DESIGNING THERMO & PHOTORESPONSIVE MATERIALS FOR BIOMEDICAL USE

Designing Dual Thermoresponsive & Photoresponsive Materials for Biomedical Applications

By

Jenny Mayra Guicela Tzoc Torres, B.Eng

A Thesis Submitted to the School of Graduate Studies in Partial Fulfillment of the Requirements for the Degree Master of Applied Science

MASTER OF APPLIED SCIENCE (2011) McMaster University

(Biomedical Engineering) Hamilton, Ontario

TITLE: Designing Dual Thermoresponsive & Photoresponsive Materials for Biomedical Applications

AUTHOR: Jenny Mayra Guicela Tzoc Torres, B. Eng. (McMaster University)

SUPERVISOR: Dr. Todd Hoare

NUMBER OF PAGES: x, 110

Abstract

Multi-stimuli-responsive materials with dual sensitivities to both temperature and light were designed and investigated for their responsive properties in aqueous media.

Amphiphilic polymers were synthesized by copolymerizing monomers of thermoresponsive N-isopropylacrylamide (NIPAM) with vinyl cinnamate (VC), using different chain transfer agents to both control the molecular weight and impart functionality of an amine-terminal or carboxylic acid- terminal end groups. Linear polymers based on pNIPAM-VC were characterized and their thermo- and photo-responsive properties confirmed by ^{1}H NMR, GPC, and UV-visible spectroscopy.

To obtain desired solubility and phase transition properties for the copolymer, latent variable methods were applied to past polymer data to identify the correlated reaction variables. -Using model inversion, the ability to predict polymer properties was possible. The outcomes helped to determine ideal reaction reagents and conditions for future designs, facilitating the synthesis of both amine-capped and carboxylic acid-capped poly(NIPAM-co-VC) polymers with high solubility and phase transition onset below physiological temperature (<37°C)

The designed poly(NIPAM-co-VC) polymers were subsequently grafted to a polysaccharide, hyaluronic acid (HA) or carboxymethyl cellulose (CMC), via carbodiimide chemistry. The graft material's mechanical strength was compromised by both the linear polymer size and the architecture (end-group-grafting) which lead to unsuitable materials.

Microgels with multi-responsive properties were synthesized by copolymerizing NIPAM with either acrylic acid (AA) or methacrylic acid (MAA) by conventional precipitation-emulsion methods. These microgels were aminated and subsequently grafted with a cinnamate pendant group. As an alternative, microgels were fabricated by microfluidics using linear polymers precursors. Both types of microgels exhibited significant deswelling upon changes in temperature, light, and pH, suggesting their potential utility as smart, photo-responsive drug delivery vehicles.

Acknowledgements

I would first like to thank God for his guidance in this journey of life. I am thankful for this wonderful opportunity that was challenging and rewarding.

Thank you to my supervisor Dr. Todd Hoare for his supportive manner and advice, and I am honoured to have worked with such an intelligent and accomplished man.

Thanks to Dr. Heather Sheardown and the 20/20 NSERC Ophthalmic Materials Network, Dr. Pelton, Dr. MacGregor and Dr. Stover for access to their equipment and their friendly group members. Particular thanks to Nick Burke for all his wise suggestions with GPC. Thank you to all my lab mates, office mates, and colleagues for their help in general. Special thanks to Rabia Mateen and Paniz Sheikholeslami for their equipment hints and analysis discussions. Thanks to Danielle Maitland and Janine Ho, for all their time and efforts. I am thankful to Emily Nichols, who provided knowledge and guidance in the application of statistical methods. It was a pleasure to work with you all.

I would like to thank all my friends for their ongoing patience, understanding, and support. Finally, thank you to my family members near and far, my parents, siblings, and their partners alike. Gracias hermano, Mario, for your smiling and calming support at all times! Thanks to my parents, Mario and Mayra Tzoc, who are my inspiration and motivators. Such hard working, dedicated people, I can only strive to be like them. Thank you for all your love and support all of the time. I love you both very much!

Table of Contents

List of Figures

List of Tables

List of Abbreviations & Symbols

~	Approximately
/	Or
AA	Acrylic acid
AESH	Cysteamine hydrochloride
AIBMe	Dimethyl 2,2'-azobis(2-methylpropionate)
Al	Aluminum
AMD	Age-related macular degeneration
CMC	Carboxymethyl cellulose
CNIB	Canadian National Institute for the Blind
conc.	Concentration
DOE	Design of experiments
DMF	*N,N*-Dimethylformamide
Eff.Dia.	Effective diameter
EtOH	Ethanol
FRP	Free radical polymerization
-g-	Graft
GPC	Gel Permeation Chromatography
H_2O	Water
HA	Hyaluronic acid
k	1000
Lab	Laboratory
Min	Minute
M_n	Number average molecular weight

M_w	Weight average molecular weight
MWCO	Molecular weight cut off
NIPAM	N-isopropylacrylamide
NPDR	Non-proliferative diabetic retinopathy
Obs.	Observed
PCA	Principal component analysis
PD(I)	Polydispersity (index)
PDR	Proliferative diabetic retinopathy
PEG	Polyethylene glycol
PEO	Polyethylene oxide
PLS	Partial least squares regression
PP	Polypropylene
ppt	Precipitate
Pre.	Predicted
PS	Polystyrene
S.#A	Sample, number, pNIPAM-co-AA linear polymer series
S.#K	Sample, number, pNIPAM-HEMA linear polymer series
S.#T	Sample, number, pNIPAM-VC linear polymer series
S.#U	Sample, number, pNIPAM-VC-AA linear polymer series
S.#W	Sample, number, pNIPAM linear polymer series
T_{cp}	Cloud point
TGA	Thioglycolic acid
THF	Tetrahydrofuran
UV	Ultra-violet
VC	Vinyl cinnamate
VPTT	Volume phase transition temperature
vs.	Versus
wt.	Weight
λ	Wavelength

Chapter 1 :

Introduction

In 2007, Canada spent an estimated $15.8 billion in vision loss care costs, and this amount is forecast to rise steadily by CNIB (Access Economics Pty Limited 2008). Due to the increasing cases of ocular degenerative disease in youth and senior populations, there is a high need for improved drug delivery systems (DDS) to deliver therapeutics and treat these diseases.

Our goal was to design biomaterials that offer desired characteristics for ophthalmic applications. Developing suitable materials is not a simple task, as the human body is an intelligent system which efficiently acts to eliminate foreign materials. The motivation of this work, to create a successful "smart" biomaterial that responds reversibly to multiple environmental stimuli (pH, temperature, and light) while being appropriate for ocular use, is outlined in Chapter 2.

Our systems were designed to exhibit dual responsiveness to temperature and light. The thermoresponsive component of the materials is poly(N-isopropylacrylamide) (pNIPAM), a polymer that in aqueous media exhibits a characteristic lower critical solution temperature (LCST)~32°C; that is, when it is exposed to a temperature higher than its LCST, the water-soluble, hydrophilic polymer collapses to forms an insoluble, more hydrophobic globule. Thus, due to the reduced affinity between pNIPAM chains and water above the LCST, physical gelation can occur driven by entropic changes. The light-sensitive component is provided by cinnamates, which have been reported to reversibly form new chemical bonds when exposed to light of certain wavelengths (λ). Unlike other responsive systems which are surgically implanted (invasive means) the fundamental idea here is to design a system that undergoes a solution-to-gel (sol-to-gel) transition spontaneously upon injection into the body, using the temperature change from room temperature to body temperature as the stimulus for gelation. This would allow for a room temperature liquid solution to be easily uptaken into a syringe and injected *in vivo*. Upon injection, the system would immediately form a gel (by NIPAM thermo-crosslinks) and then reversibly respond (via swelling or deswelling) to a light stimulus (VC photo-crosslinks) on demand. Such a system would be useful for triggered drug delivery in an ocular environment, in which low exposure of UV light is regularly tolerated.

The required incorporation of hydrophobic photoresponsive cinnamate groups into polymers to impart photosensitivity while retaining water-solubility in the final product polymers was a particular challenge throughout this thesis. Different chemistries were explored

to obtain the optimal polymeric properties using combinations of thermoresponsive, pH-responsive, light-responsive, and hydrophilic monomers to achieve the desired solubility and cloud point of the pNIPAM graft material. In a typical polymerization process, synthesis, and recovery steps are slow, and if the optimal product properties are not obtained, the design process by nature becomes highly iterative and time consuming. To address this challenge, partial least squares regression (PLS) was applied to past polymer data and used to predict future polymer properties, as described in Chapter 3. The most important benefit of PLS is that one can gain a deeper understanding of the most influential factors (obvious and non-obvious) in designing new materials and new polymerization processes.

The knowledge gained through PLS modeling was used to synthesize a dual thermo and photo-responsive polymer graft that could subsequently be conjugated to a carbohydrate to generate a thermally-gelling injectable drug delivery system. The material's chemical composition was characterized, its responsive nature examined, and cytotoxicity results discussed in Chapter 4.

In Chapter 5, methods of successfully designing microgels with multi-responsive properties were explored. These microgels were formulated both by conventional microgel precipitation-emulsion strategies and by novel microfluidics methods. By incorporating different carboxylate functional groups, some microgels showed multi-responsive properties to changes in their surrounding temperature, light, and/ or pH.

The multi-responsive materials designed in this work showed significant potential as drug delivery devices, although further testing and development will be required to translate these materials design concepts to the clinic. The methods of formulation and PLS applications can be used as efficient design tools that can save time, resources, and clarify the underlying relationships of the variables in a system.

Suitable biomaterials with multi-responsive features can offer benefits to the practitioner and patient alike. An ideal DDS would be able to respond quickly *in situ*, allow for controlled drug release by external means (by simple and safe modes), have tunable structures to accommodate different drugs, be stable, localized at the target site, offer biodegradable properties and be non-toxic *in vivo*. The designed systems exhibit many of these properties.

Chapter 2 :

Literature Review

2.1 A Closer Look at the Eye: Diseases and Treatment Options

2.1.1 The Posterior Segment of the Eye & Diseases

The eye is considered an 'immune-privileged' organ and yet its complexity does not allow for facile delivery of therapeutics to treat ocular diseases. While there are novel therapeutics and therapeutics delivery systems being designed and developed, efficient delivery systems that act at the target site for prolonged periods are still a significant clinical need to help prevent, treat, and potentially cure ophthalmic diseases.

Figure 2—1 shows a sagittal section of the adult human eye. The eye is a slightly asymmetrical sphere, with a sagittal diameter-to-transverse diameter of approximately 25mm:24mm and a volume of ~6.5cm^3 (Kolb H., Fernandez E. et al. 1995). The eye is divided into two segments:

1. Anterior segment: area from cornea to the lens inclusive, with aqueous humor
2. Posterior segment: area from lens to retina inclusive, with vitreous humor

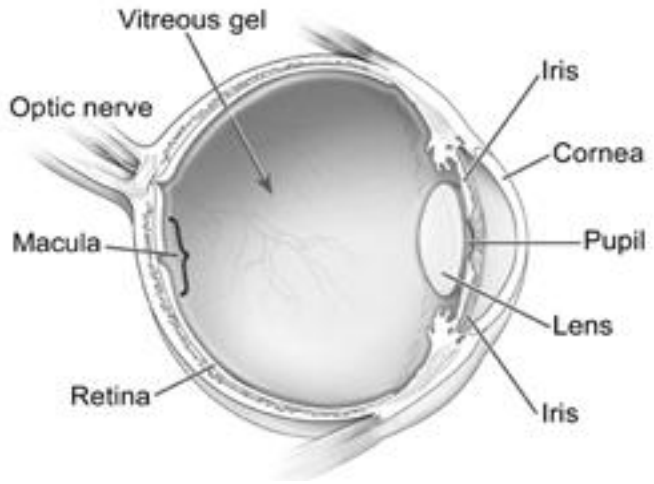

Figure 2—1: Anatomy of the eye, a sagittal view (National Eye Institute 2010)

Here the focus is to develop materials that could have potential ophthalmic applications in the posterior segment of the eye. Three of the eye tissues and related diseases are detailed in Table 2—1.

Table 2—1: Three posterior segment tissues and potential diseases affecting them

Tissue	Contents	Function	Potential Disease(s)	Source(s)
Optic nerve	➢ Second cranial nerve ➢ Made up of ~1million thread-like nerve fibers, come from retina	➢ Carries impulses to brain to interpret information as images	Glaucoma (G): ➢ Caused by increased intraocular pressure ➢ 4 classes: open-angle (OAG) is chronic, angle-closure (ACG) is acute, congenital (CG), secondary (SG)	(Health Canada. 2006; VeriMed Healthcare Network 2009)
Macula	➢ Located at center of retina ➢ Made up of cone cells (photoreceptor cells)	➢ Responsible for sharp & central vision	Age-related macular degeneration (AMD): ➢ Wet AMD (abnormal blood vessels, may leak blood/ fluid and move macula) → loss central vision ➢ Dry AMD (light-sensitive macula cells break down) → blurred vision	(Lowenstein J.I. 2011; National Eye Institute 2010)
Retina	➢ Made up of rods cells (photoreceptor cells)	➢ Network of nerves ➢ >100 million photo-sensitive cells ➢ Allows to see colour vision ➢ Receives and transports signals to optic nerve	Diabetic Retinopathy (DR): ➢ Damage of retinal vasculature ➢ NPDR-DR (mild symptoms; weak blood vessels, may form bulges "microanuerysms" → leak/swell macula) ➢ PDR-DR (advanced form; O_2 deprived retina with new fragile vessels form in retina/ vitreous that can leak → clouded vision/ detach retina causing glaucoma)	(American Optometric Association 2006)

2.2 Drug Delivery Systems: Designs & Challenges

2.2.1. Drug Release Kinetics

Drug release kinetics describes the amount of drug released from a drug delivery device as a function of time. Depending on the drug delivery system design, the release kinetics of a drug may be regulated by changing the rate of diffusion of a drug through the matrix; in this case, relationships such as Fick's first law can be used to estimate the kinetics of drug release. In other cases, drug release is driven by polymer degradation, by which the release kinetics are

regulated by the degradation kinetics of a bond between the drug and the release vehicle or the rate at which a matrix material entrapping drug is degraded away.

In typical drug dosing applications (capsules or injections) the drug release kinetics are represented in Figure 2—2(a) (green lines). In this case, drug dosing induces local increases in concentration of the drug that diminish over a short time until the next dosage occurs (spikes). Drugs are required at specific concentrations to be effective (lower limit) but can be toxic at higher concentrations (upper limit), such that drug release outside this "therapeutic window" (between the dotted lines in Figure 2—2(a)) can lead to no effect or toxic effects respectively.

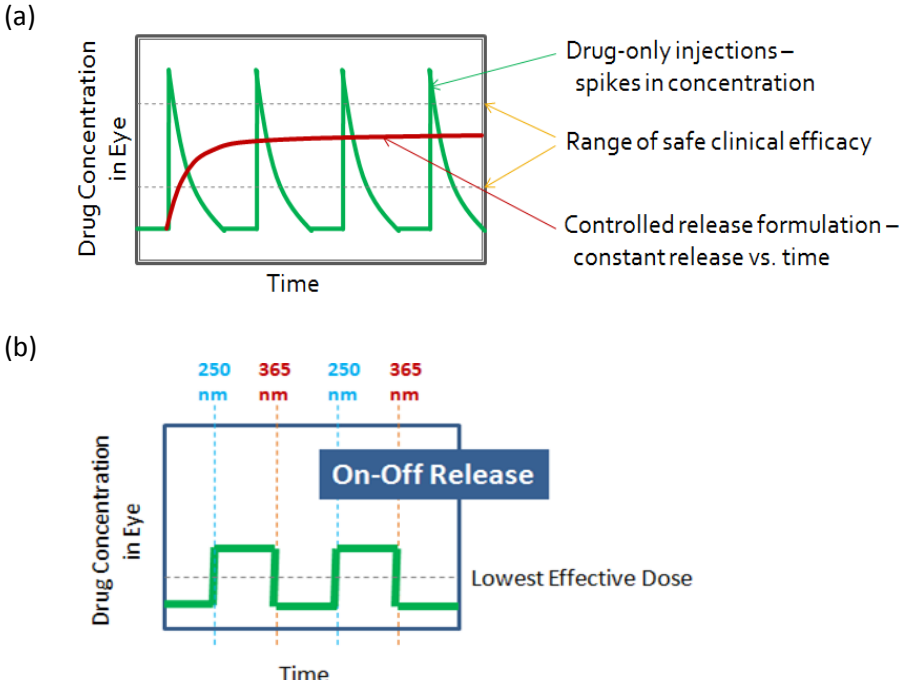

Figure 2—2: Drug release profile of (a) conventional dosing and constant release and (b) controlled 'on-off switch' release design

In most drug delivery systems, a constant release of drug over an extended period time is desired, the kinetic profile shown in (red) Figure 2—2 (a). In other cases, however, controlled 'on-off' switch drug release is desired, as shown in (green) Figure 2—2 (b). A controlled 'on-off' switch system is theoretically possible for reversible photoresponsive materials. This type of delivery system could be advantageous for intermittent drug delivery applications where "high" or "low" drug release states are desired (e.g. insulin delivery) or in the treatment of diseases where non-invasive adjustments in drug dosing are frequently required. Given the patient

discomfort associated with accessing the back of the eye through repeated injections, such an ability to trigger changes in drug release kinetics through communication with a drug delivery device has significant advantages.

2.2.2 Past Therapeutic Delivery Systems

The most common routes of drug administration are oral (capsules), topical applications (eye drops or creams), injections (intravenous, subcutaneous), and implanted devices. Novel minimally invasive ocular designs include gel/ nanoparticle drug delivery systems, iotophoresis, microneedles, drug-eluting contact lenses, and microdroplets (Weiner A.L. and Gilger B.C. 2010). Some more highly invasive methods include drug delivery by eroding and non-eroding implants, active pumps, intraocular lenses, suprachoroidal, and episcleral reservoirs (Weiner A.L. and Gilger B.C. 2010).

Established drug delivery systems for the eye exist, but most offer limited efficiency and adequacy. Novel systems, products, devices, and drugs must go through a number of clinical stages and meet the requirements of a governing body such as Health Canada's Product & Food branch or the American Food and Drug Administration (FDA) to be market-approved (FDA 2009). Today, some AMD treatments are systemic via intravenous injection or administered by regular injections into the eye every 4-6 weeks. The latter method is better in terms of site-specific efficiency, as the prior method results in significant loss of drug through the circulatory system prior to reaching the eye. Though injections are a better means of delivery, they have associated risks to the patient and patient compliance is reportedly low for this type of treatment (Access Economics Pty Limited 2008).

2.2.3 Challenges of Drug Delivery to the Back of the Eye

In order to design suitable drug delivery systems, we need to consider the following challenges:

- On average, the adult human body has an efficient immune response to foreign materials, with over 108 antibodies and 1012 different T-cell receptors available to destroy foreign materials (Heath F., Haria P. et al. 2007). Although the requirements for biocompatibility in the eye may be more relaxed than other places in the body due to

the eye's immune-privileged nature (due to the retinal-blood barrier), we must ensure that the materials (and their byproducts) are biocompatible and can be cleared from the eye.

- Injected biomacromolecules (DNA, RNA, proteins) often rapidly drain away from site and into the lymphatic system, minimizing the effectiveness and duration of the therapeutic(s) *in vivo.* As a result, localized drug delivery specifically to the targeted site would be highly desirable to reduce the fraction of "wasted" drug that does not interact with its target tissue.
- The natural inherent properties of the drug (molecular charge, size, solubility, half life, and stability) can affect the efficacy of drug. For example the drug may be denatured in the biological environment by the biomaterial used to deliver the drug and may deactivate the drug upon delivery. This is a particular concern for biomolecular drugs such as proteins or nucleotides which can be easily denatured or degraded in the body.
- The posterior segment has barriers to drugs with pharmacokinetic-pharmacodynamic interactions that are difficult to detail (Novack G.D. 2008). As a result, the potential drug interactions must be examined both *in vitro* and *in vivo*.
- Repetitive injections are undesirable for patients and risk damaging surrounding vasculature (bleeding) or the injection void could lead to infection, ophthalmitis, cataracts or even retinal detachment. As such, minimizing the frequency of injections and/or the side-effects of these injections would be desirable.

Overcoming these challenges, while considering the practicality of any drug delivery system developed, is needed to benefit all stakeholders: drug developers, auditors, physicians, and patients. In the designs proposed herein, the multi-responsive systems developed are primarily proof-of-concept systems that may lead to future drug delivery products.

2.3 Stimuli Responsive Materials

2.3.1 Responsive Materials

"Smart" materials that respond to environmental stimuli have become a subject of intense research interest in the last several years. Smart materials that respond to stimuli such

as electric field, magnetic field, temperature, light, electrochemical, and pH changes have been reported (Yoshida M. and Lahann J. 2008). A visual representation of some stimuli, and the corresponding physical response to those stimuli, is shown in Figure 2—3.

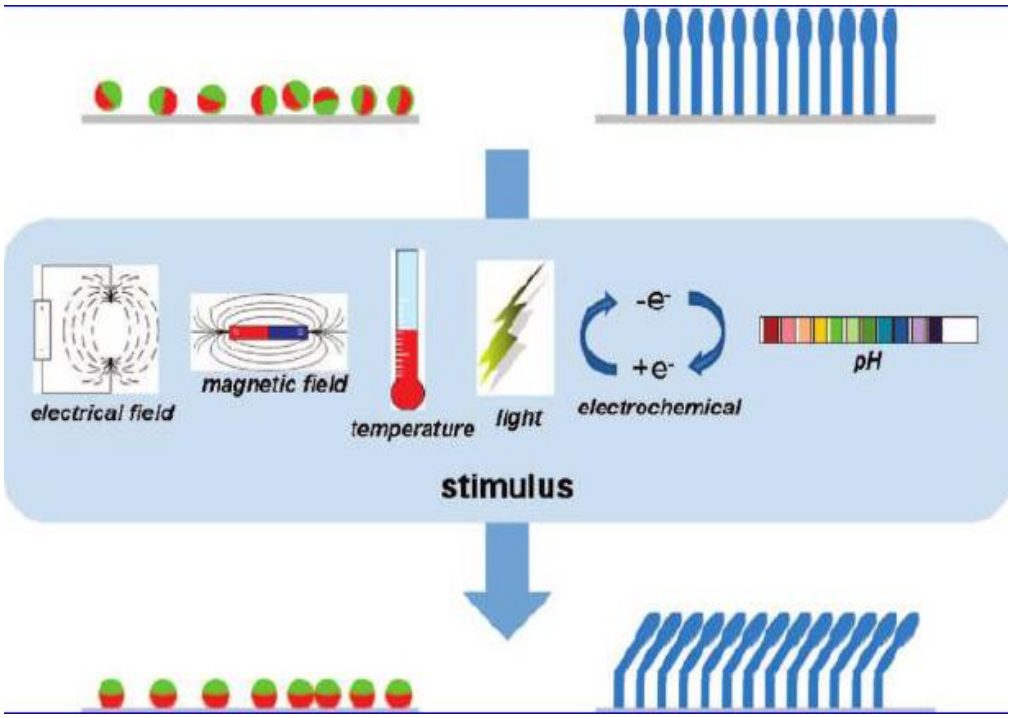

Figure 2—3: Examples of common stimuli, reprinted with kind permission (Yoshida M. and Lahann J. 2008)

Examples of responsive materials include the copolymers 2-(2-methoxyethoxy)ethylmethacrylate-co-oligo(ethylene glycol) methacrylate (p(MEO_2MA-co-OEGMA) [thermoresponsive range ~26°C to 90°C] (Lutz J-F., Akdemir O. et al. 2006), poly(acrylic acid) (PAA) [pH responsive], and poly(N-vinylcaprolactone) (PNCL) [thermal and pH responsive] (Ahn S-k., Kasi R.M. et al. 2008).

Biomaterials using smart materials have demonstrated ability as wound healing scaffolds and have been researched for their use as drug delivery systems to deliver riboflavin (Ha D.I., Lee S.B. et al. 2006), lysozyme (Zhao C., Zhuang X. et al. 2009), fibroblast growth factor (bFGF) (Andreopoulos F.M. and Persaud I. 2006), quantum dots as protein models (Sirpal S., Gattás-Asfura K.M. et al. 2007), and doxorubicin (Hu R., Chen Y-Y. et al. 2010), among other targets.

Thermoresponsive (or thermosensitive) materials that undergo a physical transformation in response to a change in their environmental temperature have attracted particular interest. The minimum temperature value at which this change occurs is usually called the lower critical solution temperature (LCST) for polymers. For hydrogels or microgels, the phase transition results in deswelling of the gel network at the volume phase transition temperature (VPTT); for linear polymers, the phase transition results in a transition from a soluble to insoluble polymer, resulting in materials with visible whitening/ precipitation at the cloud point temperature (T_{cp}). The temperature at which the polymer undergoes a phase transition varies based on the chemistry of each polymer and can be altered by copolymerization with more hydrophilic (higher LCST) or hydrophobic (lower LCST) comonomers. Therefore, thermoresponsive materials become an attractive option to be used *in vivo*, if there VPTT can be altered to a physiologically relevant range (from >25°C to <37°C); such phase transitions have been reported (Ha D.I., Lee S.B. et al. 2006), resulting in a liquid solution at room temperature to be easily injected into the body and immediately gel.

While most thermosensitive materials are of synthetic origins, some are natural and examples of each are identified in Table 2—2.

Table 2—2: Examples of thermoresponsive materials

Material	Investigated parameters/use	Source(s)
Liposomes such as dipalmitoylphosphatidylcholine, distearoyl phosphatidyl choline & cholesterol (Ch)	➢ Can encapsulate hydrophobic/ hydrophilic drugs ➢ Anti-tumor drugs studied	(Maruyama K., Unezaki S. et al. 1993; Chelvi T.P. and Ralhan R. 1995)
Poly(ethylene oxide-b-L-lactide-b-ethylene oxide) (PEO-PLLA-PEO) or (PEO-PLLA)	➢ Solutions at low concentrations formed micelles ➢ Undergo sol-to-gel transition ➢ Slow drug release (FITC-Dextran)	(Jeong B., Bae Y.H. et al. 1996)
Elastin-like peptides (ELP) such as ELP-doxorubicin (ELP-Dox)	➢ Fusion of thioredoxin with ELP (Trx-ELP) with greater than 95% recovery of protein ➢ Reacting lysine-containing ELPs with an organophosphorous cross-linker, β-[tris(hydroxymethyl)phosphino]propionic acid (THPP) under physiological conditions	(Ge X., Trabbic-Carlson K. et al. 2006; Lim D.W., Nettles D.L. et al. 2007)
Poly(N-isopropylacrylamide) (pNIPAM)- based materials	➢ Grafted with collagen/ hyaluron/ chitosan to deliver cells/ drugs	(Fitzpatrick S.D., Mazumder M.A.J. et al. 2010; Fitzpatrick S.D., Mazumder M.A.J. et al. 2011)

It should be specified that some of these materials are also thermogelling, in that they will visibly undergo a solution-to-gel (sol-to-gel) transformation to generate a viscous gel above the LCST (for example, (Fitzpatrick S.D., Mazumder M.A.J. et al. 2011). Note that a thermoresponsive material is not necessarily a thermogelling material, though the reverse terminology is true. Other examples of reported thermoresponsive materials include ,N-diethylacryamide (DEAAM), poly(ethylene oxide)-poly(propylene oxide) (PEO-PPO) copolymers (Alarcon CH., Pennadam S. et al. 2005), and thermoresponsive pNIPAM-g-chitosan-g-hyaluronic acid (CPN-HA) (Chen J-P. and Cheng T-H. 2009).

2.3.2 Design Overview

In this work, polymers, hydrogels, and microgels were designed that are both thermoresponsive and photoresponsive in nature. These products are required to have negligible toxicological effects and ideally will be transparent in aqueous media for their practical application in the eye.

2.3.2.1 NIPAM

Since NIPAM was first reported by Heskin in 1968 to have a thermal phase transition, it has been widely investigated (Heskins M. and Guillet J.E. 1968). The repeat unit of polyNIPAM is shown in Figure 2—4.

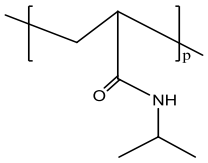

Figure 2—4: Chemical structure of monomer NIPAM

The homopolymer has a characteristic LCST ~32°C. Hence, it is a low viscosity aqueous solution at room temperature (below the LCST) and can easily be injected into the body and start to aggregate into a localized mass (~30seconds to form physical crosslinks). This behaviour originates from the balance of hydrophilic (amide linkage) and hydrophobic (isopropyl group) groups and their conformations in aqueous media. The responsive nature of NIPAM is governed

by thermodynamics where the polymer dissolution can be stated as (Rimmer S., Soutar I. et al. 2009):

$$\Delta G_{mix} = \Delta H_{mix} - T\Delta S_{mix} \quad \text{Equation 2.1}$$

where ΔG_{mix} is the Gibbs free energy, ΔH_{mix} is the enthalpy, T is the temperature, and ΔS_{mix} the entropy of the system. When ΔG_{mix} is negative, the polymer is fully dissolved and a positive ΔG_{mix} results in physical aggregation. When the surrounding temperature is below the LCST, the enthalpic effect of hydrogen bonding of water around the amide segment results in a net negative Gibbs free energy and thus a soluble polymer in aqueous media. As the surrounding temperature is increased above the LCST, the entropic cost of water structuring around the hydrophobic isopropyl groups becomes a more significant contributor to the overall Gibbs free energy, increasing the overall Gibbs free energy and resulting in associations between these hydrophobic isopropyl groups to minimize the total surface area of interaction (and thus required structuring) with water (the aggregation response). Co-polymerizations of NIPAM that alter the VPTT range from 25-50°C are shown here and by others (Bikram M. and West J.L. 2008).

2.3.3 Photoresponsive Materials

Compounds that undergo conformational changes in response to the applications of particular wavelength(s) of light are known as photoresponsive, light-sensitive, photochromes or chromophores, depending on their exact response. Photochromes have a reversible response to light which causes molecular photochemistry at specific wavelength(s) and photocleavage at other wavelength(s) to regenerate the original structure. These photosensitive molecules are an attractive choice for *in vivo* applications, specifically in the eye, because they can be triggered by an external light source. Some of the most studied photoresponsive molecules include anthracene, cinnamates, coumarin, thymine, cinnamylidene, azobenzene, spiropyran, spirooxazine, diarylethene, and fulgide (Kelly S.M. 1995; Andreopoulos F.M., Deible C.R. et al. 1996; Hulubei C. and Rusu E. 2006; Wybrańska K., Szczubiałka K. et al. 2008; Sheardown H., Brook M.A. et al. 2009; Ercole F., Davis T.P. et al. 2010; Wells L.A., Furukawa S. et al. 2011). Most

of these compounds are naturally occurring in plants and fruits and are extracted and used in cosmetics, fragrances, foods, and medicines (antiradical activity).

Coumarin moieties have been used extensively in conjugation with polymers to generate photoresponsive systems. For example, photoresponsive micelles were stabilized by block copolymers using poly(ethylene oxide)-poly(coumarin methacrylate)-poly(methacrylate) (PEO-PCMA-PMMA) (Jiang J., Qi B. et al. 2007). Cinnamates are also widely reported in the literature as photoresponsive and photocrosslinkable functional groups. For example, films made of poly(ethylene glycol) with cinnamylidene moieties (Andreopoulos F.M., Deible C.R. et al. 1996) or films prepared from α,ω-dihydroxy terminated poly(L-lactide) (PLLA) with pendent 5-cinnamoyloxyisophthalic acid (ICA) to give (PLLA/ICA) (Nagata M. and Inaki K. 2009) were reported. Other studies describe novel methods of synthesizing photoresponsive free radical-reactive monomers such as 4-(benzyloxycinnamoyl) phenyl methacrylate (BCPM) (Vijayanand P.S., Kato S. et al. 2007), esterifications of vinyl phenols/vinyl β-chloroethyl ether with cinnamic acid/ β-styrylacrylic acid, etherifications of vinyl β-chloroethyl ether with hydroxychalcones (Kato M., Ichijo T. et al. 2003). In some cases, different photochromes can be mixed to also generate photocrosslinkable systems; for example, Ito Y. and Fujita H. reported the unusual photocycloaddition of tryptamine and 3-nitrocinnamic acid (Ito Y. and Fujita H. 1999).

2.3.3.1 Cinnamates

The work presented here focused on the use of a variety of cinnamates and designs, using both copolymers of vinyl cinnamate (VC) and graft copolymers consisting of a pNIPAM backbone and trans-4-nitrocinnamic acid (NC), cinnamic acid (CA), trans-4-nitrocinnamoyl chloride (NCCl), or cinnamoyl chloride (CCl) grafts. The chemical structures of some of these photosensitive molecules are shown in Figure 2—5.

(a) (b) (c)

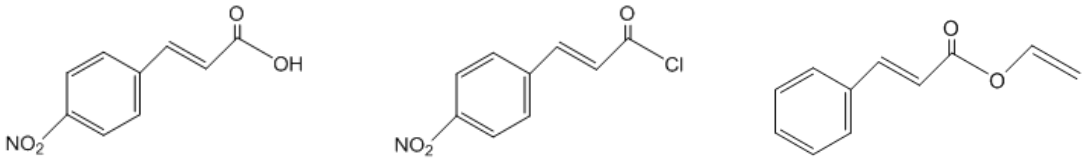

Figure 2—5: Chemical structure of (a) trans-4-nitrocinnamic acid, (b) trans-4-nitrocinnamoyl chloride, and (c) vinyl cinnamate

The copolymerization of vinyl cinnamate was a particular focus of this thesis. Since Minsk L.M et al. first reported the photocrosslinkable nature of poly(vinyl cinnamate), the monomer and polymer properties have been widely investigated (Minsk L.M., Smith J.G. et al. 1959). Most studies of the pVC homopolymer are in its solid state and examine its photocrosslinking ability but not its de-crosslinking ability. For VC, the application of light in the range of λ>305nm to 360nm has been observed to induce photo-dimerization, while the application of λ~250nm will photocleave/ de-dimerize the molecules. Irradiation causes a trans-cis isomerization as well as a [2+2] cycloaddition of the α,β-unsaturated carbonyl, forming a cyclobutane ring. While dimers are not always the most common products of the photoreaction other possible photoproducts have also been reported (Lewis F.D., Quillen S.L. et al. 1988). The photochemistry of trans-4-nitrocinnamic acid upon light application is seen in Figure 2—6.

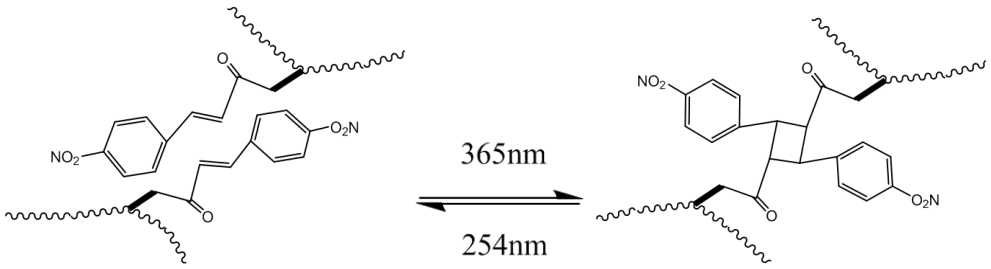

Figure 2—6: Photochemistry of trans-4-nitrocinnamic acid pendent group, upon irradiation exposure

From a quantum yield perspective, the photoreaction occurs as an excited state molecule attacks a ground state molecule according to the scheme (Schmidt G.M.J. 1971):

$$\mathrm{M} \xrightarrow{h\nu} \mathrm{M}^*$$

$$\mathrm{M}^* + \mathrm{M} \rightarrow \mathrm{M}_2$$

Where M is a monomer at ground state, M* the excited state monomer, and M_2 is the photoproduct. Upon irradiation of cinnamic acids the photoproducts are referred to as 'topotactic', as the dominant products are the α (head-to-tail, α-truxillic acid) form and β (head-to-head, β-truxinic acid) form (Atkinson S.D.M., Almond M.J. et al. 2003). In most cinnamate crosslinking processes, a combination of these structures occurs in solution, as shown in Figure 2—7.

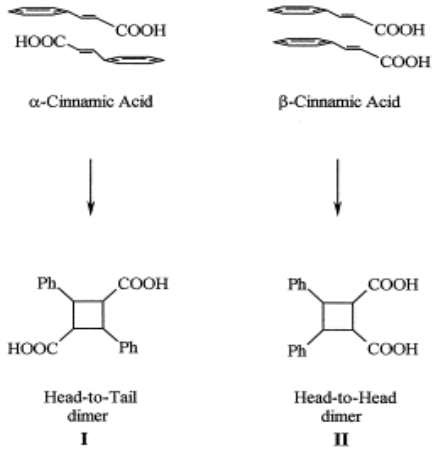

Figure 2—7: Dominant photoproducts of cinnamic acid upon irradiation (Atkinson S.D.M., Almond M.J. et al. 2003)

The rate of photocrosslinking or disappearance of photoactive –CH=CH- bond depends on the other chemical groups present. Polymers with substituted cinnamoyl chlorides possessing electron releasing or withdrawing functional groups (methoxy, chloro, nitro groups at the para position of aromatic ring) have been found to significantly affect crosslinking efficiency (Ali A.H. and Srinivasan K.S.V. 1997). Cinnamoyl compounds with a nitro substitution were shown to be the least efficient at crosslinking and thus underwent the least number of cyclobutane-type addition reactions (as confirmed by spectral studies) (Ali A.H. and Srinivasan K.S.V. 1997; Daskiewicz J-B. and Barron D. 2003; Bartsch S. and Bornscheuer U.T. 2010).

2.3.3.2 Light Applications

The electromagnetic spectrum in Figure 2—8 shows the UV bands required to initiate the photochemical reactions of cinnamates in comparison to other bands.

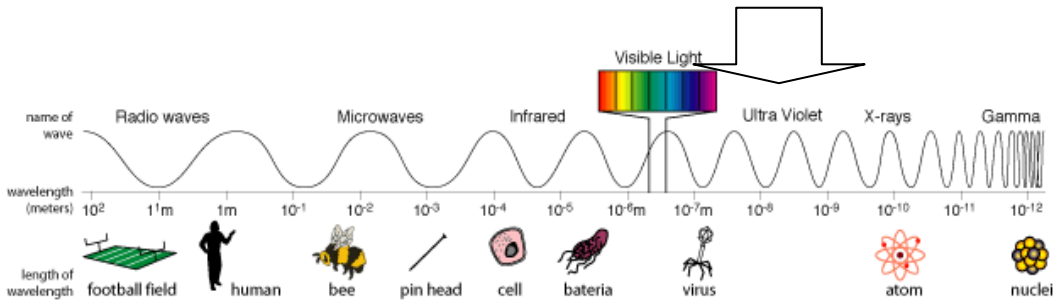

Figure 2—8: The electromagnetic spectrum (NASA Official: Netting R. 2007)

UV rays can be sub-divided into three categories as:

1. UVA (long-waved): 400nm-315nm range
2. UVB (middle-waved): 315nm-280nm range
3. UVC (short-waved): 280nm-100nm range

Here, we need both application of UVB and UVC for dimerization and de-dimerization respectively. UV light can penetrate materials with photons of the correct energy (light waves about the size/ smaller than the atom/molecules) to interact with the electrons in atoms. When light is directed to a material, adsorption of the photon energy can emit an electron from the material via the 'photoelectric effect' or cause an electron jump to a higher energy level 'excited state' that subsequently relaxes back to its ground state, re-emitting another photon in the process (Moxon E.). The emitted photon, can be measured by spectroscopy techniques (spectrophotometry, fluorescence, etc.) and is used in many analytical applications.

A disadvantage to using UV light is that prolonged exposure to UVC rays can be harmful to cells so exposure times should be limited. Excessive exposure to UV irradiation can damage cell's DNA, inhibit subsequent transcription and result in abnormal cell function (i.e. cancerous cells or cell death) (Tornaletti S. and Pfeifer G.P. 1996; Mone M.J., Volker M. et al. 2001). Exposure limits are set for irradiance of <1mW/cm^2 for exposure times >16min of UVA bands and irradiance <0.3mW/cm^2 for exposure times <16min to UVB and UVC bands (International Program on Chemical Safety 1982). The routine use of light application in ophthalmic diagnostics confirms this type of stimuli is a safe and practical method as long as it is applied within safe limits to the body.

2.4 Objectives of Current Research

Based on the stated objectives and chemistries described, the main objectives of this thesis are:

- To design water soluble polymers with dual thermoresponsive and photoresponsive properties
- To explore the most suitable chemistries for synthesizing dual responsive materials and confirm those chemistries (along with the responsive nature by appropriate characterization

- To perform *in vitro* cytotoxicity studies to assess the potential utility of these materials *in vivo*
- To apply partial least squares (PLS) modeling to better understand the influential parameters and correlations associated with the synthesis of dual responsive polymers
- To explore PLS model inversion to predict polymer properties before polymer synthesis
- To graft dual responsive linear polymers to carbohydrates to form injectable hydrogel systems useful for delivering drugs
- To fabricate dual responsive microgels for use as injectable drug delivery systems

This thesis is sectioned into three sub-projects with a corresponding chapter for each. The sub-projects include: the investigation of PLS modeling for polymer designs (Chapter 3), *in situ*-gelling graft copolymer design (Chapter 4), and microgel synthesis (Chapter 5). A representative relational flow diagram connecting the three sub-projects is shown in Figure 2—9.

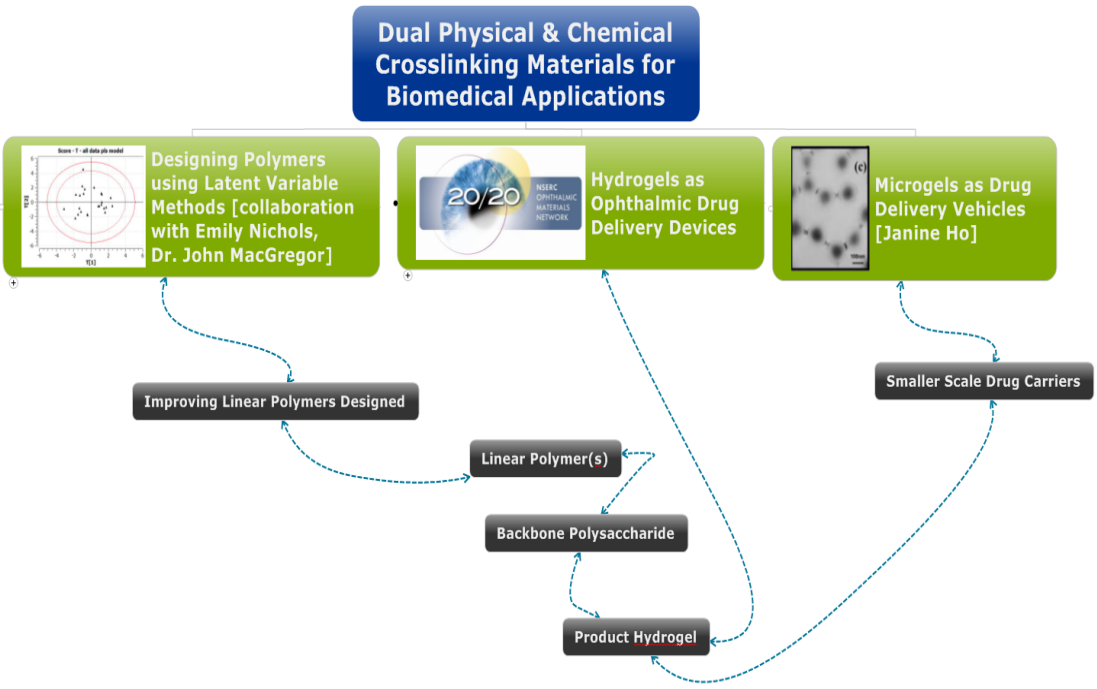

Figure 2—9: Relationships of sub-projects in this thesis

Chapter 3 :

Designing Polymers using Latent Variable Methods

3.1 INTRODUCTION: POLYMER DESIGNS & LATENT VARIABLE APPLICATIONS

3.1.1 Purpose of PLS Applications in this Work

PLS was applied in this thesis work in order to design a poly(NIPAM-co-VC) copolymer recipe that yielded a polymer with sufficiently low molecular weight for renal clearance, high solubility at room temperature, and a phase transition temperature close to that of unmodified PNIPAM (~32°C). The main challenge with these materials is to ensure thermally-driven aggregation occurs from a soluble state at room temperature (low viscosity) to a collapsed aggregated state at body temperature (high viscosity). Another challenge is the incorporation of hydrophobic VC monomers into the polymers, as hydrophobic groups tend to lower the LCST (Stile R.A., Burghardt W.R. et al. 1999; Liu L. 2003). The transition temperature must not be altered dramatically by the incorporation of photoresponsive groups in order to preserve thermally-driven gelation at a temperature between room and body temperature; however, at the same time, the amount of VC incorporation into the polymers should be maximized in order to induce maximum photo-responsiveness.

It was hypothesized that using PLS would help speed the polymer design process, make good use of the past polymer data, and obtain polymers with predictable properties in a faster/ more efficient manner compared to the traditional polymer design approaches.

Another benefit of using PLS is the possibility of learning more about the underlying relationships of the inputs (x variables) for the reactions and their influence on the polymer products (y variables), factors that may be obvious or non-obvious. Using PLS helps determine the direction of design based on experimental data. Finally, the unexpected ability to combine a wide range of seemingly unrelated polymer chemistries into one related model was ideal, essential for considering multiple types of comonomer systems that may be useful for achieving the materials design goal.

3.1.2 Traditional Polymer Design Approach

The traditional approach to designing polymers involves a highly iterative approach in which initial recipes are designed based on knowledge of the fundamental chemistry of the materials and/or literature precedents describing the synthesis of similar materials, the

reactions run, and the products characterized to assess whether the desired properties have been achieved. From start to finish, this process can take weeks, months, or even years until a suitable material is synthesized, essentially using a trial-and-error process based on qualitative assessments of previous materials. Usually, if the materials do not yield the desired properties, they are considered 'unsuccessful'; in fact, the opposite is true in that past data, if satisfactory or not, can help us better understand the systems and help formulate better polymers in the future using statistical design methods.

3.1.3 Latent Variable Methods

Statistical methods and optimization techniques such as principal component analysis (PCA) and partial least squares regression (PLS) also called projection to latent structures are useful tools to develop or improve products and processes. PLS has been previously used to reformulate food recipes, predict total antioxidant capacity (TAC) of red wines, predict polymer blended properties based on reactant properties never before tested, for gene expression data predictions, and to predict protein binding affinities among other applications (Nguyen D.V. and Rocke D.M. 2002; Catana C. and Stouten P.F.W. 2006; Muteki K. and MacGregor J.F. 2006; Versari A., Parpinello G.P. et al. 2010; Nichols E. 2011).

3.1.3.1 PCA on X or Y Data

Principal component analysis derives a small set of orthogonal and uncorrelated variables called principal components from a larger set of correlated variables (original x data variables). Similar to PLS, (detailed below), the first component in a PCA shows more variance than other components in the data set. Subsequent components represent the next highest source of variance in the data, with each component orthogonal to the preceding component. As a result, these components are defined as linear combinations of the original variables. This is helpful for data analysis and interpretation since the original variables may have correlations with each other that are obscured in their original multi-dimensional space but are highlighted when considering their representative (independent) orthogonal components. Please note that in the following sections the term component is used interchangeably with latent variable. A

detailed principal components analysis on x and y data was done before building the final model and shown in Appendix A1.

3.1.3.2 PLS Application Methods for Polymer Synthesis

In contrast to PCA, which identifies correlations between x or y data independently, partial least squares regression (PLS) methods permit identification of correlations between a range of x variables and a range of y values. This method is particularly attractive from a product design perspective, in that relationships between composition or process steps and product properties can be clearly elucidated. A step-by-step approach is outlined here which corresponds to the PLS application steps used in this work. These steps can serve as a starting point for the application of PLS to data sets to help a general user. An overview of the steps and actions taken here (steps 1 to 6) can be seen in Appendix A2. For detailed PCA & PLS fundamentals and correlation matrix calculations, refer to the literature (Fernandez G. ; Wold S., Sjöström M. et al. 1986; Kettaneh-Wold N. 1992; MacGregor J.F. and Kourti T. 1995; Esposito Vinizi V., Chin W.W. et al. 2010).

3.1.3.3 Step 1: Organizing & Compiling Data

In step 1 all past data is collected and organized into one database that is logical to the chemist as well as to the statistician. Important x variables are chosen with corresponding y variables to build **X** and **Y** matrices. In the **X** matrix, each row represents one unique recipe and its corresponding y variable in the **Y** matrix. Careful attention must be paid in expressing x and y variables (units) so that all values are meaningful and comparable; otherwise, inconsistent data will introduce incorrect relationships into the PLS model and thus yield misleading results. A particular benefit of using this approach is that PLS can identify useful correlations among the data even if there are many zeros in **X** or missing values in **Y**, such that even incomplete data sets can be analyzed. However, large amounts of missing data can result in less accurate and robust final models. As with other comparative methods, a system comprising of more observations (**X** and **Y** pairs**)** will help improve the model. Proper selection of x and y variables so that they are not themselves directly correlated in a physical sense is important; otherwise, PLS analysis would deceivingly over-fit the model. The data used to build the model is called the

"training data", as it is used to uncover key trends in the data set and "train" the model where the user can identify useful directions for materials modification.

3.1.3.4 Step 2: Building a PLS Model

Step 2 involves building the PLS model. PLS is based on the methodology of taking many non-independent variables (x and y variables) and projecting them down into a lower dimension latent variable space. A visual representation of the **X** and **Y** and key latent space matrices is shown in Figure 3—1.

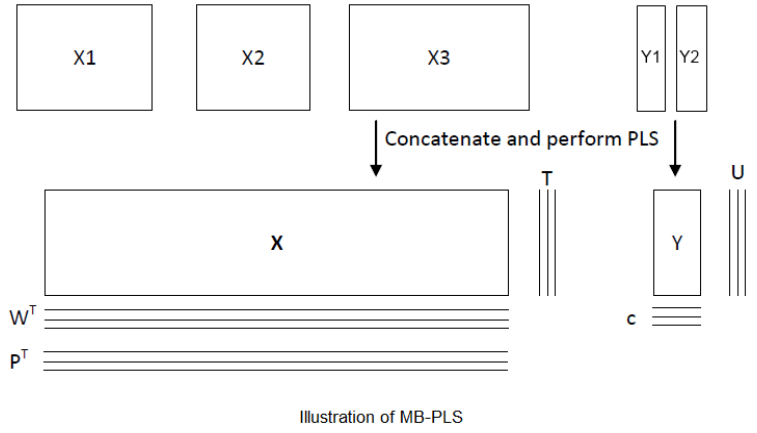

Figure 3—1: Projecting original variables into the latent variable space and a visual representation of matrices locations (ProSensus Inc. 2011)

PLS regression models the relationship(s) between **X** and **Y**, described mathematically as (ProSensus Inc. 2011):

$$\mathbf{X} = \mathbf{T} \cdot \mathbf{P}^{\mathbf{T}} + \mathbf{E} \qquad \text{Equation 3.1}$$

$$\mathbf{Y} = \mathbf{T} \cdot \mathbf{C}^{\mathbf{T}} + \mathbf{F} \qquad \text{Equation 3.2}$$

Here, **X** and **Y** are the matrices containing the x and y original variables respectively, **T** represents the latent variables, $\mathbf{P}^{\mathbf{T}}$ and $\mathbf{C}^{\mathbf{T}}$ relate the original variable to the latent variables, and **E** and **F** are residual matrices. Each column of the T matrix is a latent variable and represents one direction in the latent variable space. The T matrix is made up of values called scores that are like location coordinates of an observation in the latent variable space. The magnitude of

each score is obtained by an iterative calculation that generates weights, **W*** for the projected observations from **X** space to **T** space (Li B., Morris A.J. et al. 2004):

$$\mathbf{T} = \mathbf{X} * \mathbf{W}^{*} \qquad \text{Equation 3.3}$$

When building a model in ProMV software, the autofit feature was used in deciding the number of components. The first few components usually explain more of the variance ~70-90% in the training data (Guha R., Stanton D.T. et al. 2005). Therefore, it is important to check the number of components in a model because most of the underlying relationships are explained by these.

3.1.3.5 Step 3: Evaluating the Model

Next, the PLS model is examined for its suitability of representing the data by looking at a variety of parameters.

R2 and Q2 - R2 is the fraction of the sum of squares of all the Y variables explained by the model; the better the fit, the higher the R2 value. As more components are introduced, the value of R2 necessarily increases. Q2 represents how well the model can predict observations in the Y space; however, unlike R2, it does not necessarily increase upon the addition of more components, decreasing at some number of independent components added to the model. The aim is to reach a balance between highest R2 and Q2 to ensure the model explain the data well and can give good predictions for new observations. Values of these parameters ~1 can be difficult to attain, but it is extremely important to examine this value before using a model.

Loading bi-plot - A loading bi-plot shows the training data in the latent variable space. This plot is an overlay of two plots: the vectors of weights and loadings over a score plot (García-Muñoz S., Kourti T. et al. 2003). The correlated variables are localized in the same regions. If more than two latent variables define the data, each latent variable should be checked against all others to see correlations (clusters) and patterns evident in the latent space combination(s).

Coefficients bar plot - Each component has its own coefficients bar plot that displays the influence of each original x variables on the component, together with 95% confidence intervals (CI). For example, if an original variable (x1) has a small or “insignificant” influence on

component 1, then the coefficients bar plot would show x1 centered about ~0 with its CI equally above and below 0.

Observed vs. predicted (Obs.vs.pred.) plot - The model obs. vs. pred. plot can be viewed as a linear or time-series plot (both shown in proceeding sections). In the time-series plot, it is important to notice the magnitude and direction of the predicted set (dotted points) when comparing to the observed values (solid). In the linear version plot, a 'good' prediction is evidenced by a linear relationship.

SPE vs. HT2 - The squared prediction error (SPE) shows the distance of observations from the model plane and Hotellings T^2 (HT2) shows the distance of observations from the center of the model. These parameters can be checked individually or in the ProMV software can be plotted against each other. SPE vs. HT2 should be checked for the training data set to confirm all observations lay within both parameters' 95% CIs. Observations that lie outside the 95% CI for SPE and HT2 simultaneously are concerning and most likely distort the modeling of the whole data set.

3.1.3.6 Step 4 & 5: Exploring the Model Space (Model Inversion) & Refining

After the model is examined, the model space can be explored and inverted to find desired y values and their corresponding x values. In ProMV, the model is unconstrained in x and y such that chosen y values could lead to x values (i.e. polymer recipes) that are not practical. Therefore, after collecting all new x's based on the model guidance, these recipes may need to be refined to match the physical reality. The revised, physically-realistic x values should then be added as a 'prediction set' to the model (without the corresponding y values) to obtain the model's property prediction values for the recipe defined.

3.1.3.7 Step 6: Follow-up laboratory work

The final step is to physically make the materials and measure their properties in the lab. The new material y properties should agree with the model predicted values; otherwise, there may be some discrepancy in the model that needs investigation/ correction before proceeding. If desired, this new data can be appended to the training set and the partial least squares analysis re-run to generate new parameters and iterate the process as desired until an appropriate material is acquired.

3.2 EXPERIMENTAL: MATERIALS & METHODS

3.2.1 Materials Used

N-isopropylacrylamide (Aldrich Chemicals, Milwaukee, WI, USA) was purified by recrystallization with toluene/hexane. Acrylic acid (AA), vinyl cinnamate (VC), hydroxyethyl methacrylate (HEMA), thioglycolic acid (TGA), cysteamine hydrochloride (AESH), (all purchased from Sigma Aldrich, Canada) and dimethyl 2,2'-azobis(2-methylpropionate) (AIBMe) (Wako Chemicals, U.S.A) were used as received. The solvents *N,N*-dimethylformamide (DMF, 99.8%, Caledon Laboratories), tetrahydrofuran (THF, Fisher Scientific), toluene, hexane were all reagent grade and EtOH anhydrous grade (Caledon Laboratories). All water used was Milli-Q grade. The PBS buffer solutions were made (100mM and 10mM with pH7.3) (Ruzin S. 2005; EnCor Biotechnology Inc. 2008).

3.2.2 Generalized Polymer Synthesis

A variety of pNIPAM-based polymers were designed, with over 30 recipes made by a chain transfer free radical polymerization process (Ju H.K., Kim S.Y. et al. 2001; Dinçer S., Tuncel A. et al. 2002; Lee S.B., Ha D.I et al. 2004; Ha D.I., Lee S.B. et al. 2006; Fitzpatrick S.D., Mazumder M.A.J. et al. 2010; Fitzpatrick S.D., Mazumder M.A.J. et al. 2011). A general procedure to make these linear polymers is described below for sample S.9T (p(NIPAM-co-VC)); the exact amounts of reagents and conditions used to prepare the entire library of polymers are detailed in section 3.3.3.7. NIPAM (44.2mmol), VC (3.5mmol), and TGA (1mmol) were dissolved in EtOH (30mL) in a round bottom flask equipped with a magnetic stir bar and heated to 50°C using an oil bath, with a condenser-bubbler attached. The flask was covered with aluminum foil to prevent light-initiated crosslinking of cinnamate groups during polymerization. Nitrogen (N_2) was bubbled through the reaction mixture for 30 minutes prior to injecting the initiator AIBMe (0.5mmol). The polymerization was allowed to proceed overnight. Unreacted vinyl cinnamates or insoluble polymer fractions were isolated by adding the solution drop-wise into a beaker (400mL of H_2O) with a magnetic stir bar and allowed to stir for 48 hours; water soluble polymers remained dissolved while any unreacted hydrophobic VC monomers precipitated (ppt) and were removed via vacuum filtration. The filtrate was kept, placed into cellulose dialysis membrane(s) [MWCO

3500Da or 14kDa as per recipe designed] and dialyzed against fresh water for 8 cycles. Finally, the samples were lyophilized, weighed, and stored in the refrigerator. For samples not containing VC, the polymer reaction mixture was rotovaped (to remove excess solvent), added to ~200mL of H_2O, dialyzed [MWCO 14kDa] for 6 cycles, lyophilized, weighed, and stored at room temperature.

3.2.3 Characterization Techniques

3.2.3.1 Solubility Measurements – Qualitative Method

The solubility (transparency) of each polymer in solution for the initial training set was determined by visual inspection. Each polymer was dissolved in 100mM PBS at a conc. of 50mg/mL in 5mL of PBS. The vials were placed on a shaker for 48 hours and allowed to sit for one week at room temperature. Following this period, each sample was placed over a paper of printed text and by visual inspection ranked from highest solubility/ transparency (value of 13) to lowest solubility (value of 1). The use of qualitative measures (indicator variables) and quantitative variables were both tried separately to build PLS models in this work, where both proved to be helpful for these polymerizations.

3.2.3.2 Solubility Measurements – Quantitative Method

The solubility of each polymer was tested by adding 10%w/v polymer in 10mM PBS, using PBS as representative of physiological conditions commonly used in biological testing (EnCor Biotechnology Inc. 2008). The vials were placed on a shaker for 48 hours and allowed to sit for one week at room temperature. All samples were then placed in PS cuvettes, capped and vortexed at 2500rpm for 20 seconds before each measurement to ensure homogeneity, especially for samples with ppt formation. The % transmittance of the samples was immediately measured at λ=500nm using a DU 800 UV/Visible Spectrophotometer (Beckman Coulter). The cell temperature was set to 23°C to match the room temperature, with all temperatures confirmed by measuring the internal cell temperature directly by placing a glass thermometer into one solution, using an infrared laser thermometer pointed into the solution, and recording the computer temperature values. Five replicates were conducted on two different days (at ~1

week and ~3 weeks after the initial polymer addition) to ensure the samples solubility did not change significantly over time. The reported values are an average of 5 values.

3.2.3.3 Cloud Point Determination – Qualitative Method

The onset cloud point T_{cp} of each polymer solution was determined by visual inspection as the temperature of the polymer solutions was increased. Each polymer, 50mg/mL conc. was dissolved in a total of 5mL of 100mM PBS. The vials were placed on a shaker for 48 hours and allowed to sit for one week at room temperature. After this period each sample was placed in a water bath where the temperature was increased by 3°C increments starting from 24°C to 70°C. Samples were taken out of the water bath after 3 minute exposure to new set temperatures; this time was sufficient such that the sample temperature read by an infrared thermometer matched the bath display temperature. The temperature at which the sample visually became 'cloudy' was recorded as the T_{cp}. Smaller, 1°C temperature ramps were conducted if required to increase the accuracy of the cloud points measured. The temperatures reported represent an average of three measurements using the laser pointed into the solution vial and into the water bath.

3.2.3.4 Cloud Point Determination – Quantitative Method

The T_{cp} was determined spectrophotometrically by measuring the %transmittance of light (λ=500nm) while increasing the temperature of the solutions. Each polymer was dissolved in 10mM PBS at a conc. of 10%w/v. The vials were placed on a shaker for 48 hours and allowed to sit for one week at room temperature. All samples were then placed in PS cuvettes and agitated for 20 seconds using a vortex operating at 2500rpm before each temperature measurement. The sample cells were subjected to heating from 10°C to 65°C, with 3°C or 5°C increments. After each temperature increase, a 5 minute wait time was employed to ensure the temperature was at equilibrium and the samples had time to come up to that temperature. The sample was quickly vortexed to ensure mixing of any aggregates followed by measurement of the sample transmittance immediately. The temperature was measured by three different means: the computer value given, a laser thermometer aimed into the solution, and by a glass thermometer placed into the solution. The glass thermometer was noted to be the most accurate value such that only those temperatures are reported herein. Duplicate runs were

done for some polymers to confirm the phase change values. The T_{cp} was calculated by finding the average value between the final constant (baseline) %transmittance (corresponding temperature) and the first major drop in %transmittance (corresponding temperature).

3.2.3.5 Characterization by Nuclear Magnetic Resonance Spectroscopy

The chemical composition of each polymer was confirmed using ^{1}H NMR (Bruker 200MHz spectrometer). Lyophilized polymers (10mg/mL) were dissolved in deuterium oxide (0.7mL) with 32 scans per spectra collected. Spectra were analyzed by finding characteristic hydrogen peaks corresponding to the theoretical polymer structure and integrating the areas (comparing areas on 1:1: hydrogen basis) to calculate the mol% of a given reactant relative to another reactant detailed in section 3.3.3.5 (Hoare T. and Pelton R. 2004; Selvam P., Babu K.V. et al. 2005; Zhao C., Zhuang X. et al. 2009)

3.2.3.6 M_n, M_w, & PDI by Gel Permeation Chromatography

Both DMF and THF GPC were explored to determine the molecular weights (M_n, M_w) and PDI of the linear polymers using PEG and PS standards respectively. Samples of pNIPAM (PolymerSource and Sigma-Aldrich) with M_n range (~2kDa-125kDa) were run in each solvent system to obtain more accurate calculations of the M_n and M_w of NIPAM based materials relevant to PS and PEG standards (Agilent Technologies 2000).

3.2.3.7 Statistical Analysis

PCA and PLS methods were applied to analyze x and y and data respectively using ProSensus MultiVariate software (ProSensus Inc. 2010).

3.3 Results & Discussion: Model Evolution & Outcomes

The model building process is based on continuous improvements and an original model is not necessarily the best or final model to characterize the system. Here the original model (the training set used to begin the materials design) and the final model are described, with emphasis on both their creation and their respective results.

3.3.1 The Original Model: Polymer Characterization and Modeling Results

3.3.1.1 The X & Y Data Overview

The first series of polymers synthesized were used as an initial training set to identify general trends in the data. The PLS model was built by combining the reactant amounts (**X**) and operating reaction conditions (**Z**) into one final matrix **X**. A visual representation of the original data matrices is shown below in Table 3—1.

Table 3—1: Data table of x and y variables used to generate initial model

Polymer ID	NIPAM [%moles]	AA [%moles]	VC [%moles]	HEMA [%moles]	AIBMe [moles l/moles M]	TGA [moles CTA/moles M]	AESH [moles CTA/moles M]	EtOH inverse conc. [L/moles M]	DMF inverse conc. [L/moles M]	Rxn Temp [°C]	Cond. [Y/N]	Solubility [%transmittance]	Cloud Point [°C]
S.1W	100.00	0	0	0	0.0136	0	0.0419	0	0.226	70	1	2	
S.5A	86.33	13.67	0	0	0.0039	0.0215	0	0.391	0	50	1	11	30
S.8A	91.70	8.30	0	0	0.0041	0.0228	0	0.415	0	55	0	9	34
S.9A	84.67	15.33	0	0	0.0038	0.0211	0	0.383	0	55	0	12	34
S.12A	86.25	13.75	0	0	0.0047	0.0219	0	0.391	0	55	1	10	32
S.13A	81.54	18.46	0	0	0.0044	0.0207	0	0.369	0	55	1	13	31
S.2K	86.33	0	0	13.67	0.0039	0.0195	0	0.391	0	60	1	4	
S.3K	89.43	0	0	10.57	0.0081	0.0244	0	0.407	0	55	0	6	
S.4K	66.67	0	0	33.33	0.0033	0.0667	0	0.111	0	55	1	7	43
S.5K	72.14	0	0	27.86	0.0056	0.0418	0	0.279	0	50	1	5	41
S.1U	68.81	15.59	15.59	0	0.0042	0.0166	0	0.312	0	65	1	8	29
S.4T	91.70	0	8.30	0	0.0050	0.0249	0	0.415	0	65	1	3	31
S.5T	91.70	0	8.30	0	0.0050	0.0249	0	0	0.415	65	1	1	45
S.5U	57.80	26.61	15.60	0	0.0092	0.1376	0	0	0.688	59	1		
S.6U	72.02	24.93	3.05	0	0.0028	0.0360	0	0.554	0	52	1		
S.6K	72.48	14.18	0	13.34	0.0024	0.0361	0	0.361	0	43	1		
S.7K	84.74	0	0	15.26	0.0089	0	0.0138	0.295	0	48	1		
S.6T	85.53	0	14.47	0	0.0064	0	0.0129	0	0.643	58	1		

3.3.1.2 The X Data

The initial model contained recipes and data for 13 polymers which are denoted as the training data in the model. The last five samples (in bold and italics) were the prediction set (not yet synthesized) to be used to investigate the model's predictability of y variables. Chemistry codes are defined in the 'List of Abbreviations and Symbols' section.

The chemistries assessed include NIPAM homopolymer or NIPAM copolymerized with AA, HEMA, VC or a combination of these. A common variable in all recipes was NIPAM, such that the thermoresponsive properties of the polymer were of particular interest. AA was selected

primarily to incorporate reactive functional groups (carboxylic acids) into the polymer to serve as reactive sites for aminations and subsequent conjugation of a cinnamate moiety. Residual –COO- groups are also ionized at physiological pH, increasing the phase transition temperature of the hydrogel as previously shown (Yin X., Hoffman A.S. et al. 2006). Similarly, HEMA is more hydrophilic than NIPAM and contains a pendant hydroxyl group as a prospective site for conjugation of a cinnamate group. VC is a polymerizable monomer that contains a cinnamate group, facilitating cinnamate incorporation directly in the polymer backbone (versus side group grafting of cinnamate moieties from AA or HEMA chemistries); however, the monomer is water-insoluble and relatively hydrophobic, significantly reducing the phase transition temperature of NIPAM upon copolymerization. Indeed, a maximum incorporation limit was observed where above this limit the product copolymer was insoluble in water and could not be further tested. The highest amount of VC incorporated here was ~10mol% (by titration results detailed in Chapter 4). Two chain transfer agents were also assessed to control the polymer molecular weight and attach a defined functional group at the polymer chain end: AESH (terminal amine) and TGA (terminal carboxylic acid). AIBMe was used to initiate all polymerizations.

Recipe trials varying more than one input (x variable(s)) at a time among 7 possible reactants (4 monomers, 1 initiator, 2 chain transfer agents) and 4 possible process conditions (2 potential solvents, reaction temperature, if a condenser with continuous nitrogen bubbling (=1) or a N_2 filled balloon (=0) was used to purge oxygen from the system) were designed and polymers synthesized according to the recipes shown in Table 3—1. The x variables were appointed as the most influential variables that may affect the polymer properties (y variables).

3.3.1.3 Y1, Solubility – Qualitative

An important y requirement for these polymers is solubility at room temperature; otherwise, the polymers would associate together even prior to injection and an *in situ* gelling hydrogel could not be effectively designed. The polymers were ranked for solubility by visual inspection with the least soluble (~1) to most soluble polymer solutions (~13) shown in Figure 3—2.

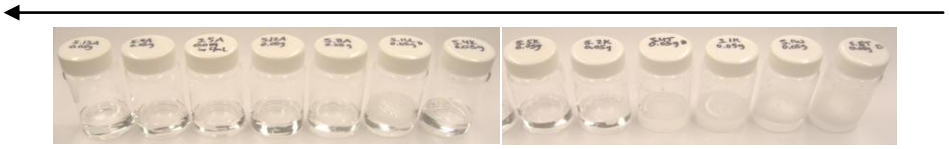

Figure 3—2: Visual ranking for polymer solutions from (right) lowest to (left) highest solubility

The polymers solutions with NIPAM (homopolymer) and those with VC and HEMA incorporated resulted in the lowest solubility and highest ppt formation at room temperature. These trends were likely attributable to a combination of the high salt concentration of the PBS media used which caused a 'salting-out' effect for pNIPAM-HEMA-based chemistries and the high hydrophobicity of polymers with high VC contents in VC-based chemistries, both of which effectively lower the LCST of the polymer (López-León T., Ortega-Vinuesa J.L. et al. 2006). This hypothesis was supported given that lowering the temperature of these samples (refrigeration) allowed for full dissolution of the polymers.

3.3.1.4 Y2, Cloud Point – Qualitative

Most polymer solutions assayed exhibited a cloud point temperature (T_{cp}) due to their thermoresponsive character. It was desired to have products with T_{cp} above room temperature but below physiological temperature (i.e. 23°C < T_{cp} < 37°C), enabling the final graft product to be a free-flowing solution at room temperature but a physically-associated hydrogel at body temperature. Most samples showed a T_{cp} upon heating, including samples that had some ppt at room temperature showed a change and became milky (two T type chemistries, NIPAM-co-VC).

Since polymer solubility at a specific temperature and cloud point are physically related (i.e. cloud point describes the temperature at which a polymer switches from soluble to insoluble), more quantitative measures of y's were sought (final model). It is worth noting that the phase transition of linear poly(NIPAM) is concentration and solution dependent; for example, at low concentrations, poly(NIPAM) in media has higher T_{cp} values in water (~3°C higher) compared to its T_{cp} at lower concentrations in aqueous media (Tong Z., Zeng F. et al. 1999). Furthermore, a critical fraction of NIPAM is required in a copolymer for phase transition behavior to be observed; for example, reports have suggest a minimal amount of NIPAM (from ~60–30mol%) is needed to see a T_{cp} effect in aqueous media for NIPAM-co-HEMA (Arıca M.Y.,

Öktem H.A. et al. 1999; Shen Z., Terao K. et al. 2006). These physical limits were considered when selecting the prediction set.

3.3.1.5 Examination of Initial Model

The initial model had five components with a cumulative R2 ~0.96 and a cumulative Q2~0.65 shown in Table 3—2 and Figure 3—3. The SPE vs. HT2 did not have observations in their 95-99%CI therefore all original observations were kept to build this initial model.

Table 3—2: Initial model R2 and Q2 values for each component

Latent Variable No.	R2	Q2
1	0.6940	0.1940
2	0.0630	0.1667
3	0.1585	0.1647
4	0.0262	0.1069
5	0.0179	0.0150

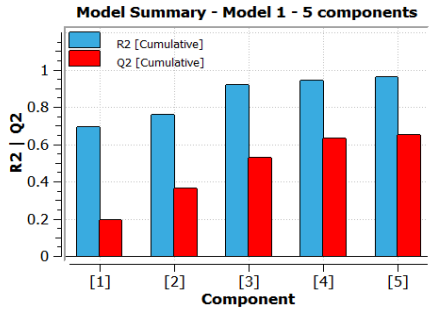

Figure 3—3: Bar plot of initial model components

Figure 3—4 is the loading bi-plot, where observations of similar chemistries are clustered together. From the bi-plot, solubility is correlated to the use of EtOH as the reaction solvent, as they sit together in the top left quadrant of the T2 vs. T1 space. The observations (blue triangles) span the latent variable space with clusters of chemistries clumped together close to their feed monomers. For example, most K (pNIPAM-HEMA) type chemistries are situated in the lower right quadrant and type A (pNIPAM-AA) chemistries in the top left quadrant.

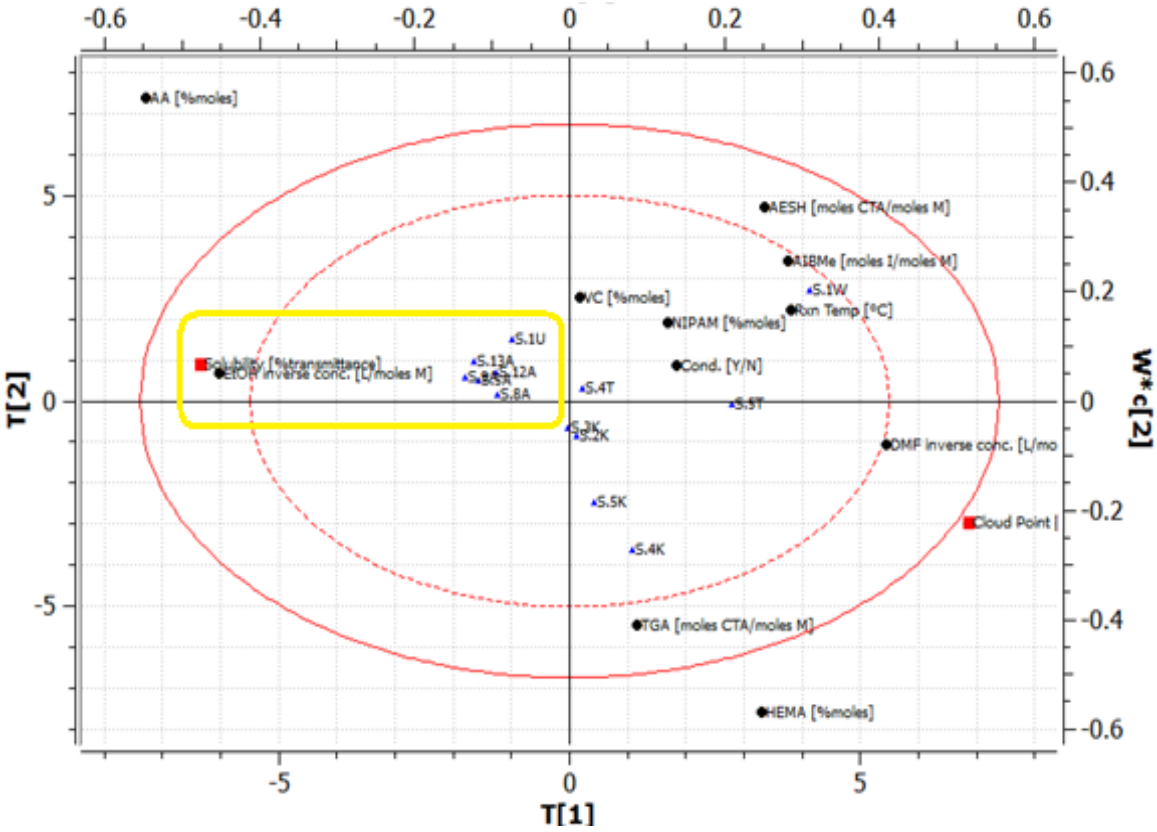

Figure 3—4: Loading bi-plot for the initial model. The solid red line represents the 99%CI and dashed red line the 95%CI for observations (blue triangles). The original x variables are shown as black dots and y variables are red squares in the plot.

From proximal observations, it can be stated that polymerizations using a higher reaction temperature, more DMF as the reaction solvent, and HEMA or VC as functional comonomers will lead to the formation of less soluble polymers. The area highlighted in yellow shows the most successful polymers with high solubility as desired and characterized in the lab.

The most important relationships are that the monomers (AA and HEMA) are oppositely correlated (i.e. AA incorporation results in more soluble products) and that the solvents (EtOH and DMF) are oppositely correlated (i.e. reactions performed in EtOH yield more soluble products. Also the observations show that the product solubility is increased by using certain comonomers in increasing solubility of HEMA<VC<AA with NIPAM. The trend shown is most likely due to the hydrogen bonding between HEMA alcohol to NIPAM carbonyl that create interchain associations, and VC provides lower solubility due to its hydrophobic nature.

3.3.1.6 Exploration of Initial Model

To 'explore' the model space, ProMV offers a tool to view the score plot with past observations in the latent variable space. The option comes about by inverting the model and allowing the user to explore the latent variable space. The user can select a position in the latent variable space where desirable properties are achieved and obtain a recipe (with a squared prediction error SPE=0) on the plane. The resulting (unconstrained) recipes were adjusted for practical purposes (given the limitations described previously) for synthesis in the lab. These adjusted recipes of interest were then entered into the model as a prediction set. The corresponding predicted y variables for these reactions were obtained by using the obs.vs.pred. option in ProMV.

3.3.1.7 Polymer Prediction Set of Initial Model

The prediction set polymers (Table 3—1 in bold and italics) were used as a prediction set (i.e. initially not synthesized but later made and characterized in the lab) and their y variables compared with the model prediction results. The solubility and cloud points from the model versus the lab results are given in Table 3—3 and Table 3—4 respectively. The obs.vs.pred. plots (as time series, Figure 3—5 and Figure 3—6) show the actual y values (solid black line) and the model prediction of those y values (dotted line) for the training data. In the tables, the blank spaces are left blank to state that the cloud points were below room temperature and thus not measurable using the method employed. The new polymer recipes (green line) are the model predictions for the y values only. The model does a good job of predicting both the trends and magnitudes of the y variables, with a match of ~70% (in magnitude) for y1 predicted. In this case, the predicted model values of cloud point are not as accurate; this illustrates the potential weakness of this (or any) model in accurately predicting parameters when limited input information is provided for a specific parameter. By the absence of data, the model assumes the data is missing, not below the measurement range; thus, prediction errors for similar formulations are observed. However, for parameters or compositions with adequate model inputs, the results suggest that model inversion is an excellent tool that can be used to predict certain polymer properties of new compositions of polymers based on existing data of polymers prepared using similar chemistries and/or similar methodologies.

Table 3—3: Solubility of training data set (in black) and prediction set (in green)

Solubility of Polymer in PBS [ranked 1-13]		
Sample ID	Predicted by Model	Observed in Laboratory
S.5A	10	11
S.8A	9	9
S.9A	10	12
S.12A	9	10
S.13A	10	13
S.1W	0	2
S.4T	7	3
S.5T	2	1
S.1U	9	8
S.2K	7	4
S.3K	7	6
S.4K	5	7
S.5K	6	5
S.5U	**3**	**10**
S.6K	**12**	**12**
S.6U	**10**	**6**
S.7K	**6**	**5**
S.6T	**1**	**1**

Table 3—4: Cloud point of training data set (in black) and prediction set (in green)

Cloud Point Temp [°C]		
Sample ID	Predicted by Model	Observed in Laboratory
S.5A	30	30
S.8A	31	34
S.9A	30	34
S.12A	31	32
S.13A	30	31
S.1W	47	
S.4T	36	31
S.5T	43	45
S.1U	32	29
S.2K	35	
S.3K	35	
S.4K	38	43
S.5K	36	41
S.5U	41	47
S.6K	26	38
S.6U	30	
S.7K	36	
S.6T	45	

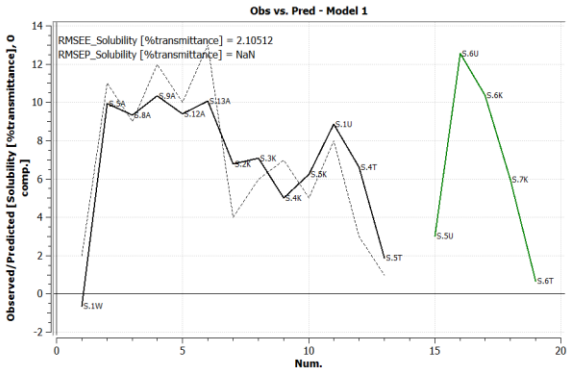

Figure 3—5: Obs.vs.pred. time series plot showing solubility of training data set (in black) and prediction set (in green). Dotted lines are the model prediction and solid lines are lab measurement values

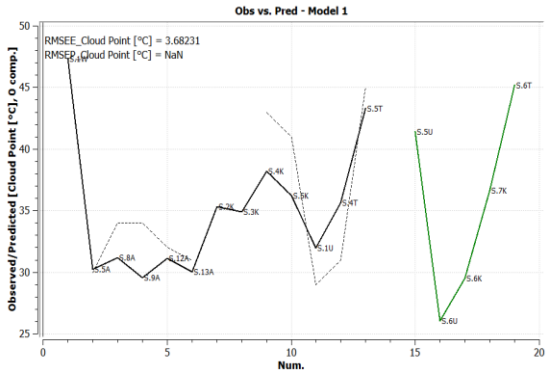

Figure 3—6: Obs.vs.pred. time series plot showing solubility of training data set(in black) and prediction set (in green). Dotted lines are the model prediction and solid lines are lab measurement values

3.3.2 Solvent Screening

Given both qualitative observations and model predictions, a clear difference in polymer properties was observed depending on the type of solvent used for the polymerization reaction. It was therefore of interest to investigate which type of solvent would lead to the desired solubility and cloud points for these recipes. Since the x variables are correlated and not independent, a design of experiments (orthogonal factorial design) approach could not be used with our system (Wold S., Sjöström M. et al. 1986). The most suitable alternative for our system was to perform experiments of a 'mixing design' with three variables (three types of solvents) as depicted in Figure 3—7 (a). Poly(VC-co-AA-co-NIPAM) polymers were made in either pure solvents EtOH or THF or DMF (corresponding to triangle vertices) or in a combination of 2 solvents (along the triangle edges). With all other inputs constant (amounts of monomers, temperature, purification methods) the triangle results for solubility and cloud point are shown in (b) and (c) respectively. Note that all monomers, chain transfer agent, and initiator were freely soluble in each solvent.

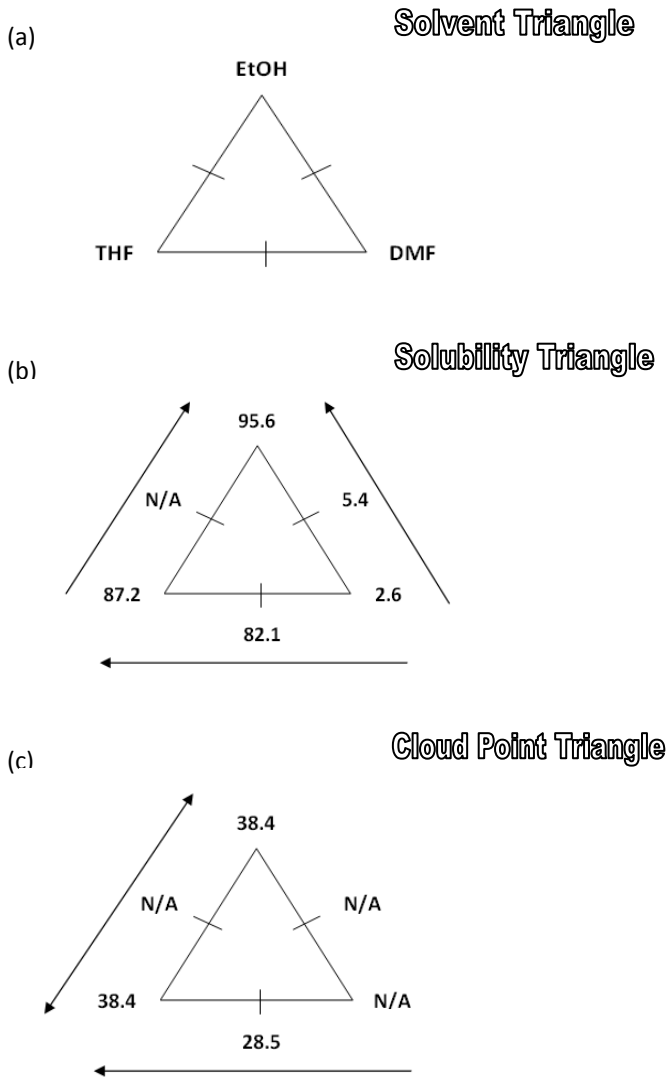

Figure 3—7: Mixing design solvent triangles with (a) solvent types, (b) solubility results, (c) cloud point results for the corresponding solvents. The notation N/A denotes data that could not be collected due to (in figure b) the sample was not available to test or (in figure c) the cloud point could not be determined since the polymers were insoluble in aqueous media.

The results indicate a trend in decreasing solubility in the order EtOH > THF > DMF. These differences are most likely attributable to hydrogen bonding interactions between the solvents and one or more of the constituent monomers, altering the copolymerization kinetics and thus the solubility of the resulting polymer, although further study would be required to comment specifically on the mechanism (Bokias G. and Hourdet D. 2001; Hansen C.M. 2004; Yu T.L., Lu W-C. et al. 2004; Shen Z., Terao K. et al. 2006; Murugan N.A., Hugosson H.W. et al. 2008).

3.3.3 The Final PLS Model: Polymer Characterization and Modeling Results

3.3.3.1 The X & Y Data Overview

In order to improve the model, more y's were sought out and the qualitative y's were measured explicitly by quantitative strategies. This moves away from ranking-based approaches which (although useful for first implementing the model) may lead to non-relevant correlations in data if the ranking intervals are not consistent.

3.3.3.2 The X Data

The same x variables from the initial model along with the addition of three new x variables were used to build the final model: reaction time (hrs), dialysis membrane molecular weight cut-off (MWCO), and whether the polymer was dialyzed against basic conditions (yes=1, no=0). Basic dialysis was conducted to ensure ionization of any acrylic acid groups, maximizing the solubility of the polymer being dialyzed. These three variables were included in that they can each potentially influence the polymer chain chemistry and molecular weights of the final, purified polymer that is analyzed.

3.3.3.3 Y1, Solubility – Quantitative

The polymers were dissolved in a lower salt concentration physiological buffer 10mM PBS and the solubility was quantified by the amount of light transmitted through the sample (%transmittance). For this test, most of the polymers were visually soluble and clear, with the % transmittance on average >80%. Only poly(NIPAM-co-VC) polymers showed lower transparency values at the constant temperature tested (23°C), reasonable given that the copolymers only have hydrophobic (VC) groups attached to NIPAM.

3.3.3.4 Y2, Cloud Point – Quantitative

The new onset cloud points were determined by measuring the %transmittance while changing the temperature and calculating the onset values. As mentioned previously, the phase transition is a concentration-dependent phenomenon and the quantitative method for the final model (conc. 10mg/mL) is different from the qualitative method of the initial model (conc. 10mg/mL) so different T_{cp}'s are expected. Figure 3—8 shows visually how the samples changed

below (a) and above (b) the LCST. Aggregates formed (NIPAM) in some samples that floated or sunk to the bottom, therefore each sample was vortex mixed immediately before measuring to obtain the most accurate representation of the light passing through the media.

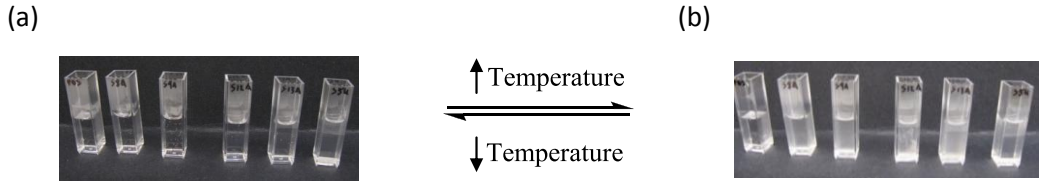

Figure 3—8: Photographs of cloud point testing (a) below LCST and (b) above LCST. From left to right in each image, sample: PBS, pNIPAM-co-AA variations (4 middle samples), and pNIPAM-VC-AA.

A typical cloud point determination plot for these samples is shown in Figure 3—9 (a) to (c), where the glass thermometer readings (taken inside the cells) were used to calculate the T_{cp} reported. As the polymers were heated above their LCST, they transitioned from clear to opaque, confirming their thermoresponsive nature.

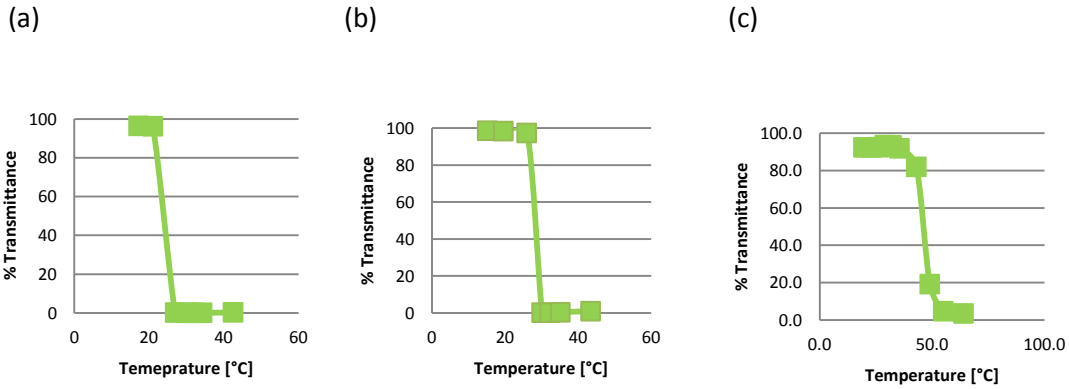

Figure 3—9: Typical cloud point temperatures from lowest to highest values measured for polymer (a) S.8T poly(NIPAM-co-VC), (b) S.1W poly(NIPAM), and (c) S.1Ur2 poly(NIPAM-VC-AA).

3.3.3.5 Y3, NMR Actual Ratio of Copolymerization

^{1}H NMR spectra were analyzed for most polymers made to confirm the chemistry and calculate the actual amount of monomer copolymerized with NIPAM. Figure 3—10 shows a representative spectrum for S.13A pNIPAM-co-AA used to calculate the mol% AA (mol AA per mol NIPAM) in the polymer.

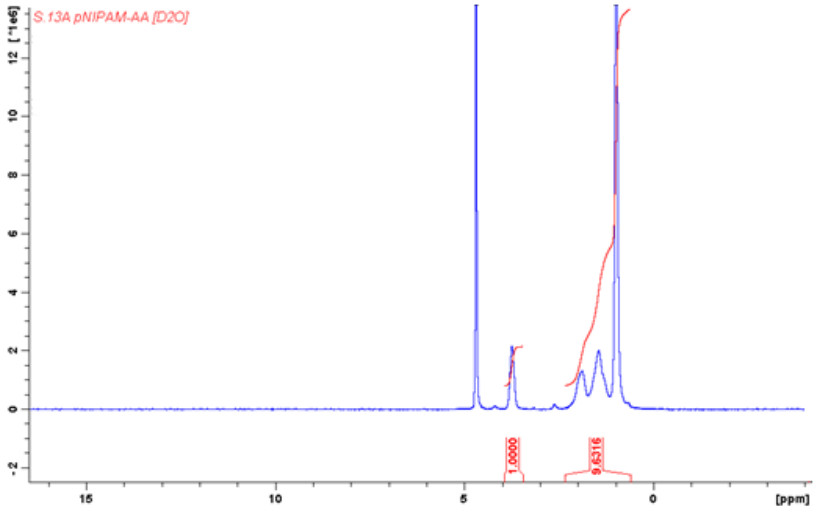

Figure 3—10: ^{1}H NMR of S.13A pNIPAM-co-AA in D_2O

Chemical shift (δ) values representing relevant chemistries in this polymer include:

0.5ppm-1.2ppm from the methyl groups -(CH_3)$_2$ from NIPAM

1.2ppm-1.8ppm from the methylene groups -(CH2) from NIPAM and AA

1.8ppm-2.5ppm from the methinyl groups -(CH) from NIPAM and AA

Each mole of NIPAM contributes a total of 9H to this region and AA contributes 3H. This region is integrated and 9H (due to NIPAM) subtracted from this integral; the result is divided by 3 (3 H/mole AA), the value was then compared to the area of NIPAM's characteristic methinyl proton (δ~3.8ppm) to obtain the ratio of AA:NIPAM in the copolymer (Hoare T. and Pelton R. 2004). A similar approach but using characteristic peaks for HEMA (δ~3.9ppm representing one methylene group) and VC (δ~6-8ppm representing five aromatic hydrogens and two methinyl hydrogens of the cinnamate chain) to obtain the mol% of each comonomer per NIPAM.

3.3.3.6 Y4, Number Average Molecular Weight M_n

The number average molecular weights of selected samples were collected using gel permeation chromatography using DMF and THF as the eluting solvents. Literature GPC analysis of pNIPAM-based polymers have generally been problematic, with observed elution times often leading to much higher or lower molecular weight values than anticipated (Lambeth R.H., Ramakrishnan S. et al. 2006). In an attempt to improve measurements, some polymer solutions were heated at specific temperatures for specific times while LiBr was added to other samples

to minimize potential column interactions (PolymerSource ; Zeng F., Tong Z. et al. 1999; Ganachaud F., Monteiro M.J. et al. 2000; Masci G., Giacomelli L. et al. 2004; McHale R., Aldabbagh F. et al. 2007; Yusa S-i., Yamago S. et al. 2007; He X., Wu X. et al. 2011). None of these trials significantly changed the elution time or peak shape and therfore were not continued (details not reported). The most suitable solvent found to effectively dissolve a wide range of polymer chemistries was THF, using PS standards as a reference polymer to calculate M_n, M_w, and PDI values. To obtain the most accurate values possible, standard pNIPAM samples were run (designated 'pNIPAM STD') with known M_n values from commercial suppliers. A plot of pNIPAM STD molecular weight calculated using PS as a reference compared to the supplier's reported M_n value (M_n measured vs. M_n actual, shown in Appendix A3) was subsequently used as a more accurate reference to calculate all polymer molecular weights as follows (Izunobi J.U. and Higginbotham C.L. 2011):

$$M_n = \frac{\sum N_i M_i}{\sum N_i} \qquad \text{Equation 3.5}$$

$$M_w = \frac{\sum N_i M_i^2}{\sum N_i} \qquad \text{Equation 3.6}$$

The previous (PS) and adjusted (pNIPAM STD) molecular weights are shown in Table 3—5.

Table 3—5: GPC calculated molecular weights with PS standards and pNIPAM standards (in bold)

Sample ID	Contents	Retention Time [min]	M_n [Da]	M_w [Da]	PDI [M_w/M_n]	**M_n new**
1W	pNIPAM	18.33	9,264	29,269	3.16	**11,202**
1A	pNIPAM-AA	21.58	4,583	10,766	2.35	**5,248**
6K	pNIPAM-HEMA-AA	25.73	1,240	1,825	1.47	**1,802**
7K	pNIPAM-HEMA	18.15	17,419	39,259	2.25	**24,716**
6T	pNIPAM-VC	20.78	9,793	16,386	1.67	**11,958**
9T	pNIPAM-VC	25.60	1,650	2,959	1.79	**2,189**
1U	pNIPAM-VC-AA	26.83	1,151	2,737	2.38	**1,719**
2K STD	pNIPAM	26.80	3,130	14,416	4.61	**3,668**
10.3K STD	pNIPAM	21.40	6,947	8,855	1.27	**8,092**
32K STD	pNIPAM	18.23	21,616	40,795	1.89	**33,225**
125K	pNIPAM	17.00	52,430	96,057	1.83	**128,066**

Note that samples S.6T and S.9T represented the same chemistry prepared in different solvents (DMF and EtOH respectively). An overlay chromatograph of three chemistries is shown

in Figure 3—11. The largest M_n sample shown here is rated at 30kDa pNIPAM STD (blue crosses) and the other samples tested are eluding at later times that correspond to a smaller M_n values calculated. All sample polymers measured were in the target range (~2kDa to 30kDa), chosen such that the polymers would be small enough to be excreted by the kidneys (Rockel A., Hertel J. et al. 1986) but still sufficiently large to undergo a phase transition.

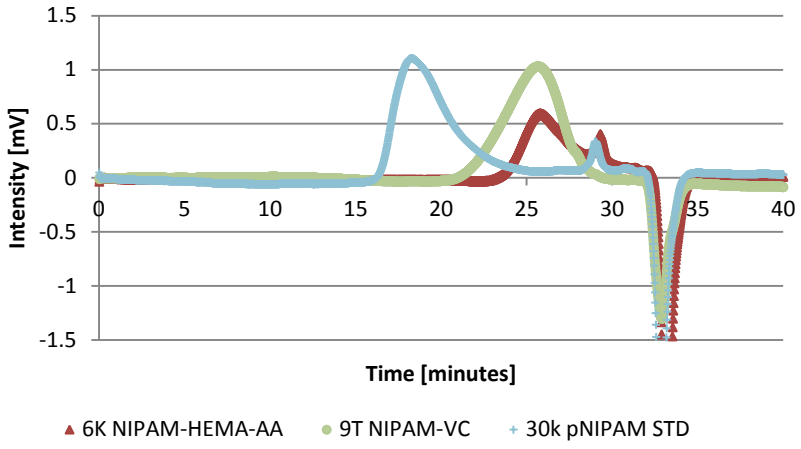

Figure 3—11: GPC chromatogram showing three representative NIPAM polymers

3.3.3.7 Results of Final Model

The tabulated results for PCA and PLS modeling are shown in Table 3—6. The PCA on X data and PCA on Y data results are presented in Appendix A1. The final model is detailed here.

Table 3—6: Compiled x and y data for final PLS model

Polymer ID	NIPAM [%moles]	AA [%moles]	VC [%moles]	HEMA [%moles]	AIBMe [moles I/moles M]	TGA [moles CTA/moles M]	AESH [moles CTA/moles M]	EtOH inverse conc. [L/moles M]	DMF inverse conc. [L/moles M]	THF inverse conc. [L/moles M]	Reaction temperature [°C]	Condenser [Y/N]	Reaction time [hours]	Dialysis MWCO [Da]	Dialyze against basic envmt	Solubility [%transmittance]	Cloud Point [°C]	NMR actual ratio AA/NIPAM [mole%]	NMR actual ratio VC/NIPAM [mole%]	NMR actual ratio HEMA/NIPAM [mole%]
S.1W	100.00	0	0	0	0.0136	0	0.0419	0	0.226	0	70	1	24	14,000	0	94.0	28.1	0	0	0
S.2W	100.00	0	0	0	0.0065	0	0.0291	0	0.323	0	65	1	24	3,500	0	94.2	28.1	0	0	0
S.1A	86.33	13.67	0	0	0.0039	0.0215	0	0.391	0	0	50	1	24	14,000	0				0	0
S.5A	86.33	13.67	0	0	0.0039	0.0215	0	0.391	0	0	50	1	24	14,000	0	92.6	45.0	8.74	0	0
S.8A	91.70	8.30	0	0	0.0041	0.0228	0	0.415	0	0	55	0	24	14,000	0	97.9	52.5	8.55	0	0
S.9A	84.67	15.33	0	0	0.0038	0.0211	0	0.383	0	0	55	0	24	14,000	0			13.95	0	0
S.12A	86.25	13.75	0	0	0.0047	0.0219	0	0.391	0	0	55	1	24	14,000	0	97.2	60.5		0	0
S.13A	81.54	18.46	0	0	0.0044	0.0207	0	0.369	0	0	55	1	24	14,000	0	93.5	40.0	21.05	0	0
S.2K	86.33	0	0	13.67	0.0039	0.0195	0	0.391	0	0	60	1	24	14,000	0	94.8	28.1	0	0	14.02
S.3K	89.43	0	0	10.57	0.0081	0.0244	0	0.407	0	0	55	0	24	14,000	0			0	0	24.19
S.4K	66.67	0	0	33.33	0.0033	0.0667	0	0.111	0	0	55	1	24	14,000	0	93.6	25.8	0	0	41.02
S.5K	72.14	0	0	27.86	0.0056	0.0418	0	0.279	0	0	50	1	24	14,000	0	96.6	28.1	0	0	
S.6K	72.48	14.18	0	13.34	0.0024	0.0361	0	0.361	0	0	43	1	24	14,000	0	92.8	52.5	28.52	0	32.12
S.7K	84.74	0	0	15.26	0.0089	0	0.0138	0.295	0	0	48	1	24	14,000	0	95.2	27.2	0	0	10.76
S.4T	91.70	0	8.30	0	0.0050	0.0249	0	0.415	0	0	65	1	24	14,000	0			0	7.53	0
S.5T	91.70	0	8.30	0	0.0050	0.0249	0	0	0.415	0	65	1	24	14,000	0			0	2.34	0
S.6T	85.53	0	14.47	0	0.0064	0	0.0129	0	0.643	0	58	1	24	14,000	0	49.6	23.0	0	3.14	0
S.7T	92.66	0	7.34	0	0.0105	0.0210	0	0	0	0.629	50	1	6	14,000	0	69.3	24.8	0	3.29	0
S.8T	92.66	0	7.34	0	0.0105	0.0210	0	0	0.629	0	50	1	6	3,500	0	46.4	23.0	0	5.27	0
S.9T	92.66	0	7.34	0	0.0105	0.0210	0	0.629	0	0	50	1	6	3,500	0	86.8	27.3	0	3.46	0
S.5U	57.80	26.61	15.60	0	0.0092	0.1376	0	0	0.688	0	59	1	24	14,000	0	90.5			7.00	0
S.6U	72.02	24.93	3.05	0	0.0028	0.0360	0	0.554	0	0	52	1	24	14,000	0	90.3			1.39	0
S.1U	68.81	15.59	15.59	0	0.0042	0.0166	0	0.312	0	0	65	1	24	14,000	1	93.1		23.35	10.77	0
S.1Ur1	68.81	15.59	15.59	0	0.0042	0.0166	0	0.312	0	0	55	1	12	3,500	0	95.6	38.4		3.27	0
S.1Ur2	68.94	15.53	15.53	0	0.0037	0.0155	0	0.311	0	0	55	1	12	3,500	0	96.3	44.1			0
S.1Ur3	68.81	15.59	15.59	0	0.0042	0.0166	0	0	0	0.312	50	1	6	3,500	0	87.2	38.4			0
S.1Ur4	68.81	15.59	15.59	0	0.0042	0.0166	0	0	0.312	0	50	1	6	3,500	0	2.6			4.23	0
S.1Ur5	68.81	15.59	15.59	0	0.0042	0.0166	0	0.146	0	0.146	50	1	6	3,500	0					0
S.1Ur6	68.81	15.59	15.59	0	0.0042	0.0166	0	0.146	0.146	0	50	1	6	3,500	0	5.4			3.50	0
S.1Ur7	68.81	15.59	15.59	0	0.0042	0.0166	0	0	0.146	0.146	50	1	6	3,500	0	82.1	28.5		4.08	0
S.1Ur11	68.81	15.59	15.59	0	0.0042	0	0.0125	0	0.312	0	60	1	12	3,500	0	89.1	37.0			0
S.1Ur12	68.85	15.58	15.58	0	0.0037	0.0168	0	0.312	0	0	55	1	12	3,500	0	0.9				0

3.3.3.8 PLS Final Model

The final model was initially made using all the data collected in Table 3—6. Using all the data did not result in a good model. One of the reasons was the large amount of missing data. While PLS is tolerant of missing data to some extent, for GPC data, there were too many observations (>30 polymers) and not enough sample results (GPC > 50% missing data); as a result, GPC data were eliminated from this version of the model. Dependent variables in both the x and y domains were also omitted; for example, the y variable 'theoretical ratio' was omitted because it directly represented other x variables (feed amount of monomers x_1-x_4).

With a few other trials to express concentration in different units, the final model was constructed.

The model was built using 14 x variables, 5 y variables, and using the autofit option in the software, 3 latent variables were generated with R2 ~0.5719 and Q2 ~0.3811. The training data set includes all the observations for the 30 polymer recipes synthesized in the lab excluding S.1U pNIPAM-VC-AA. The decision to exclude this observation was due to the fact that the model indicated this polymer to be an extreme outlier in the 95-99%CI for both SPE and HT2 plot (not shown); physically, this polymer was exposed to an extra 'dialyze against basic environment' purification step unique to all the other polymers tested. This suggests that long-term basic dialysis may modify the composition of the polymer and/or the dialysis membrane, changing what fractions of polymer are retained inside the dialysis bag or the chemistry of the polymer itself. The SPE vs.HT2 plot for the final model is shown in Figure 3—12, indicating no extreme outliers and thus its suitability for the rest of the data.

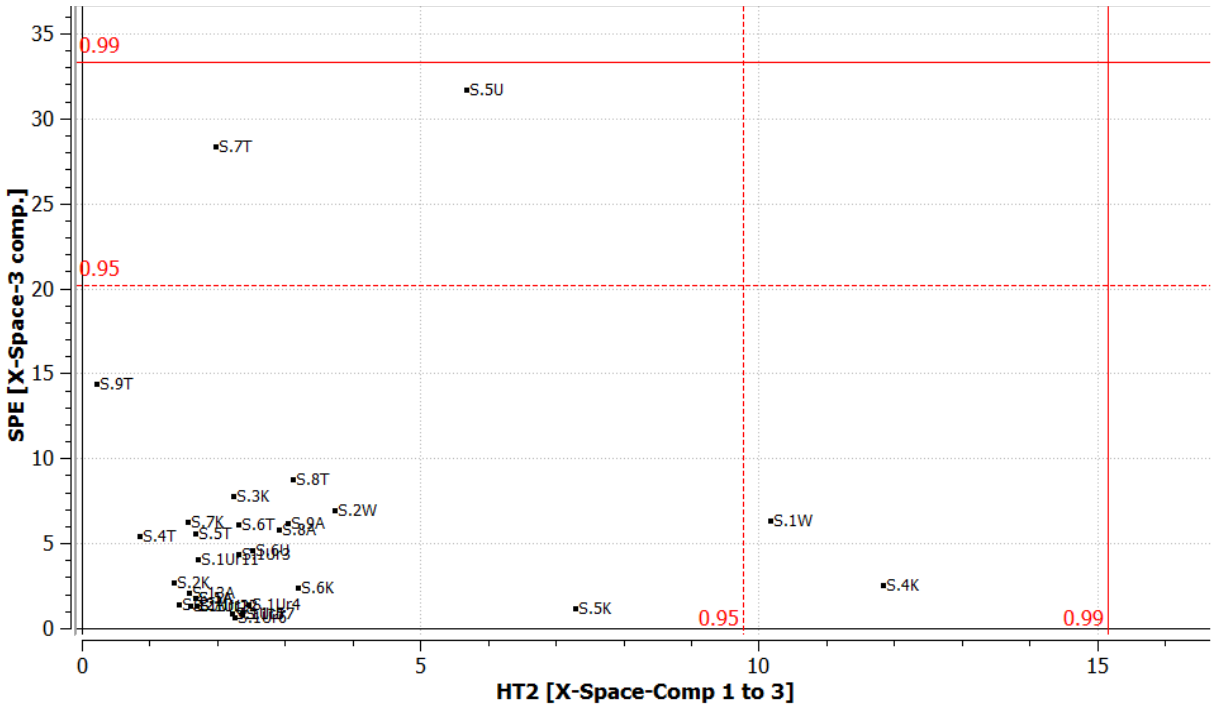

Figure 3—12: SPEvs.HT2 for final model, showing observations are in acceptable range

Figure 3—13 is the loading bi-plot of T2vs.T1. Surprisingly, solubility and HEMA/NIPAM (actual NMR) are close together in this space, though they are not as closely related in T3 space (not shown). This means that increasing the amount of HEMA in the polymer resulted in increased solubility. This is opposite to the correlation observed in the initial model, where the copolymerization of NIPAM and HEMA led to some of the most insoluble polymers. This difference is likely due to the lower salt concentration of PBS used here, which does not "salt out" the HEMA-containing polymers at the test temperature.

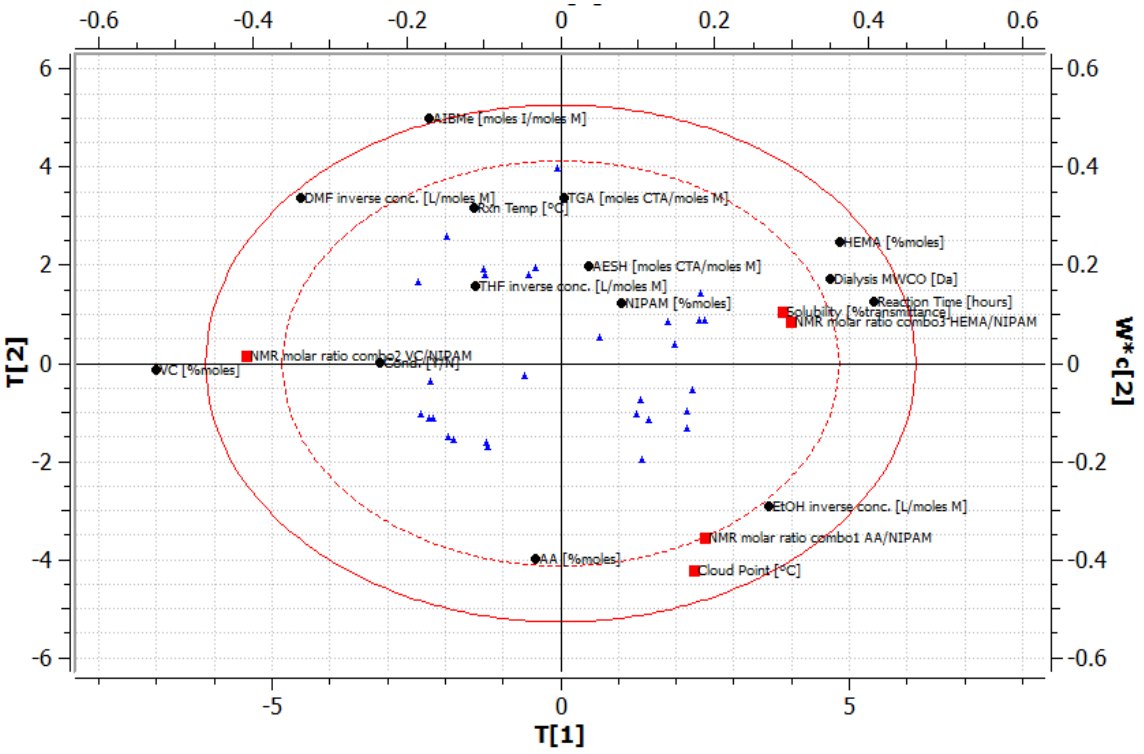

Figure 3—13: T2vs.T1 loading bi-plot for the final model

The final model suggests that the use of DMF as the polymerization solvent is the most negatively correlated variable to both cloud point and solubility than any other solvent used. This echoes the result of a mixing design experiments described in section 3.3.2, where cloud points and solubilities were measured for pure and 50:50 mixtures of DMF, THF, and EtOH.

To determine the 'best' CTA to use for these chemistries, we can look at their locations in T1 and T2 space. Since AESH lies closer to solubility and both chain transfer agents lie far from the cloud point, it could be seen as a better option for these chemistries. The amine terminal

functional group is also easier to graft to the carboxylic acid-functionalized carbohydrates to be used as graft platforms in the dual thermo/photoresponsive polymer design. Also of note is that both CTAs move opposite to the cloud point, suggesting that the use of more CTAs tends to decrease the cloud point; this is consistent with the cloud point being more influenced by the (somewhat hydrophobic) chemistry of the CTA as the average polymer chain length becomes shorter.

In the first component, the monomers AA and HEMA are negatively correlated with DMF, suggesting that hydrogen bonding interactions occur with both these comonomers that influence polymerization and/or polymer solubility. This result suggests that EtOH is the best polymerization solvent to use to maximize polymer solubility while balancing the T_{cp}.

The amounts of initiator and VC are oppositely correlated with solubility and T_{cp}. This correlation is likely due to the increase in polymer hydrophobicity at higher VC concentrations and the formation of shorter chains with higher AIBMe concentrations, increasing the overall influence of both the initiator and chain transfer agent end groups on the resulting polymers on the overall polymer properties and thus reducing polymer solubility in water.

The coefficients plot indicates the level and direction of each x variable per y variable for the three components. In viewing Figure 3—14, the coefficients plots for solubility (a) and cloud point (b) the following observations can be made:

- Solubility is most positively influenced by using larger reaction times and larger dialysis MWCO while negatively influenced by incorporating more VC groups. The first two factors suggest that higher molecular weight polymers are more soluble than lower molecular weight polymers, consistent with the initiator correlation identified in the bi-plot discussion.
- The T_{cp} is higher when the AA content is higher and EtOH is used as the reaction solvent, while increasing initiator or HEMA concentrations have the opposite effect. Intrachain hydrogen bonding between HEMA and NIPAM could reduce T_{cp}, while the hydrophobic end group from the initiator also decreases the cloud point in cases where more initiator is present, the polymer chains are shorter, and the initiator chemistry has a larger role in determining the overall properties of the polymer.

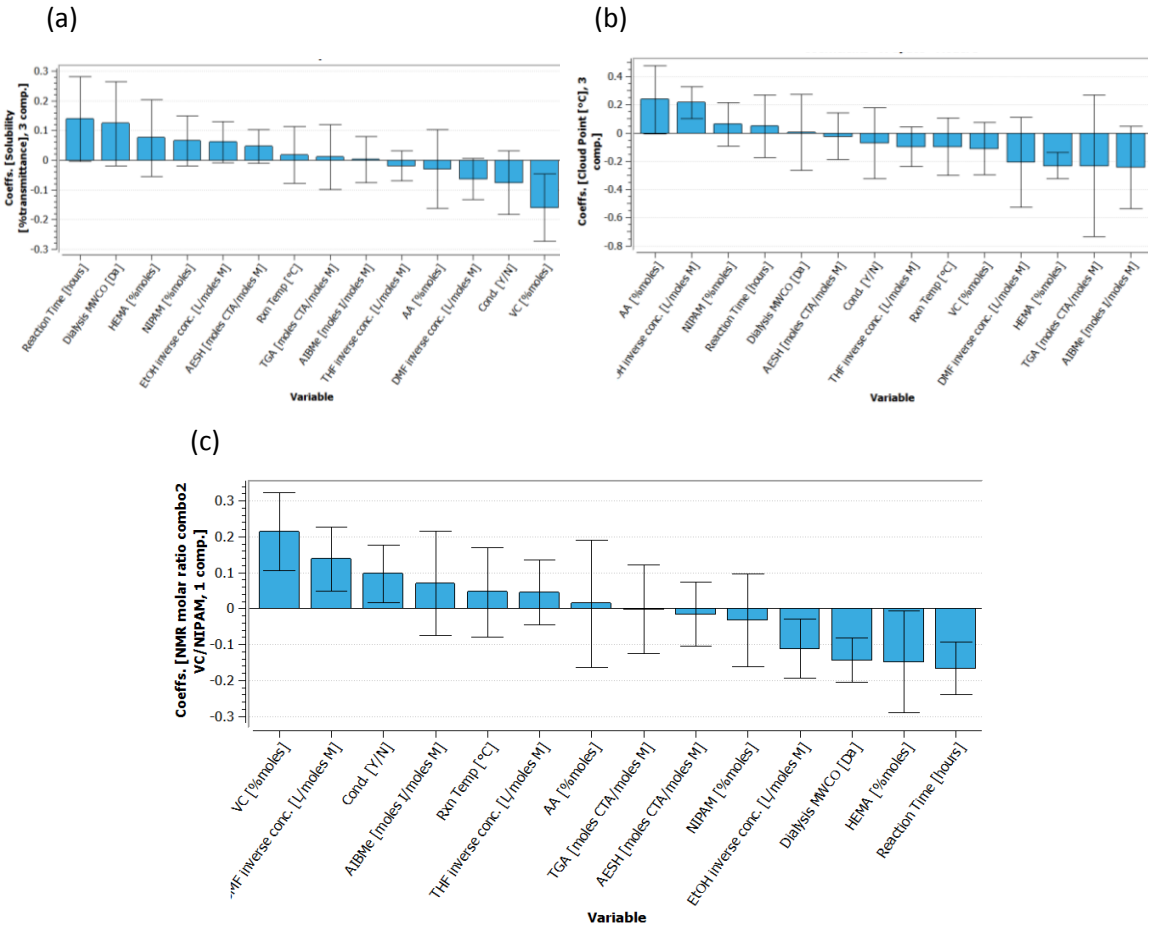

Figure 3—14: The coefficients plot for (a) solubility for T1, (b) cloud point for T1, and (c) actual NMR molar ratio VC/NIPAM for T1

The coefficients plot for VC (actual NMR molar ratio) in Figure 3—14 (c) suggests the reaction time has an inverse effect on the amount of VC actually incorporated into the recovered polymer fraction; the physical meaning behind this observation is unclear. More interestingly, purifying methods are also significant in that using higher MWCO causes a decrease in the amount of VC in the recovered polymer sample. This suggests that low molecular weight fractions (lost during the dialysis with a higher MWCO) are richer in VC, an observation consistent with the incorporation of slower reacting monomers (such as VC) with lower propagation rate constants into polymers.

With the help of PLS modeling, polymers that exhibited "desirable" properties in terms of solubility and phase transition temperature were made and used to graft to a carbohydrate

(Chapter 4). Three types of linear polymers labeled S.6T pNIPAM-VC(AESH terminated), S.9T pNIPAM-VC(TGA terminated), and S.1U pNIPAM-VC-AA(TGA terminated) were selected to be grafted. The PLS data organization, qualitative measurements of properties, and the loading bi-plot of the final model helped identify the most correlated variables in the initial polymerizations and the variables that lie closer to increased product solubility while maintaining cloud point in our range of desired values.

3.4 CONCLUSIONS & RECOMMENDATIONS

3.4.1 Conclusions

In summary, PLS was successfully applied to design smart thermoresponsive polymers with desired properties. Specifically, we have shown that:

- Building a model using indictor rankings (y variables in the initial model) results in an acceptable model with good prediction of solubility for future polymers, as long as the polymers in the training set have clearly different solubilities
- Quantitative measurements were used to obtain comonomer incorporation (NMR), chain length (GPC), cloud point (UV-vis spectroscopy) that verify the successful synthesis of these combination chemistries that show thermoresponsive properties
- To achieve a highly soluble polymer, it was found that the presence of HEMA is more beneficial to improve solubility over all other monomers used
- The amount of AA has a strongest positive correlation with the T_{cp} compared to all other monomers used
- The most influential operating conditions on final properties of polymer with NIPAM copolymerized with VC are the reaction time and dialysis membranes MWCO used
- Hydrophobic terminal end initiator can decrease the cloud point of the final polymer product, if used in large quantities, forming shorter chains
- Both CTAs are more positively correlated with polymer product solubility and negatively correlated with cloud point. The use of AESH (amine-terminal group) as a chain transfer agent is preferred to the use of TGA because it has a closer relation to solubility.

- From the PLS modeling results, three linear polymers were selected to be grafted onto carbohydrates (Chapter 4) and they had desired functional CTAs as well as high solubility and an acceptable range of cloud point values

3.4.2 Recommendations

The following represent additional possible implementations of the PLS model to learn more about how to design smart thermoresponsive polymers with desired applications:

- Make separate models for each chemistry, if a sufficient number of observations are at hand, to learn the underlying correlations and explore the model for predictions of y variables
- Prune the model to remove variables with minimal influence (from PCA examination)
- Make a model with all x variables for each y variable of interest; for example if there are 5 y variables, there would be 5 separate models made. This approach may give insight into influential parameters on each y that may not be evident in this overall model.
- Incorporate wisely chosen interaction terms into the model (predefined and preset). The interaction terms are an option in the software, where the user can identify pairs of suspected x variables that individually are different compared to when they are used together and affect the output properties differently. This option was explored for the final model but may be better suited for individual y model designs.
- Use constrained model inversion (Matlab coding) to determine optimal recipes to achieve specific y values. The current approach identifies desirable and less desirable compositions, but does not necessarily define an optimized composition.
- Take a point in the latent variable space and make, (and characterize) one polymer at a time, updating the model in an incremental fashion to move through the space following a response surface methodology. This should help define the system which may be similar to a standard Rosenbrock's function, where there exists areas that are feasible regions, constraint boundaries, and infeasible regions (The MathWorks Inc. 2000).

Chapter 4 : Rapidly Gelling Thermo-Photo Polymers

4.1 INTRODUCTION: POLYMERIC SYSTEMS

4.1.1 Overview of Design

A variety of thermally-gelling polymer systems have been reported, as discussed in the introduction to this thesis. Thermoresponsive materials are beneficial as they are rapidly responsive and do not require any chemical or physical intervention to deswell in the physiological environment; on the other hand, the physical nature of the interaction makes such materials usually prone to dissolution over time in the infinitely diluting conditions of the body and the network crosslink density is harder to control compared with chemical approaches. To address these challenges, the designed polymers include a secondary crosslinking mechanism using cinnamates which can reversibly crosslink and de-crosslink by the application of specific wavelengths of light, generating a structure analogous to that shown in Figure 4—1.

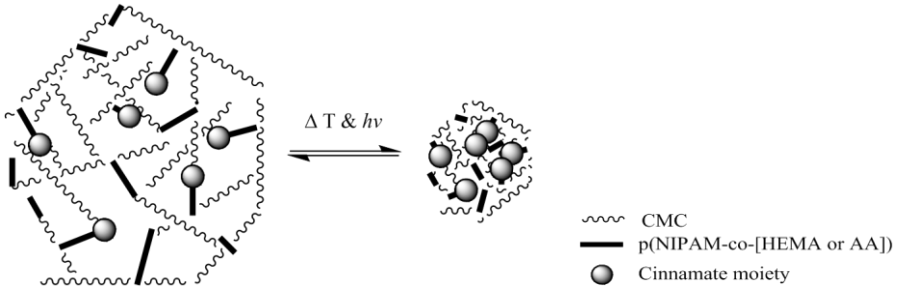

Figure 4—1: Hypothesized drug release systems with thermo and photoresponsive nature

The combination is useful as the pNIPAM physical crosslinks can rapidly gel a solution-like precursor and immobilize it in the body while the cinnamate chemical crosslinks can be used to stabilize the network, add/subtract mechanical strength to the network, and increase/decrease the diffusion coefficient of a drug through the polymer network. This design is convenient to the physician and patient alike and the chemistry can be altered to change the theoretical drug loading or drug release as required.

Poly(vinyl cinnamate) (pVC) is a photoresponsive polymer that has been studied for its potential applications in photoresists, nonlinear optics, and liquid crystals displays (LCDs) (Lee J-W., Kim H-T. et al. 2001; Yoo J-H., Cho I. et al. 2004). VC copolymers were explored here as part of a potential biomaterial when copolymerized with NIPAM. The pNIPAM-VC polymers (Chapter

3) will then be further grafted to a carbohydrate (hyaluronic acid (HA) or carboxymethyl cellulose (CMC)) to form a hydrogel material as a potential drug delivery system. These carbohydrates were chosen to help stabilize the polymers (with their high hydrophilicity), improve the mechanical strength of the hydrogel, potentially reduce the biological response to the material by mimicking natural extracellular matrix materials, and provide defined degradation mechanisms (by hydrolysis or enzyme degradation). While HA has been grafted with NIPAM in other studies, non photo-responsive compounds or comonomers such as N-acryloyloxysuccinamide (NAS) or gelatin have been added, primarily to facilitate fast gelling capability (Ohya S., Nakayama Y. et al. 2001; Fitzpatrick S.D., Mazumder M.A.J. et al. 2011). Others use similar compounds to make very different products such as HA-bioten-collagen as scaffolds (Segura T., Anderson B.C. et al. 2005), gelatin-NIPAM ECM scaffolds (Ohya S., Nakayama Y. et al. 2001; Ohya S. and Matsuda T. 2005), and NIPAM-g-HA-gelatin gels (Chen J-P., Leu Y-L. et al. 2011). However, dual thermo/photo-responsive hydrogel based on pNIPAM chemistry system has yet to be reported.

4.1.2 Polymer Materials in Designs

4.1.2.1 Classes of Designs

There were two main routes of chemistries that were investigated for the conjugation of photosensitive moieties onto NIPAM based chains:

1. Copolymerizing NIPAM with a functional monomer such as AA or HEMA (as discussed in Chapter 3), and grafting a cinnamate moiety: trans-4-nitrocinnamic acid (NC), cinnamic acid (CA), trans-4-nitrocinnamoyl chloride (NCCl), or cinnamoyl chloride (CCl)
2. Copolymerizing NIPAM with VC directly (as discussed in Chapter 3)

These thermo and photo-responsive materials were subsequently grafted to a carbohydrate (HA or CMC) to provide a highly water-binding backbone that can effectively build viscosity and create strong hydrogels even at low to moderate degrees of crosslinking.

4.1.2.2 Hyaluronic Acid

Hyaluronic acid (HA) is a biopolymer, a glycosaminoglycan that is naturally found in the body which helps to lubricate/ cushion joints, and is known for its extracellular matrix (ECM) mimicking action that facilitates cellular migration and proliferation (West D.C., Hampson I.N. et al. 1985; Haserodt S., Aytekin M. et al. 2011). HA is composed of repeating disaccharide units containing β-D-*N*-acetylglucosamine and D-glucuronic acid to form polymers that can range from hundreds to millions of Daltons in size. HA is synthesized by three groups of HA synthases (HAS) and is degraded by hydrolysis and hyaluronidases (Hyal) where five Hayl genes plus one pseudogene exists in the human genome (Philipson L.H. and Schwarts N.B. 1984; Csoka A.B., Scherer S.W. et al. 1999; Itano N., Sawai T. et al. 1999). It was reported that only Hyal1 and Hyal2 enzymes are the dominant players which breakdown HA. Hayl2 is reportedly attached to a cell membrane by gycosylphospatidylinositol, and the enzyme acts by splitting HA chains into 20kDa segments which are then trapped by endocytic vesicles and further degraded by Hyal1 (Csoka A.B., Frost G.I. et al. 2001; Rai S.K., Duh F-M. et al. 2001).

As a biomaterial, HA is attractive because it has carboxylic acid groups (one per repeat unit) and hydroxyl groups (three secondary hydroxyl groups and one primary hydroxyl per repeat unit) that facilitate extremely high water binding while also providing multiple potential reactive sites for grafting (nucleophilic –OH and electrophilic –COOH). It should be noted that HA's degradation products may impede antiangiogenic activity and inhibit the interaction of fibronectin with collagen (West D.C., Hampson I.N. et al. 1985); however, in our case of ophthalmic applications, incorporating HA is anticipated to be an excellent choice since the native vitreous humor contains a high fraction of HA.

4.1.2.3 Carboxymethyl cellulose

Carboxymethyl cellulose was also used as a model carbohydrate backbone for elucidating the optimal grafting chemistry since it has similar solubility and functionality relative to HA while being significantly less expensive.

4.2 EXPERIMENTAL: MATERIALS & METHODS

4.2.1 Materials Used

Most materials used and suppliers are described in Chapter 3. Hyaluronan powder (NaHy) 176kDa-350kDa (Lifecore Biomedical), CMC both 250kDa and 700kDa (Sigma-Aldrich), ethylene diamine (EDA) (Fisher Scientific), Hydrochloric acid (HCl) (0.1M from McMaster ABB Store), *N*-(3-Dimethylaminopropyl)-*N*'-ethylcarbodiimide hydrochloride (EDC) and N-hydroxysuccinimide (NHS) (Sigma-Aldrich), and 2-propanol (reagent grade, 99.5% , Caledon Laboratories) were used as purchased. All water was Milli-Q grade unless otherwise stated. Phosphate buffered saline (10mM PBS, pH 7.3) and 2-(*N*-morpholino) ethanesulfonic acid (MES, pH 5.5) buffers were made.

4.2.2 pNIPAM-VC-AA and pNIPAM-co-VC Synthesis

Detailed syntheses are described are in Chapter 3 section 3.3.3.7 for samples S.1U (TGA-carboxylate terminated), S6T (AESH-amine terminated) and S.9T (TGA-carboxylate terminated).

4.2.3 HA-EDA or CMC-EDA Synthesis

CMC (200kDa, 1.5g) was dissolved in MES (0.1M, 150mL, pH 5.5) in a round bottom flask equipped with a magnetic stir bar at room temperature. In a separate beaker, EDA (0.7597mL) and NHS (3x molar excess) were dissolved in MES (40mL), then added to beaker 1, and finally EDC (3x molar excess) was added to the polymer solution. This reaction was allowed to proceed at room temperature for 4 hours, dialyzed (MWCO 50kDa) for 6 cycles, lyophilized, weighed and stored at room temperature (CMC based) or fridge (HA based).

4.2.4 pNIPAM-VC(AESH)-graft-HA Synthesis

Sample S.6T, pNIPAM-VC(AESH-amine terminated), was grafted onto the carboxylic acid groups of HA via carbodiimide chemistry. In a beaker, HA (0.100g) was dissolved in MES buffer (0.1M, pH 5.5, 80mL). In a separate beaker, 0.0182g of pNIPAM-VC(AESH) was dissolved in MES buffer(0.1M, pH 5.5, 80mL). Upon dissolution, beaker 2 was combined with beaker 1 and NHS then EDC (5x molar excess of each) was added. The reaction beaker proceeded for 6 hours at

room temperature. The final product was purified by dialysis (MWCO 50kDa), lyophilized, weighed, stored, and refrigerated. The reactants were in mole ratios of HA: pNIPAM-VC(AESH) as 1.00: 50.00 of their functional groups respectively.

4.2.5 pNIPAM-VC-AA(TGA)-graft-CMC-EDA (for both CMC250kDa/700kDa)

The linear polymer S.9T pNIPAM-VC(TGA) (-carboxylate terminal groups) was grafted to the amine groups of CMC-EDA by carbodiimide chemistry. Typically, CMC-EDA (0.200g) was dissolved in MES (0.1M, pH 5.5, 60mL) in beaker 1. In beaker 2, sample pNIPAM-VC(TGA) was dissolved in the same MES solution buffer. Upon dissolution, beaker 2 was combined to beaker 1, at which point both NHS and EDC (5x molar excess of each) were added. The reactants were in mole ratios of CMC: pNIPAM-VC(TGA) as 1.00: 2.00 of their functional groups respectively.

4.2.6 Characterization by Nuclear Magnetic Resonance Spectroscopy

^{1}H NMR spectra were obtained on a Bruker 200 MHz spectrometer at room temperature with 32 scans recorded for 10mg/mL samples dissolved in D_2O.

4.2.7 UV Irradiation

Vinyl cinnamate-functionalized pNIPAM polymers were dissolved in 2-propanol (20mM) and placed under a UV light source (CUREZONE) with λ~350nm and power ~18W/cm^2. Irradiation times of 0, 5, and 25 minutes were tested in triplicates for each sample.

4.2.8 M_n Determination by Gel Permeation Chromatography

GPC was conducted as described in Chapter 3 section 3.2.3.6. Samples were tested in both DMF and THF solvent GPC columns with 0. 5 and 1.0L/min flow rates respectively.

4.2.9 Potentiometric-Conductometric Titration

Potentiometric-conductometric titrations of samples with acid groups were performed by dissolving 50mg polymer into 50mL water. HCl was added drop-wise to adjust the initial solution to pH~2.5. Samples were then titrated with NaOH (0.1M), added with a delta pH/mV of 80, minimum single injection of 0.0010mL to a maximum single injection of 0.04mL with 45

seconds between each injection, recording pH and conductivity as a function of the volume base added (Mandel PC Titrator).

4.2.10 UV-Vis Spectroscopy Measurements

Vinyl cinnamate-functionalized pNIPAM-based polymers (20mM) were dissolved in 2-propanol and absorbance was measured as a function of wavelength using a UV-vis spectrophotometer (DU 800 UV/Visible Spectrophotometer, Beckman Coulter, software version 3.0). Measurements were conducted before and after irradiation exposure and triplicates of each sample were measured.

4.2.11 Cell Cytotoxicity Studies

The following steps were completed for the cell viability MTT assay:

1. Sterilize polymers for 4 hours (2 hours each side) with UV radiation and dissolve in compatible cell media
2. Use trypsin to remove cells from the plate, count the cells and plate desired number (25,000 3T3s per well, 50,000 C2C12s per well, 100,000 RPEC and HCEC per well) with 1mL of media. Cell media for HCEC: Keratinocyte serum-free medium (includes bovine pituitary extract and epidermal growth factor supplement) + 1% Penecillin-Streptomycin and the RPEC media: Dulbecco's Modified Eagle Medium: Nutrient mixture F-12 + 10% fetal bovine serum + 5% Penecillin-Streptomycin.
3. Leave cells in well for 24hrs to adhere and stabilize
4. Remove 1 mL of media
5. Add polymer-media solution and media to wells in various proportions (to a total of 1mL) to achieve desired concentrations for testing
6. Incubate cells with polymer solutions for 24hrs
7. Reconstitute MTT stock solution in PBS and sterile filter to get a concentration of 4mg/mL MTT in 10mM PBS.
8. Dilute the MTT stock solution to 0.4mg/mL with serum-containing media
9. Remove 1mL of polymer solution
10. Rinse each well with 0.5mL media and remove the media

11. Add 150μL of diluted MTT stock solution to each well
12. Expose cells to MTT solution for 4hrs
13. Add 250μL DMSO to each well
14. Shake plates for 20 minutes or until purple formazen has dissolved
15. Transfer 2x200μL of MTT-DMSO solution from 24-well plate to a 96-well plate
16. Use the plate reader to take readings at 540 and 700nm (baseline)

4.3 RESULTS: CHARACTERIZATION, RESPONSIVE PROPERTIES & *IN VITRO* TESTING

4.3.1 Cinnamate Incorporation via Graft-to Approaches

Light-sensitive polymers were synthesized by which cinnamates were grafted to the linear HEMA or AA-NIPAM copolymer by reaction of pNIPAM-AA-EDA or pNIPAM-co-HEMA polymers with NC or NCCl via carbodiimide (using EDC) or esterifications (using DCC and triethylamine) chemistry respectively (Zheng Y., Andreopoulos F.M. et al. 2001; Pecinovsky C.S., Hatakeyama E.S. et al. 2008; Samimi H.A., Mamaghani A. et al. 2009). In each of these graft-to approaches, the number of sequential reactions required and the order of reactions (depending on chemical groups reacting) both had a strong influence on the reaction kinetics and final product formed. For example, it was found that a product polymer CMC-EDA grafted to polymer NIPAM-AA(TGA)-EDA-NC had low water solubility due to extremely high amounts of grafting that essentially used up most carboxylic acid groups. In another case, NIPAM-AA(TGA)-g-CMC-EDA-NC compared with a similar material NIPAM-AA(TGA)-EDA-NC-g-CMC revealed that the former was opaque and lower amounts of CMC were grafted (based on NMR analysis, Figure 4—2). However, the clear polymer did not undergo a phase transition although it maintained the characteristic clear and transparent properties we desired. Overall, all polymers prepared by a graft-to method were either insoluble or did not undergo a thermal phase transition.

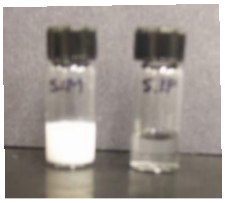

Figure 4—2: Photograph of product 1 and 2 of CMC-g-NIPAM based materials

4.3.2 Cinnamate Incorporation via Vinyl Cinnamate Copolymerization

4.3.2.1 Linear Polymer Systems

As an alternative to grafting, vinyl cinnamate could be incorporated as a comonomer in the pNIPAM polymer synthesis, eliminating one (or, in the case of acrylic acid-functionalized polymers, two) grafting steps and improving our control over the final product properties. The copolymers thought to have the most suitable properties were S.1U, S.6T and S.9T based on Chapter 3 final model analysis.

Polymer S.6T (pNIPAM-VC(AESH)) was characterized by proton NMR (Figure 4—3) with selected characteristic hydrogen peaks assigned on the spectrum.

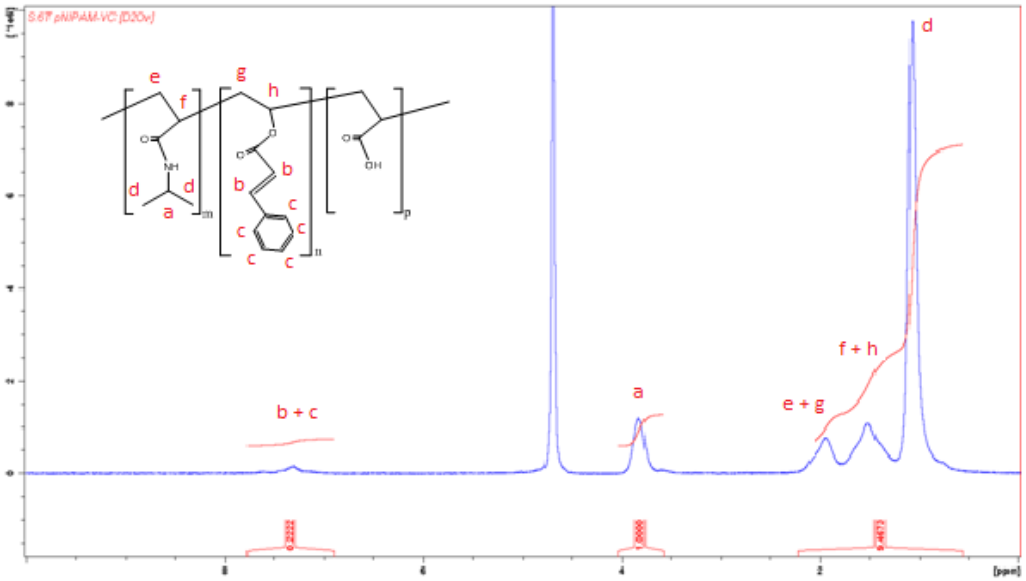

Figure 4—3: ^{1}H NMR of pNIPAM-co-VC(AESH) in D2O, with the characteristic hydrogens labeled

The aromatic protons give characteristic peaks from 7.0ppm to 8.0ppm (representing 5H)(Kim H-T. and Park J-K. 1998). The cinnamate unit (-CH=CH) gives doublets (due to coupling of –CH protons with each other) in the region of 6.3ppm to 7.3ppm, characteristic for the trans isomer of cinnamic acid (Ali A.H. and Srinivasan K.S.V. 1997). The relative mole fraction of VC per NIPAM was calculated using the ratio of VC (6.8-7.8ppm) to NIPAM (3.7ppm) peak areas, divided by the number of hydrogens represented by each peak (7 H/mol VC:1 H/mol NIPAM), yielding a VC content of 3.14mol% in the resulting polymer.

Polymer S.1U pNIPAM-VC-AA was found to have ~10mol%AA incorporated (by NMR and titration results) which agrees with its stoichiometric proportions.

Table 4—1 shows the polymer properties resulting from each of the three "best" p(NIPAM-VC) polymers while Figure 4—4 shows solubility and cloud point data for each polymer. The 'T' type chemistries (copolymers of NIPAM and VC) always had less than <10mol% VC regardless of the feed monomer mix used; in contrast, the 'U' type chemistry (copolymer of NIPAM, VC, and AA) incorporated a significantly higher amount of VC. Thus, the presence of AA appears to assist with VC incorporation, an effect that may be attributable to the copolymerization ratios between each of the tested monomers and/or the solubility of the growing polymer with or without the polar AA residues in the polymerization solvent used (ethanol). The number average molecular weights of the linear polymers, standardized by pNIPAM references of known molecular weight, were collected in THF as detailed in Chapter 3, which may influence the LCST properties of the polymers.

Table 4—1: Linear polymer properties

Sample ID	Contents	CTA Type & Amount [mol CTA/ total mol monomers]	VC/NIPAM [mol% feed]	Solvent	Reaction Time [hours]	Dialysis MWCO [Da]	VC/NIPAM [mol% NMR]	M_n Adjusted [Da by GPC]
S.6T	pNIPAM-VC	AESH [0.0129]	16.92	DMF	24	14,000	3.14	11,958
S.9T	pNIPAM-VC	TGA [0.0210]	7.92	EtOH	6	3,500	3.46	2,189
S.1U*	pNIPAM-VC-AA	TGA [0.0100]	22.66	EtOH	24	14,000	10.77	1,719

*This material was dialyzed against a basic environment, resulting in increased yield

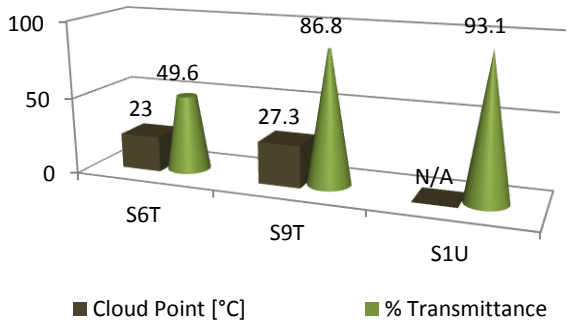

Figure 4—4: Cloud point temperature and solubility of three pNIPAM-VC copolymers (measured in 10mM PBS and concentrations of 10mg/mL); N/A indicates that the cloud point was not detectable at this lower polymer concentration tested (LCST > 60°C).

The cloud point onset (NIPAM aggregation) is at room temperature for S.6T, where the polymer would need to be refrigerated to ensure fully dissolution, the phase transition occurs at 23°C so that the value of transmittance (solubility) at that temperature is lower than the other polymers. However, S.6T's conjugation chemistry is favorable given that an amine-terminated polymer may be grafted on a carboxylic acid-containing carbohydrate in a single synthetic step. Polymer S.9T has a similar composition but a significantly lower molecular weight, reducing the cloud point to just above room temperature while significantly improving the solubility. S.1U has the shortest chain size (M_n) and highest acid content; it is soluble and had a desired cloud point (~29°C at 50 mg/mL) but no detectable cloud point at 10 mg/mL. At higher concentrations, S.1U would be the best graft material, as it has high solubility at low temperature and the highest amount of VC incorporated of all synthesized copolymers; at lower concentrations, S.9T would be a better choice. All three polymers were further characterized for photoresponsive properties and in vitro testing.

4.3.2.2 Hydrogel Grafted Systems

Two hydrogel precursor materials were investigated where linear polymer S.6T was grafted to HA to form '5Z' HA-g-NIPAM-VC(AESH) and linear polymer S.9T was grafted to CMC to form '6Z' CMC(250kDa)-EDA-g-NIPAM-VC(TGA) and '7Z' CMC(700kDa)-EDA-g-NIPAM-VC(TGA). Polymers were grafted to carbohydrates by carbodiimide chemistry to form an amide bond (Hoare T. 2009). The anticipated architecture of all hydrogels is a brush-like structure with a polysaccharide backbone and pNIPAM chains as the brushes, as depicted in Figure 4—5. This architecture may be a good design for pNIPAM chains that are larger than the ones used here but since the pNIPAM chains here are shorter, this hydrogel physical crosslinking (NIPAM effect) was limited.

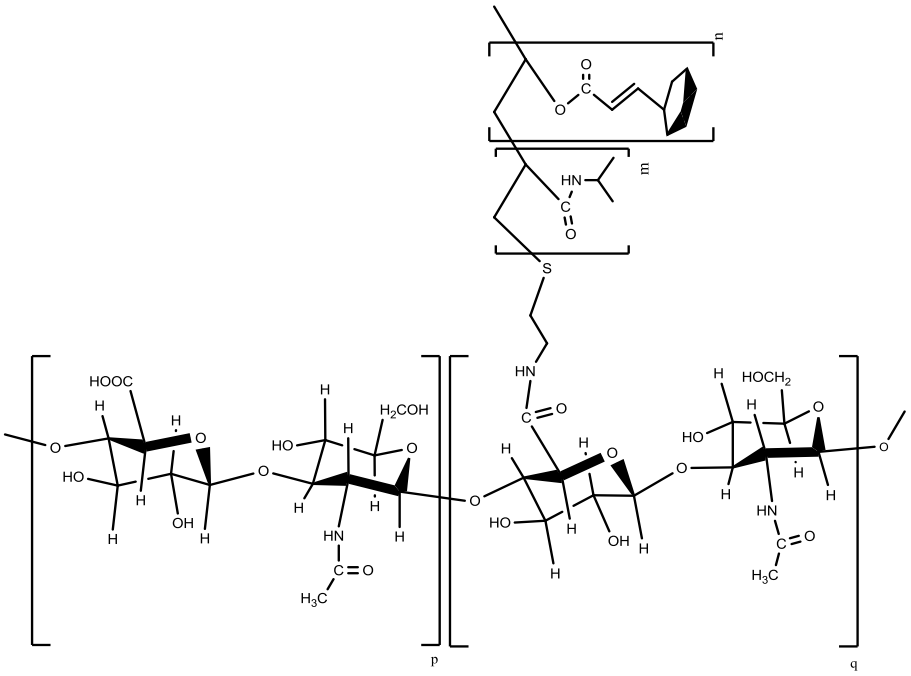

Figure 4—5: Hydrogels with a brush-like architecture with HA backbone and pNIPAM-VC grafted arms

Table 4—2 shows the estimated graft polymer properties, based on gravimetric measurements of the weight of material reacted and recovered (Chen J-P. and Cheng T-H. 2006):

$$\text{Grafting ratio (GR)} = \frac{(W_{HA-g-pNIPAM-VC} - W_{HA})/MW_{pNIPAM-VC}}{W_{HA}/MW_{HA}} \qquad \text{Equation 4.1}$$

$$\text{Degree of grafting (DG)}[\%] = \frac{\text{GR}}{\text{no.functional groups polysaccharide}} \times 100 \qquad \text{Equation 4.2}$$

$$MW_{HA-g-pNIPAM-VC} = MW_{HA} + MW_{pNIPAM} \times GR \qquad \text{Equation 4.3}$$

Table 4—2: Estimated graft polymer properties based on gravimetric measurements

Sample ID	wt of NIPAM-VC [g]	wt of polysaccharide [g]	DG [%]	MW estimated [Da]
5Z	0.0821	0.1000	2.202	499,700
6Z	0.2666	0.2000	12.54	478,977
7Z	0.2666	0.2000	16.46	1,522,115

Both the 250kDa CMC (sample 6Z) and the 700kDa CMC (sample 7Z) tested had ~40wt% graft yield of EDA on their carboxylic acid groups (as noted by conductometric titration results) and those were used to make the hydrogels presented as 6Z and 7Z; correspondingly, both have similar graft yields (13-16%), although the higher molecular weight polymer has more p(NIPAM-co-VC) grafts per chain. The amine-terminated sample exhibited significantly lower graft yield, likely due to the lower solubility of S.6T.

4.3.2.3 Photochemistry

The photosensitivity of native VC and of the polymer S.7T (exact same recipe as S.9T but using THF as a solvent) was determined by dissolving the materials at a concentration of 20mM in 2-propanol and irradiating with the UV source. Absorbance values as a function of wavelength and UV irradiation are shown in Figure 4—6. The solvent 2-propanol was chosen because it could dissolve both the reference VC (hydrophobic and insoluble in water or PBS) and polymer (water soluble) and did not absorb light in the characteristic wavelengths we were examining, unlike DMF and THF.

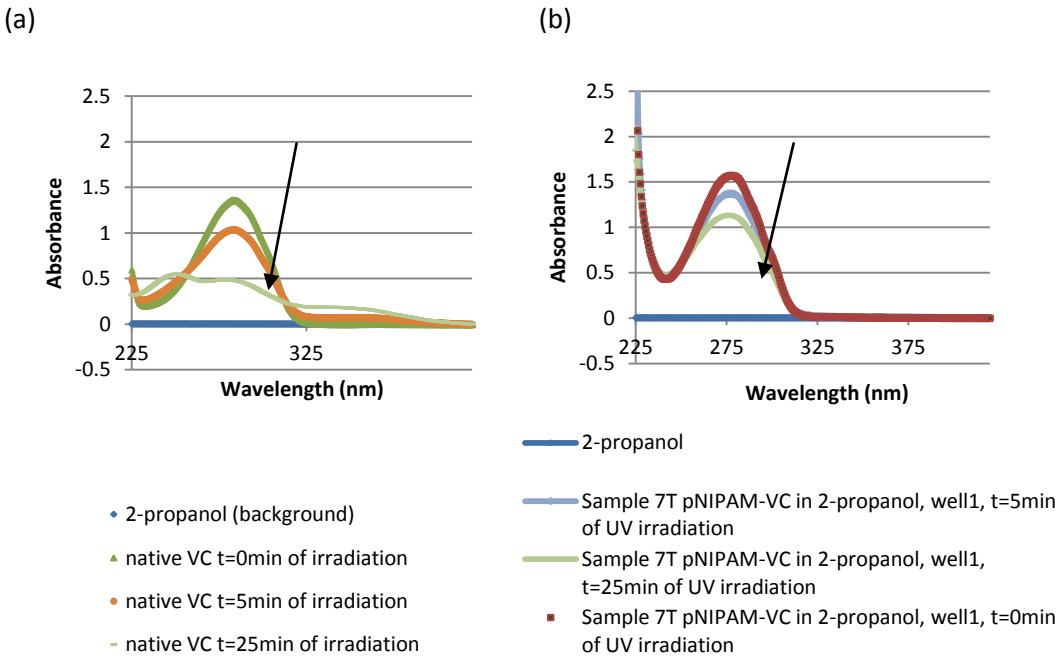

Figure 4—6: Continual UV irradiation of (a) native VC and (b) S.7T pNIPAM-VC leads to a decrease in the maximum characteristic absorbance (arrows show trend)

For all tested cinnamate groups, the maximum absorbance of the ethylenic carbons (-C=C-) occurs at λ_{max}~280nm (on average). This bond absorbance decreases as the chromophore dimerizes to form the crosslinked, four-member ring, such that crosslinking can be monitored over time. In accordance with the Beer-Lambert law, the measurement of characteristic absorbance is linearly proportional to the concentration of that compound; therefore the values of absorbance can be used to calculate the chemical crosslinking i.e. formation of cyclobutane rings (Balaji R. and Nanjundan S. 2002). In both native VC and the polymer S.7T, an increase in UV exposure caused the peak absorbance to decrease. An increase in UV exposure also caused a shift in the value of λ_{max} where the values were ~3nm lower (on average). At the highest irradiation time (25min), the native VC began to show more than one peak in the absorbance spectrum with a shift of absorbance to ~275nm (indicating the dimerized product) and 2 isosbestic points (254nm, 313nm) confirming the occurrence of trans-cis isomerization progression during irradiation. This spectral shift is not observed in the polymer sample, likely due to the lower mobility of polymer-grafted cinnamate groups relative to small molecule cinnamates.

The amount of crosslinking that occurred is directly related to the absorbance measured at each time point. Therefore, the crosslinking efficiency of the photoactive chromophore (-CH=CH-) can be calculated, equating the % decrease of (-CH=CH-) absorbance to the % crosslinks formed (Ali A.H. and Srinivasan K.S.V. 1997):

$$\%\ crosslinking = \left|\frac{A_t - A_0}{A_0}\right| \times 100\% \qquad \text{Equation 4.4}$$

Here, A_t represents the absorbance at time t (0, 5 or 25 minutes) and A_0 is the initial absorbance value, the values of absorbance are reflective of the number of VC groups present in the sample. The amount of crosslinked VC groups per initial amount of VC group can be seen in Figure 4—7.

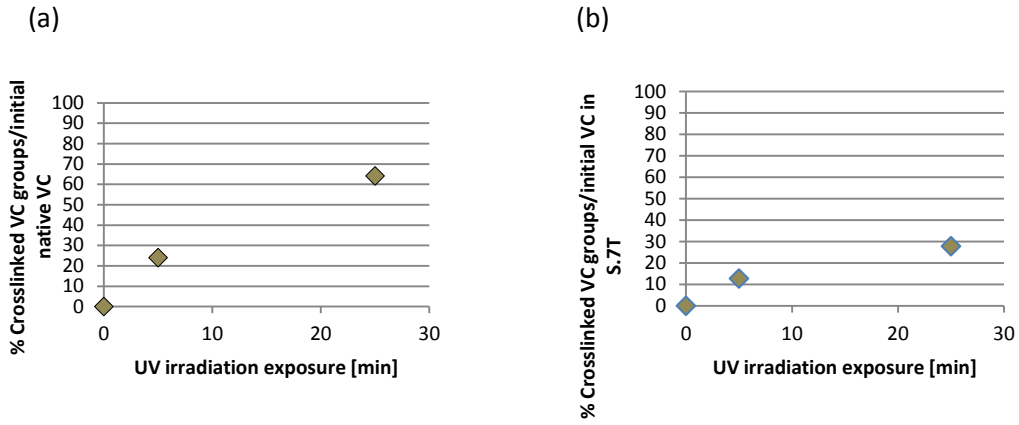

Figure 4—7: %crosslinking of VC groups in (a) native VC and (b) polymer S.7T pNIPAM-VC

Relatively high (~30%) cinnamate crosslinking could be achieved in the polymer solutions after 25 minutes of UV irradiation, confirming that this chemistry can be used to generate covalent, photo-triggered bonding.

It should be noted that UV irradiation (20min) of sample of S.1U (74mg/mL) in 2mL of PBS was found to make a visible gel without the requirement of carbohydrate grafting. This polymer, which contained AA residues, binds significantly more water and thus is more capable of gelling at a given concentration than the p(NIPAM-co-VC) polymers. This result is evidence that that the chemical crosslinks alone can form a hydrogel network.

4.3.3 *In Vitro* Studies

Human corneal epithelial cells (HCEC) were exposed to different concentrations of both linear polymers and hydrogels (generated by UV crosslinking concentrated solutions of the cinnamate-containing polymer specified in each graph) using MTT cytotoxicity studies. Overall, the results of the relative cell viability (HCEC) verify the materials tested are of low cytotoxicity. Figure 4—8 shows no cytotoxicity of S.1U toward HCEC at all concentrations tested in comparison to its reference (cells with no polymer present). These results are in agreement with other similar results, where pNIPAM chains (<10kDa) were shown to have non-toxic effects when administered orally to mice (up to 4000mg/kg body wt) (Malonne H., Eeckman F. et al. 2005).indeed, *t*-tests indicate that measured viabilities are significantly higher than the cell-only control in the presence of any of the tested polymers at higher concentrations ($p < 0.05$). These

results confirm the lack of toxicity of the cinnamate group on HCEC and indeed suggest that HCEC cells may favorably propagate on surfaces with adsorbed vinyl cinnamate copolymers.

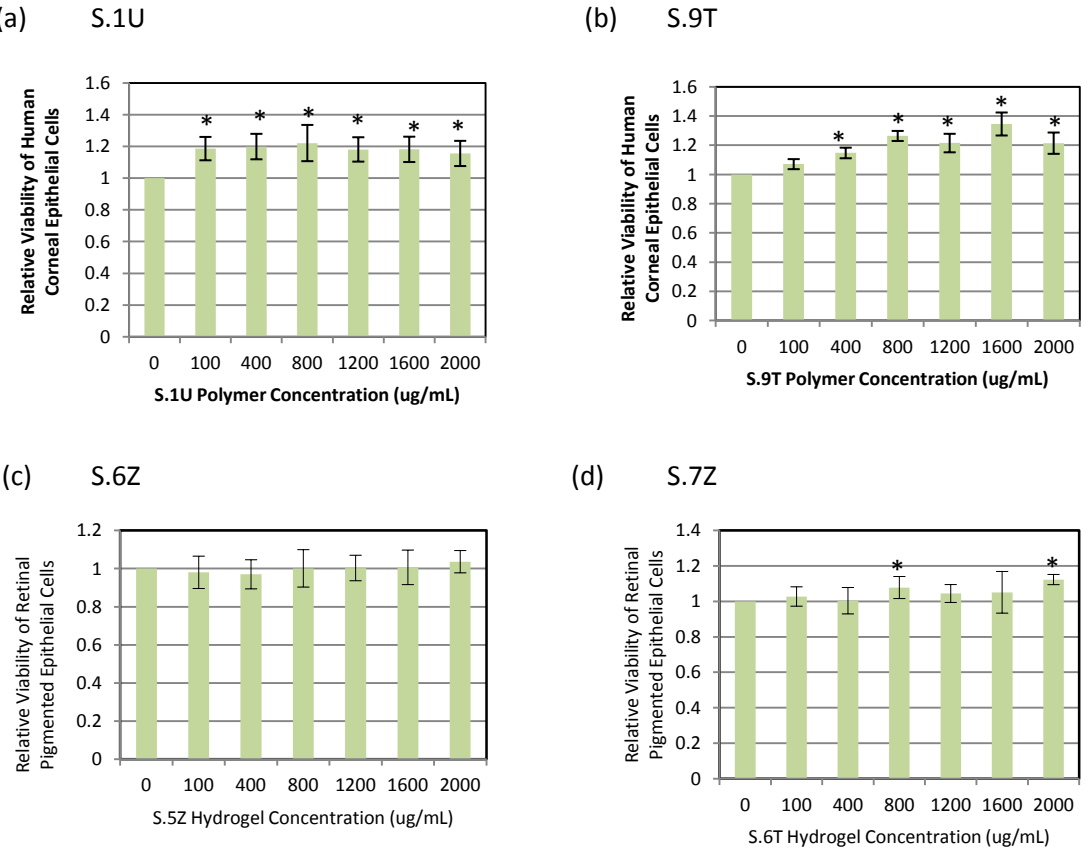

Figure 4—8: The relative cell viability of human corneal epithelial cells for various material concentrations (a) S.1U, (b) S.9T, (c) S.6Z hydrogel, and (d) S.7Z hydrogel samples. Asterisk (*) signifies a statistically different mean for that concentration tested (compared to control cells) as determined by a t-test ($p<0.05$).

MTT results for retinal pigment epithelial cells (RPEC) are shown in Figure 4—9. The results indicate that none of the polymers tested induced significant toxicity on RPE cells, even at concentrations that would be considered "high" for *in vitro* cytotoxicity assays (> 1 mg/mL). This suggests that these polymers would be amenable to potential use *in vivo*.

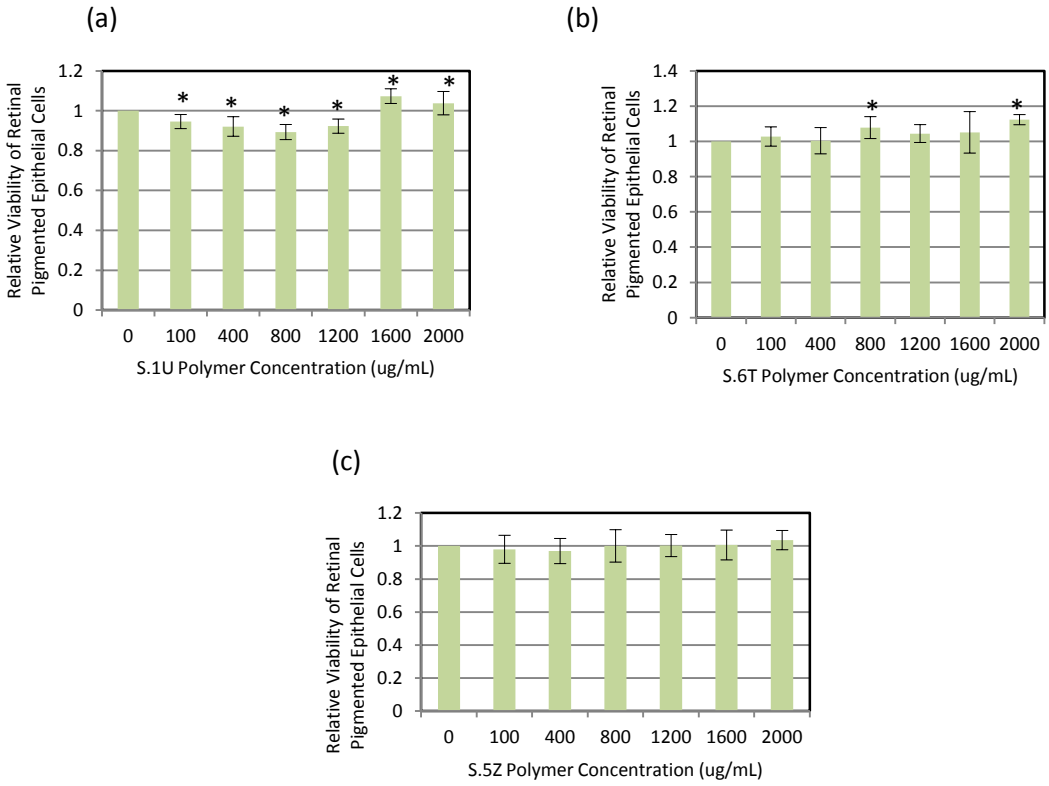

Figure 4—9: The relative cell viability of retinal pigment epithelial cells for various material concentrations (a) S.1U, (b) S.6T, (c) S.5Z. Asterisk (*) signifies a statistically different mean for that concentration tested (compared to control cells) as determined by a t-test ($p<0.05$).

4.4 Discussion: Synthesis & Responsive Properties

4.4.1 Material Characterization

4.4.1.1 Synthesis Challenges

In order to successfully make and recover these polymers, a series of challenges were overcome to improve reactivity of monomers, solubility of final product, and the final product yield ultimately recovered. The key challenge was in dealing with the characteristic low solubility of cinnamates/ derivatives in water, as even small quantities of water would cause cinnamates to precipitate. Guided by the PLS model described in Chapter 3, a variety of single and co-solvents were tested to determine the best reaction medium. Correspondingly, a trade-off

existed between cinnamate concentration in the final polymer and the solubility of the final polymer. While many studies have reported materials with pVC and cinnamates or their derivates conjugated onto polymers, those systems are generally used as photoresists and are not intended to be water soluble, limiting the use of such chemistries in the context of this work. In the end, using the PLS model results helped determine the best monomers, reaction conditions, and monomer ratios to achieve high solubility and intermediate cloud point temperatures while maximizing the cinnamate residues to form water soluble polymers.

Polymer purification and isolation procedures were also found to be critical for facilitating pure products and high yields. The reaction media was added drop-wise to a large quantity of water to dissolution all soluble cinnamate containing polymer products while precipitating the unreacted VC monomer, with the solution mixed for 2 days to ensure all possible polymers were recovered. Performing these steps in reverse (adding a large volume of water to the reaction media) results in significantly lower polymer product yields.

4.4.1.2 Physical Characterization

From the observations of material properties the linear polymers designed maintain their thermosensitive properties as desired. The cloud points for the linear polymers ranged from room temperature to above physiological temperature, depending on the composition and concentration tested. The PLS model is particularly useful in this regard to estimate the cloud point of the polymer and thus its potential utility in the ultimate application. The copolymerization of AA with pNIPAM-VC polymers improved solubility and transparency of polymers. Future optimization of the AA concentration that improves solubility but results in a slightly lower cloud point than sample S.1U (below physiological temperature) appears to be an attractive course of future study. Using AESH as a chain transfer agent in place of TGA is also preferable, since pNIPAM-VC(AESH) had significantly longer chains (M_n, enabling improved interpolymer interactions) and an amine end group that can be directly conjugated to the carboxylic acid-containing carbohydrates.

The current generation of graft polymers did not exhibit sufficient physical gelation at any concentration to result in a hydrogel-like material as observed by other similar graft polymers (Cho K.Y., Chung T.W. et al. 2003; Gattás-Asfura K.M., Weisman E. et al. 2005; Ha D.I.,

Lee S.B. et al. 2006; Tan H., Ramirez C.M. et al. 2009). Literature suggests that the weak mechanical strength of the resulting materials could be due to the use of small linear polymers (M_n low) grafted to the polysaccharide as well as the architecture of the hydrogels (linear polymer terminal end group grafting) (Fitzpatrick S.D., Mazumder M.A.J. et al. 2010). In pNIPAM based films, the architecture has been shown to significantly affect the thermosensitivity, as an increase in chain size may improve gelation of hydrogel (Plunkett K.N., Zhu X. et al. 2006). For S.1U-grafted hydrogels, the strong concentration dependence of the cloud point temperature (as noted in section 4.3.2.1) may also contribute to its lack of gel formation under the gelation conditions used. Together these factors lead to undesired swelling and impeded thermoresponsive properties of the final materials. Another factor that needs to be considered is the hydrogen bonds that can be formed between the carbonyl groups of NIPAM/ VC with the many hydrogens of the backbone polysaccharide which can effectively bond those brush-arms to the carbohydrate. This could hamper the thermo and/ or photoresponsive nature of the final material (Ghosh P., Hutadilok N. et al. 1994), potentially by distorting the local symmetry in cinnamate residues (Khan M., Brunklaus G. et al. 2008).

4.4.1.3 Photochemistry

The existence of the isosbestic point for VC samples was debated for years, some researchers declaring this was not observed. Until recently solid pVC studies report this observation and this supports the fact that irradiation causes cycloaddition induced by isomerization along with dimerization as observed in this work with native VC monomers in 2-propanol (Williams J., Rubin M. et al. 1969; Egerton P.L., Pitts E. et al. 1981; Ali A.H. and Srinivasan K.S.V. 1997; Perny S., Le Barny P. et al. 2000; Perny S., Le Barny P. et al. 2000).

An important observation is that in NC-polymer systems (NC grafted to HEMA or AA–co-NIPAM or CMC-EDA polymers), a colour change was noticed either during the conjugation reaction and/ or upon irradiation of the samples. This was thought to be due to some chemical crosslinking occurring, or due to impurities or potential degradation of the nitrocinnamates. A colour change of solution is usually indicative of a chemical change if the chromophores are responsive to wavelengths that cause a colour change in the visual spectrum (Garcia A., Marquez M. et al. 2006). Chemical crosslinking of cinnamates has been reported to occur upon

application of extremely high temperatures; if cinnamates are exposed to temperatures >200°C for 30 to 60min, thermal degradation occurs through the carbonyl bond to create a free radical cinnamate that can form new crosslinks, as evidenced by DSC, FTIR, TGA, and mass spectra studies (Paczkowski J. 1991; Kim H-T. and Park J-K. 1998). This is highly unlikely to occur in this work, as the reaction requires much higher temperatures than those used here (25-80°C range). Another possibility is that an impurity in the system (or the synthesis solvent) acts as a sensitizer, which absorbs energy and excites the NC which explain the possible crosslinking but not the colour change (Ravve A. 2006). The final alternative would be that there are some chromophores present in the system (either supplier grade or created) that absorb light and result in the visible colour change. However, it should be emphasized that vinyl cinnamate copolymers do not undergo an analogous colour change upon irradiation, suggesting that the nitro group may be involved in the colour generation.

For VC-containing copolymers, the incorporation of different hydrophilic comonomer segments can affect not only the chain solubility but also the extent of crosslinking possible. It was reported that for liquid crystal systems, the chromophore's alignment layers and pretilt can be changed by incorporated different architectures and molecular polarity entities (Naciri J., Shenoy D.K. et al. 2004). Including crosslinking density in a future PLS model may provide a method to optimize the monomer mixture to achieve both goals.

In our calculations of % crosslinking, we refer to the amount of chemical crosslinks formed relative to the total number of original chromophores present, as is typically reported (Ali A.H. and Srinivasan K.S.V. 1997). It should be acknowledged that 100% dimerization and de-dimerization is not realistically attainable (Ali A.H. and Srinivasan K.S.V. 1997; Geelen P.A.P. 2008) due to variations in the local density of chromophores, the polymer chain size and flexibility, and the 'absorbance efficiency' of the light source used (i.e. if λ_{max} is closer to the actual λ_{max} of chromophore, more crosslinking should occur). An alternative to calculate the number of photosensitive units reacted or unreacted is by monitoring IR spectra (Berrada M., Carriere F. et al. 1996), although this is typically less accurate than the UV technique used in this study.

4.5 CONCLUSIONS & RECOMMENDATIONS

4.5.1 Conclusions

The following conclusions can be made based on the data presented in this chapter:

- The physical crosslinking of NIPAM was evident in the onset of cloud points measured
- The photosensitivity of the polymers was not altered by the reaction and showed the ability to crosslink more upon longer UV irradiation exposure times at temperatures above the phase transition temperature of the pNIPAM polymer (analogous to the conditions at which physiological crosslinking would occur)
- The architecture of the hydrogels, graft molecular weight, and graft cloud point all influences the hydrogel's mechanical strength and stability
- The polymers S.1U (pNIPAM-VC-AA), S.6T (pNIPAM-VC), polymer S.9T (pNIPAM-VC), and graft material S.5Z (HA-g-pNIPAM-VC), S.6Z (CMC-EDA-g-pNIPAM-VC), and S.7Z (CMC-EDA-g-pNIPAM-VC) are nontoxic to human corneal epithelial cells and retinal pigment epithelial cells, suggesting potential applicability of these materials in both the front and back of the eye

4.5.2 Recommendations

There are a number of recommendations that could help improve the final hydrogel properties:

- The grafting can be done using the same basic chemistry but incorporating more reactive functional groups on the linear polymer to attach to the carbohydrate, effectively changing the hydrogel architecture
- Hydrogels with increased strength will be pursued by: (a) tuning the AA content of p(NIPAM-co-VC-co-AA) copolymers to lower the cloud point to <30°C; (b) increasing the molecular weight of the polymer by using lower quantities of AESH as the chain transfer agent; (c) increase the effective graft density by tuning solvent conditions to expand or contract the pNIPAM polymer coil

- Once a suitable formulation is identified, rheology and drug release studies can be conducted
- Drug release studies on hydrogels formed by direct photocrosslinking of p(NIPAM-co-VC-co-AA) polymers are currently being investigated
- Decrosslinking wavelengths can be applied to attempt to reverse the chemical crosslinking process, with the efficacy of decrosslinking tracked by gravimetric swelling and chromophore UV measurements as a function of irradiation time
- Finally, with the materials that have hydrophobic VC incorporated, the possible delivery of hydrophobic drugs could be investigated, as the VC residues could act as both photocrosslinking sites and drug depots

Chapter 5 : Thermoresponsive and Photoresponsive Microgels

5.1 INTRODUCTION: MICROGELS & THEIR FABRICATION

5.1.1 Microgels

Microgels are large molecular weight, covalently crosslinked polymer networks that have mean diameters ranging from 50nm to 5µm (Hoare T. 2006). Microgels can be considered small scale hydrogels, with measurable water swelling properties as the solvent quality changes, but macroscopically behave as colloidal particles that have sphere-like structures. Due to their small dimensions and high surface area, microgels have been explored for applications in drug delivery systems (DDS) (Hoare T. 2006; Vinogradov S.V. 2006; Sivakumaran D. 2010)

Stimuli-responsive microgels can be made with tunable properties in order to load and release drugs as required for treatments. For example, a pNIPAM-based microgel can be swollen in a good solvent (at low temperature), where the macrostructure becomes more porous, to allow for drug uptake or the diffusion of drug out of previously loaded microgels. Exposing this system to temperatures above the volume phase transition temperature (VPTT) will induce de-swelling/shrinkage that can either drive a burst release of a drug payload or entrap drugs inside a less porous network, depending on the chemistries involved. The more "smart" properties can be designed into a microgel, the more flexibility in drug release kinetics can be achieved, making dual stimulus-responsive microgel systems potentially beneficial to use in DDS.

With all the potential benefits of microgels, there are also some limitations that need to be overcome to fabricate a good microgel system. One main limitation includes the traditional emulsion method of synthesizing microgels that results in non-biodegradable materials unsuitable for *in vivo* applications. Another challenge is obtaining monodisperse particles, particularly outside of the 100-1000nm particle size range that can be achieved using pNIPAM-based emulsion syntheses. In general, larger size microgels tend to have higher polydispersity, which can lead to unanticipated immune responses or hard-to-control drug release kinetics. The aim of this chapter was to leverage our previous demonstrated ability to design thermoresponsive polymer chains containing photo-crosslinkable cinnamic acid functional groups via both graft and copolymerization approaches (Chapter 4) to design and characterize dual thermo- and photo-responsive microgels. Such materials would offer multiple possible (and reversible) triggering options *in vivo* to facilitate a range of potentially novel and useful drug

release kinetics. Microgel systems that incorporate a coumarin moiety (UV light responsive) or a spiropyan photochrome (visible light responsive) have been reported. (Garcia A., Marquez M. et al. 2006; He J., Yan B. et al. 2011). The system devised here incorporates the use of cinnamates which should have more efficient crosslinking and are more practical (than visible light responsive materials) with the goal of potential *in vivo* applications rarely reported.

5.1.2 Fabricating Microgels by Emulsion Reactions

Thermoresponsive microgels and nanogels can be made by simultaneously polymerizing and crosslinking NIPAM, a crosslinker, and other monomers (often hydrophilic in nature) in an emulsion-type reaction (Pelton R.H. and Chibante P. 1986). This method is robust over a large range of synthesis conditions and results in highly monodisperse particles with well-defined sizes. Other methods have also been reported to synthesize microgels or nanogels in cases where the thermal phase transition is not available to drive particle nucleation and growth. As an alternative method of fabrication, Kadlubowski's research focus is on a novel method where macromolecules of high molecular weights are exposed radiolysis (short intense pulses of electrons) in dilute aqueous solutions where the product radicals react with the macromolecules to form polymer radicals under specific conditions to obtain new covalently crosslinked microgels (Kadlubowski S. 2009). Other methods of microgel formation include novel membrane emulsification for water-oil (W/O) (hydrophobic Shirasu porous glass (SPG) membrane) or monodisperse W/O/W emulsions (hydrophilic SPG membranes), which have been demonstrated to deliver the anticancer drug epirubecin (Nakashima T., Shimizu M. et al. 2000).

5.1.3 Fabricating Microgels by Microfluidics

Microfluidics enables the generation of highly monodisperse water-in-oil emulsion droplets that can subsequently be gelled to form microgels via a range of different chemical or physical techniques (Tumarkin E. and Kumacheva E. 2009). For example, monodisperse dextran-HEMA microgels with ~10µm diameter have been generated using a T-shaped junction in-line droplet microfluidic geometry (De Geest B.G., Urbanski H.P. et al. 2005). Microfluidic microgel fabrication has also been reported for water/oil/water (W/O/W) set-ups and for set-ups using a

two-tier flow mixing flow channel set-up (hydrophobic then hydrophilic continuous flow in series) (Okushima S., Nisisako T. et al. 2004), and alginate-calcium carbonate stream with acidic stream to form alginate gel droplets (Amici A., Tetradis-Meris G. et al. 2008). This method of fabrication is particularly useful to make the multi-responsive microgels with diameters of more than 1µm diameter. The target size is useful in attempts to minimize the immune system's response by minimizing endocytosis by macrophages *in vivo*.

A microfluidics chip for performing on-chip mixing of reactive polymers has recently been developed in our lab. The chip design, shown in Figure 5—1, uses a geometry that includes separate microchannels that are filled with liquids (reactive polymer solutions) that meet at a junction point and flow together through a small channel for a short time before being cut by shear force with a perpendicular immiscible flow to make a microgel droplets (usually W/O phases). The flow rates, channel size, mixing channel length, nozzle diameter,and junction geometry can be altered to change the properties of the final microgel particles. The polymer A and B streams for the purposes of this project are detailed in the next sections.

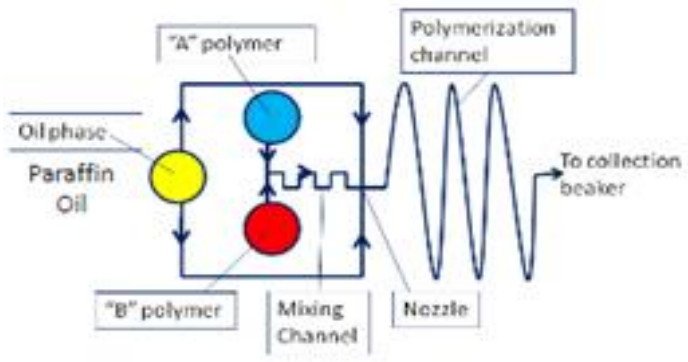

Figure 5—1: Microfluidic chip with two inlet channels that mix and are cut by shear force at the nozzle (Kesselman L., Shinwary S. et al. 2011)

5.2 EXPERIMENTAL: MATERIALS & METHODS

5.2.1 Materials Used

NIPAM was purified from recrystallization from toluene/ hexane (Sigma-Aldrich), 1-ethyl-3-(3-dimethylaminopropyl)carbodiimide (EDC), N-hydroxysuccinimide (NHS), acrylic acid

(AA), methacrylic acid (MAA), N,N'-methylenebis (BIS), ammonium persulfate (APS), trans-4-nitrocinnamic acid (NC), cinnamic acid (CA) (all from Sigma-Aldrich), ethylene diamine (EDA) (Fisher Scientific), pentane (>98%) (Caledon Labs.), and hydrochloric acid (HCL) (0.1M from McMaster ABB Store) were all used as purchased. All water used was Milli-Q grade. MES buffer solutions were made (0.1M and pH 5.5).

Various molar ratios (of functional group AA) coded as low 'L', medium 'M', and high 'H' microgels were fabricated, the letter indicating the amount of commoner AAwt% in the microgel as (L=low) 8.6, (M=Medium) 12.7, and (H=High) 21.95wt% of functional group respectively.

5.2.2 Microgel 1, Step 1 Synthesis: p(NIPAM-AA(BIS))

For 3M-1 microgel, NIPAM (1.4g), AA (0.232g), and BIS (0.1g) were dissolved in water (150mL) in a round bottom flask with 3 outlets. The flask was stirred with a magnetic stirrer (300rpm) and heated to 70°C. Two outlets of the flask were closed with rubber stoppers with the middle outlet connected to a condenser with a bubbled unit attached. The system was purged with N_2 gas for 30 minutes prior to injecting the initiator, APS (0.1g) in water (5mL) solution. The reaction was allowed to continue for 24 hours. Upon completion, the reaction mixture was cooled and dialyzed (using a MWCO 14kDa membrane) with a minimum of 6 cycles of dialysis against fresh water followed by lyophilizing, weighing and storing at room temperature. At this stage, the microgel was designated by a "series number (3 represents AA co-monomer), amount of comonomer letter (L/M/H), and reaction step (1-3) completed" code; for example, 3M-1 is a pNIPAM-AA microgel with 12.7wt% AA in the recipe prior to modification with cinnamates.

The same reaction procedure was followed to make 3L-1 and 3H-1 microgels by changing the mass of AA used to 0.15g and 0.45g respectively.

5.2.3 Microgel 1, Step 2 Synthesis: p(NIPAM-AA(BIS))-EDA

Microgel 1 was recovered and further functionalized with an amine group on some of the acrylic acid groups by carbodiimide chemistry. Various degrees of functionalization were explored, with a sample recipe as follows: microgel 1 (0.8g) was dissolved in one beaker of MES (100mL, 0.1M, pH 5.5). In a second beaker, EDA (0.2402g) was dissolved in MES (5mL, 0.1M, pH

5.5). Upon full dissolution, beaker two was combined with beaker one and the NHS (0.8678g) then EDC (0.7662g) was added. The reaction was allowed to proceed at room temperature under magnetic stirring (300rpm) for 4 hours. The product was placed in a membrane (MWCO ~14kDa), dialyzed against fresh water for 6 cycles, lyophilized, weighed, and stored at room temperature. Following the above step, this microgel was designated as 3M-2.

5.2.4 Microgel 1, Step 3 Synthesis: p(NIPAM-AA(BIS))-EDA-NC

The step 2 microgel was further reacted to conjugate either NC or CA, which both contain a carboxylate end group that can be grafted to the free amine groups (from EDA grafting) on the microgels by carbodiimide chemistry. For example, microgel 3M-2 (NIPAM-AA-EDA, 0.5g) was dissolved in MES (80mL, 0.1M, pH 5.5) in one beaker. In a separate flask, NC or CA (0.3698g) was dissolved in 5mL of DMF, stirring until fully dissolved. The NC/CA solution was added to the first beaker drop-wise, and NHS (0.5424g) followed by EDC (0.4789g) was added. The reaction was allowed to proceed at room temperature under magnetic stirring (300rpm) for 4 hours. The product was placed in a membrane (MWCO ~14kDa), dialyzed against fresh water for 8 cycles, lyophilized, weighed, and stored at room temperature. Following the above step, this microgel was designated as 3M-3 (with a N or C representing NC or CA used in this step).

5.2.5 Microgel 2 Synthesis: p(NIPAM-MAA(BIS))-EDA-NC

Similar to the above 3 reaction steps, methacrylic acid was substituted for acrylic acid (on a molar basis), with microgels labeled as series ‘4’. In step 1, the microgel was prepared in the presence of 0.2g SDS surfactant, dissolved in step 1 along with the monomer, to synthesize microgels with a lower particle size.

5.2.6 Microgel 3 Synthesis: p(NIPAM-co-AA-EDA) + p(NIPAM-VC-AA)

For microfluidics microgel fabrication, combinations of previously-synthesized linear polymers were used. Polymer A (S.6E), an EDA-grafted pNIPAM-AA polymer, was made by reacting S.1.1 pNIPAM-AA (7wt% AA by titration) with EDA, NHS and EDC as described in section 4.2 in a molar ratio of 1:10:3:7 respectively. Polymer B (S.1Ur6) is a p(NIPAM-VC-AA) copolymer, synthesized according the protocol described in section 3.3.4.

Polymer A (free amine groups) and polymer B (free carboxylic acid groups) can be crosslinked inside the microfluidics chip using carbodiimide chemistry.

Polymer S.6E (0.0131g), NHS (0.0336g) and EDC (0.0688g) were dissolved in 4mL of water in a glass vial and loaded into a syringe (polymer A inlet, Figure 5—1). Polymer S.1Ur6 (0.0108g) was dissolved in 3mL of water and loaded into a second syringe (polymer B inlet, Figure 5—1). The flow rate of paraffin oil and polymer flow into the chip was varied until monodisperse spherical droplets were formed at a flow rate of 0.95: 0.03mL/hr (oil: polymer). The reaction conditions were optimized and observed for 1 hour until stable monodisperse microgels were being made (both at the exit and along the channel, as monitored by light microscopy). The reaction was allowed to continue overnight at the set conditions, and chip outlet product was collected in a centrifuge tube (100mL) and precipitated with pentane, permitting extraction of the particles from the oil. The product collected was photographed in an aqueous suspension which was subsequently isolated by centrifugation, washed with pentane (5X) (to ensure complete removal of paraffin oil, with the aqueous phase kept through each extraction cycle), and the purified microgels in water were re-photographed using a light microscope. As with all polymers made with cinnamate groups present, the samples were covered with Al foil to ensure photosensitive groups were not exposed to light.

5.2.7 Characterization by Nuclear Magnetic Resonance Spectroscopy

^{1}H NMR spectra were obtained for the microgels on a Bruker 200 MHz spectrometer at room temperature with 80 scans and 4.5mg samples dissolved in D_2O.

5.2.8 Dynamic Light Scattering Measurements

Particle size of the microgels was determined using dynamic light scattering (Melles Griot HENe laser) with a 632.8nm light source. Detection was conducted using a 90° angle and photomultiplier tube detector (Brookhaven Instruments Corporation). The data was analyzed with a BIC TurboCorr digital correlator and software version 3.34. Lyophilized microgels were suspended in Milli-Q water at a conc. of 1mg/mL. All measurements reported had an intensity count between 80-250kilocounts per second, a count rate sufficiently large for statistical accuracy but sufficiently low that multiple scattering does not occur. Each measurement lasted

~2minutes at 25°C; 5 repeats (unless otherwise denoted by '*') were conducted for each sample and average values of effective diameter are reported with error bars representing the standard deviation. Temperature versus size measurements for the best microgel tested were conducted over the range of 10°C to 50°C at 5°C increments, with the average of 3 repeats reported together with their standard deviation.

5.2.9 UV Irradiation

Sample microgels (1mg/mL in water) were placed under a UV light (CUREZONE) with a wavelength λ=350nm, and power ~18W/cm^2 for 20 minutes. Microgels were subsequently returned for DLS testing to compare effective diameter with prior-to- irradiation samples.

5.2.10 Potentiometric-Conductometric Titration

Potentiometric and conductometric titration of samples with acid groups (pNIPAM-AA and pNIPAM-MAA before and after amination) was performed by dissolving 50mg polymer into 50mL water. HCl was added drop-wise to have an initial solution pH~2.5. Samples were then titrated with NaOH (0.1M), added with a delta pH/mV of 80, minimum single injection of 0.0010mL to a maximum single injection of 0.04mL with 45 seconds between each injection, recording pH and conductivity as a function of the volume base added (Mandel PC Titrator). A sample microgel conductometric-titration is shown in Appendix A4.

5.3 Results: Material Characterization & Responsive Properties

5.3.1 Microgel 1 Series Characterization

AA was copolymerized with NIPAM using a conventional precipitation-emulsion protocol. A summary of the AA-NIPAM microgels synthesized is shown in Table 5—1 and Table 5—2. The low degree of functionalization of microgel 3L-1 was not further pursued, as too low amounts of AA did not allow for much of NC/CA conjugation to occur (Step 3). Microgel 3M-3C generated some macroscopic aggregates that obstructed the light scattering data, so the microgels were filtered twice and re-analyzed to obtain diameter data. Note that the effective diameter values do not necessarily increase with the addition of more AA in the original

microgel formulation.

Table 5—1: Properties of series 1 microgels, pNIPAM-AA based

p(NIPAM-AA) Microgels					
Sample ID	3L-1	3M-1	3M-2	3M-3C	3M-3C filtered
Contents	pNIPAM-AA	pNIPAM-AA	pNIPAM-AA-EDA	pNIPAM-AA-EDA-CA	pNIPAM-AA-EDA-CA
Feed AA [wt%]	8.60	12.60	N/A	N/A	N/A
Product AA [wt%]	7.24	12.26	5.70	N/A	N/A
Eff.Dia. [nm]	1,111 ± 27	1,295 ± 32	644 ± 25	147,231 ± 16,079*	1,271 ± 310*

*denotes sample value as an average of 3 measurements

Table 5—2: Properties of series 1 microgels, pNIPAM-AA based, with higher ('H') amounts of AA

p(NIPAM-AA) Microgels						
Sample ID	3H-1	3H-2	3H-2	3H-2	3H-C	3H-3N
Contents	pNIPAM-AA	pNIPAM-AA-EDA	pNIPAM-AA-EDA	pNIPAM-AA-EDA	pNIPAM-AA-EDA-CA	pNIPAM-AA-EDA-NC
Feed AA [wt%]	21.95	N/A	N/A	N/A	N/A	N/A
Product AA [wt%]	20.68	3.85	3.85	3.85	N/A	N/A
Eff.Dia. [nm]	1,240 ± 23	3,506 ± 1862* (at pH~3)	5,027 ± 831 (at pH~7)	5,505 ± 844 (at pH~10)	N/A	N/A

*denotes sample value as an average of 3 measurements

In the medium series AA, the addition of EDA (reaction step 2) caused the particle size of the microgels to decrease by ~50%, likely due to the formation of an amphoteric (dual cationic/anionic) microgel that is partially crosslinked by ionic bridges. The addition of CA (reaction step 3) resulted in an increase in the microgel size (comparable to the original microgel size) but also resulted in the production of significant aggregate fractions. The addition of the relatively hydrophobic graft likely reduces the hydrophilicity of the interface and promotes inter-particle interactions via hydrophobic associations upon collision, increasing the particle size of the cinnamate-grafted microgel. Microgels with higher acrylic acid contents (the "H" series) exhibited evidence of aggregation following EDA modification, although the sample size was lower at low pH and higher at high pH than at intermediate pH values. This is characteristic

swelling behavior for amphoteric microgels with both cationic and anionic charges due to the formation of charge bridges in the materials (Ogawa K., Nakayama Y. et al. 2003).

It is also worth noting that in all reactions where NC or CA was used (reaction step 3), CA dissolved faster in DMF (without needing to be heated) and stayed soluble throughout the whole reaction, resulting in a better suspended graft microgel. NC was poorly soluble in DMF (before and during reaction) and its final products had more precipitate formation. Similar solubility issues have been reported for NC by others (Leitzke A., Reisz E. et al. 2001). While NMR gives only limited quantitative information due to slow relaxation times in hydrogel systems, ^{1}H NMR results on these grafted microgels showed that cinnamate graft density scaled with the number of reactive functional groups in the microgel; 3M-3CA had ~0.45mol% CA per mol NIPAM conjugated while 3H-3NC contained ~1.95mol%NC and 3H-3CA contained ~1.80mol% CA conjugated. However, while suspended microgels with desired properties could be isolated by filtration, significant aggregate fractions were observed in all formulations tested,

5.3.2 Microgel 2 Series Characterization

To improve the colloidal stability of cinnamate-grafted microgels, MAA was co-polymerized with NIPAM in traditional precipitation-emulsion microgel synthesis and the microgels characterized. MAA is known to localize in the microgel core during a free radical copolymerization with NIPAM (Hoare T. and McLean D. 2006), reducing the presence of hydrophobic cinnamates at the microgel-water interface and thus hypothesized to improve colloidal stability. Table 5—3 shows the MAA content and size of MAA-NIPAM microgels prepared. Only the high 'H' amount of MAA series chemistry was continued for conjugation purposes. Analysis of ^{1}H NMR for 4H-3C resulted in ~0.24mol% CA/mol NIPAM conjugated onto the microgel, although NMR results are likely to be less accurate for core-functionalized microgels due to slow proton relaxation. Note that a small amount of SDS (0.2g) was added during the polymerization to reduce the particle size, as MAA-NIPAM copolymerizations are known to generate larger microgels than AA-NIPAM copolymerizations (Hoare T. and Pelton R. 2004).

Table 5—3: Properties of series 2 microgels, pNIPAM-MAA based, with higher ('H') amounts of MAA

p(NIPAM-MAA) Microgels				
Sample ID	4H-1	4H-2	4H-3C	4H-3N
Contents	pNIPAM-MAA	pNIPAM-MAA-EDA	pNIPAM-MAA-EDA-CA	pNIPAM-MAA-EDA-NC
Feed MAA [wt%]	21.95	N/A	N/A	N/A
Product MAA [wt%]	14.16	5.96	N/A	N/A
Eff.Dia. [nm]	365 ± 3	950 ± 266	554 ± 189*	1,682 ± 55*

*denotes sample value as an average of 3 measurements

5.3.3 Microgel 2 Photochemistry

Using the protocol developed for the linear VC-containing polymers (section 3.3.3.7), the light sensitivity of the microgels was investigated. Figure 5—2 shows the effective diameter of 4H-3C microgels as a function of temperature before and after UV irradiation.

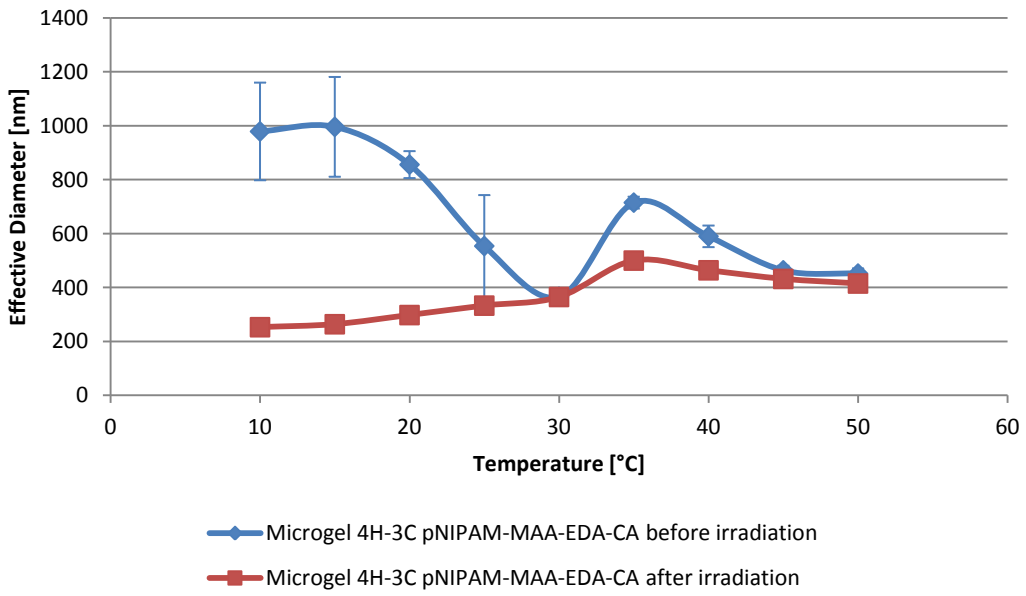

Figure 5—2: Changes in effective diameter of microgel particles as a function of temperature before UV irradiation (blue) and after irradiation for 20min (red)

The original microgel (blue squares) had a phase transition (midpoint VPTT) ~25°C; this phase transition temperature is ~7°C lower than that observed for unmodified pNIPAM hydrogels, consistent with the incorporation of a more hydrophobic monomer unit into the microgels. The VPTT for these microgels is also much broader compared to the linear polymer previously detailed (Chapter 2 and 3), consistent with other microgel measurements (Larsson A., Kuckling D. et al. 2001). The particle slightly increases at 35°C, likely indicating limited particle aggregation above the phase transition temperature, but continues to decrease at higher temperatures as the aggregates continue shrinking but do not aggregate further. This type of behaviour, with particles aggregating above the VPTT, has been previously noted when heating pNIPAM-AA-chitosan nanoparticles (Jung H., Jang M.K. et al. 2009).

Following a 20 minute UV irradiation exposure, the same microgel was re-analyzed over the same temperature range (red squares). Comparing data below the phase transition temperature (no evidence of aggregate formation), the microgel deswells dramatically, with a volume decrease by ~67% observed between the swollen state (20°C) microgel before and after irradiation. This data confirms that UV crosslinking of CA groups occurred to significantly increase the internal crosslink density of the microgel and thus changed the degree of swelling. As the particle is then heated, the effective diameter increased slightly over the full temperature range tested, again indicating the occurrence of aggregation. Interestingly, at high temperatures, the size of the UV crosslinked and non-irradiated microgels equilibrate to approximately the same size value. This observation is consistent with cinnamate groups present in the interior of the microgel, the surface chemistry of the microgel (and thus the aggregate size due to inter-particle interactions) is minimally changed by the UV crosslinking reaction. Overall, the data indicates: (a) UV irradiation can induce a large volumetric deswelling transition below the phase transition temperature and (b) the thermal transition of cinnamate-grafted thermoresponsive microgels can be turned “off” by UV irradiation.

5.3.4 Microgel 3 Characterization

Microgels were synthesized by using a microfluidic chip, where the initial-to-final microgel formation steps are visualized by the light microscopy images in Figure 5—3. Initial trial and error flow rates in (a) resulted in the formation of large microgel globs, until the best

continuous (polymer solutions and oil) flow rates were determined in (b) that formed somewhat polydisperse microgels in (c). After 4 weeks, larger and smaller microgel particles are evident, suggesting the occurrence of Ostwald ripening in the emulsion and thus incomplete gelation of the two precursor particles inside the microgel droplets. The efficiency of the carbodiimide-mediated crosslinking reaction between the A and B polymers requires further investigation.

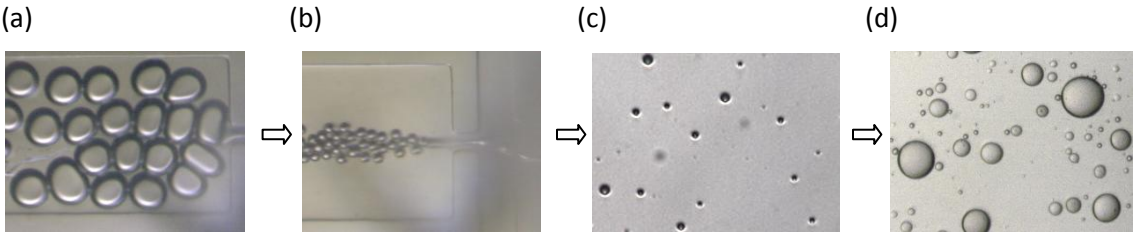

Figure 5—3: Light microscope images of (a) microgels formed under trial conditions, (b) microgels at optimal conditions, (c) microgel particles collected immediately, and (d) after 4 weeks in water

5.3.5 Microgel 3 Photochemistry

The microfluidic microgels were viewed before and after UV irradiation for 10 minutes as shown in Figure 5—4. Microgels are visibly distorted from essentially perfect spheres (before irradiation) to irregular objects (after irradiation), suggesting the occurrence of photocrosslinking between VC residues. Due to the anisotropy of the irradiated particles, it was difficult to measure absolute size data on these samples; however, qualitative observations suggested small size decreases on average upon irradiation.

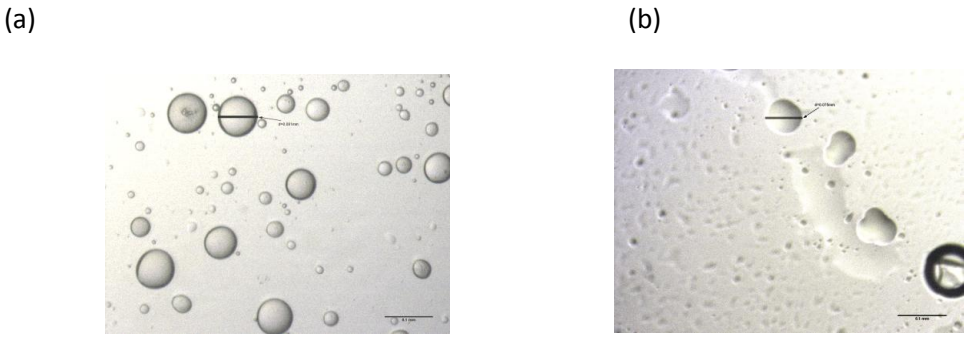

Figure 5—4: Light microscope images of microgels (a) before UV irradiation and (b) after irradiation for 10 min

5.4 Discussion: Responsive Properties

Figure 5—5 shows the chemical structure of AA versus MAA that were chosen to be co-polymerized with NIPAM to form the base microgels.

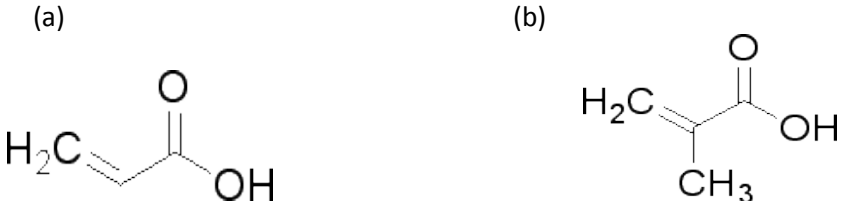

Figure 5—5: Chemical structure of (a) AA and (b) MAA copolymerized with NIPAM

Based on the different copolymerization ratios between AA and NIPAM compared to MAA and NIPAM, MAA is primarily incorporated into the microgel core during a standard microgel polymerization while AA is incorporated throughout the bulk of the microgel. As such, the CA grafts are incorporated primarily in the core for MAA-NIPAM microgels but throughout the microgel in AA-NIPAM microgels. We hypothesize that the improved stability of MAA-NIPAM microgels is attributable to this "hiding" of hydrophobic functional groups away from the microgel surface, which remains relatively hydrophilic to promote microgel stability.

The microgels produced were shown to be in fact triply sensitive, with swelling responses also observed as a function of pH. For example, the 3H-2 pNIPAM-MAA-EDA microgel was tested at various pH values and the effective diameter at a pH 3 was smaller than at higher pH values which suggests these microgels swelled to a greater extent in basic conditions due to the ionized residue carboxylic acid groups (AA) and amine groups (EDA) (Tan B.H., Ravi P. et al. 2006; He J., Yan B. et al. 2011). Graft yields and functional monomer concentrations in the initial microgel could thus be modified to tune the pH/temperature/photoresponsive response balance in these microgels to generate highly functional smart materials

During the cinnamate conjugation reaction, there is a possible undesired reaction that could occur where neighbouring amine groups react with free AA instead of the carboxylic acid groups of the cinnamates. This would ultimately decrease the size of the microgels (new covalent bonds within) and decrease the amount of cinnamate that can be conjugated. The small addition of the NC/CA groups (by NMR analysis) suggests that low amounts of NC are

present though the recipe amounts of NC were all > 1 molar excess NC to EDA. Steric limitations may also contribute to this relatively low NC/CA conjugation yield, as these two grafts were relatively large (MW of NC is ~193.16Da and MW of CA is ~148.16Da) and may thus either block adjacent reactive sites upon conjugation or diffuse very slowly through the microgel phase. It should be noted that NMR results must be interpreted cautiously in hydrogels, particularly those with functional groups of interest in the core where solvent relaxation occurs very slowly relative to in free solution. However, even given these results the number of light sensitive moieties that were conjugated were sufficient to cause an decrease in particle size upon irradiation (Schmidt G.M.J. 1971); indeed, the crosslinking achieved results in a ~30-fold volumetric deswelling transition and an effective turning off of the thermal phase transition. As such, higher graft yields are likely unnecessary to make highly functional smart microgels.

The incorporation of CA and the crosslinking of CA-based microgels were demonstrated to be more efficient compared to the NC-based microgels. This is consistent with the effect of benzene ring substituent on crosslinking previously noted in the literature (see section 2.3.3.1).

Microfluidics-generated microgels also show clear visual photocrosslinking, developing dimples and anisotropic shapes after irradiation. However, the significant change in particle size distribution before and after 4 weeks of storage indicates possible incomplete crosslinking in these materials, leading to Ostwald ripening of the microgel phase to form larger particles over time. Future studies will crosslink the VC-containing polymer with ethylene diamine only, reducing the number of grafting reactions required for effective crosslinking.

5.5 Conclusions & Recommendations

5.5.1 Conclusions

In summary:

- Dual thermoresponsive and photoresponsive microgels were fabricated by a conventional precipitation-emulsion reaction followed by carbodiimide chemistry to incorporate light responsive moieties

- Despite low levels of CA conjugated, upon 20 minutes of UV irradiation, the microgels crosslinked, inducing ~67% deswelling by volume below the phase transition temperature and effectively "turning off" the thermal phase transition
- A small pH trial confirmed that the AA microgels are also pH sensitive and cause a decrease in microgel size at lower pH values, opening the door to the synthesis of triply-responsive microgels by balancing the ratio of reactive groups present
- Microfluidics was a successful method of fabricating microgels that dimpled in response to UV irradiation
- The incorporation of CA instead of NC as a cinnamic acid photochrome is recommended

5.5.2 Recommendations

The following experiments should be conducted to confirm and improve upon the existing microgel formulations:

- Microgels with higher acid contents and lower EDA graft yields should be synthesized to enable the production of triply responsive (pH, temperature, light) microgels
- Microgels should be prepared with different SDS loadings in order to test the particle stability and size changes as a function of irradiation
- Drug release studies should be conducted to track the release of a macromolecular (bovine serum albumin~67kDa) and small molecule (Coumassie Blue~833Da) model drug as a function of UV irradiation (Wells L.A. 2010)
- Microfluidic microgels can be prepared using ethylene diamine (together with EDC/NHS) as the A inlet and the p(NIPAM-VC-AA) polymer as the B inlet to simplify the crosslinking chemistry used and attempt to reduce the Ostwald ripening observed in this study
- Macromolecular drug (bovine serum albumin) can be entrapped inside microfluidic microgels on-chip and its release tracked as a function of time both before and after UV irradiation
- De-crosslinking studies can be performed by irradiating microgels at a lower wavelength to study the potential reversibility of the photoswelling (and drug delivery) responses

Chapter 6 :

Conclusions

In conclusion,

- The successful synthesis of thermoresponsive and photoresponsive materials (structure and properties) was confirmed by ^{1}H NMR, GPC, potentiometric and conductometric titrations, and UV-vis spectroscopy
- Novel multi-responsive microgels were fabricated using microfluidics (rarely reported)
- UV irradiation of cinnamate-containing materials resulted in dimer formation and chemical crosslinking; this was both demonstrated in bulk hydrogels (pNIPAM-co-VC-co-AA polymer solutions gel upon irradiation) and in microgels (cinnamate-grafted microgels deswell and distort following UV irradiation)
- It was evident in both linear polymers and microgels that chemical crosslinking due to the chromophore dimerization was much more effective at reducing particle size than physical interactions between NIPAM residues
- Cytotoxicity studies using front and back of the eye cells (HCEC and RPEC respectively) exposed to concentrations of linear polymers and hydrogels suggest these materials are relatively non-toxic
- Demonstrated the successful application of PLS modeling to polymerization data to design polymers with target properties of smart polymeric systems
- Different PLS models were made using qualitative and quantitative measuring techniques to build models that proved to be useful in predicting polymer properties and uncovering obvious and non-obvious correlations in the original reactants and reaction conditions
- The application of PLS modeling to past polymer data helped determine the importance reaction conditions such as reaction time and dialysis membrane size in a wide range of chemistries all modeled together (rarely reported)

References

Access Economics Pty Limited (2008). The cost of vision loss in Canada, CNIB and the Canadian Ophthalmological Society**:** 124.

Agilent Technologies (2000). Polymer analysis by GPC-SEC, Agilent Technologies**:** 8.

Ahn S-k., Kasi R.M., et al. (2008). "Stimuli-responsive polymer gels." Soft Matter **4**(6): 1151-1157.

Alarcon CH., Pennadam S., et al. (2005). "Stimuli responsive polymers for biomedical applications." Chemical Society Reviews **34**(3): 276-285.

Ali A.H. and Srinivasan K.S.V. (1997). "Synthesis, Characterization, and Studies on the Solid-State Crosslinking of Functionalized Vinyl Cinnamate Polymers." Journal of Applied Polymer Science **67**.

American Optometric Association (2006, November 2006). "Diabetic Retinopathy." Retrieved March 2 2011, from http://www.aoa.org/diabetic-retinopathy.xml.

Amici A., Tetradis-Meris G., et al. (2008). "Alginate gelation in microfluidic channels." Food Hydrocolloids **22**(1): 97-104.

Andreopoulos F.M., Deible C.R., et al. (1996). "Photoscissable Hydrogel Synthesis via Rapid Photopolymerization of Novel PEG-Based Polymers in the Absence of Photoinitiators⊥." Journal of the American Chemical Society **118**(26): 6235-6240.

Andreopoulos F.M. and Persaud I. (2006). "Delivery of basic fibroblast growth factor (bFGF) from photoresponsive hydrogel scaffolds." Biomaterials **27**(11): 2468-2476.

Arıca M.Y., Öktem H.A., et al. (1999). "Immobilization of catalase in poly(isopropylacrylamide-co-hydroxyethylmethacrylate) thermally reversible hydrogels." Polymer International **48**(9): 879-884.

Atkinson S.D.M., Almond M.J., et al. (2003). "The photodimerisation of the [alpha]- and [beta]-forms of trans-cinnamic acid: a study of single crystals by vibrational microspectroscopy." Spectrochimica Acta Part A: Molecular and Biomolecular Spectroscopy **59**(3): 629-635.

Balaji R. and Nanjundan S. (2002). "Studies on Photosensitive Homopolymer and Copolymers Having a Pendant Photocrosslinkable Functional Group." Journal of Applied Polymer Science **86**: 1023-1037.

Bartsch S. and Bornscheuer U.T. (2010). "Mutational analysis of phenylalanine ammonia lyase to improve reactions rates for various substrates." Protein Engineering Design and Selection **23**(12): 929-933.

Berrada M., Carriere F., et al. (1996). "Photoinduced Polymerization of Bisimides as Models for New Soluble Side-Chain-Substituted Negative-Type Photosensitive Polyimides." Chemistry of Materials **8**(5): 1022-1028.

Bikram M. and West J.L. (2008). "Thermo-responsive systems for controlled drug delivery." Expert Opinion: Drug Delivery **5**(10): 1077-1091.

Bokias G. and Hourdet D. (2001). "Synthesis and characterization of positively charged amphiphilic water soluble polymers based on poly(N-isopropylacrylamide)." Polymer **42**(15): 6329-6337.

Catana C. and Stouten P.F.W. (2006). "Novel, Customizable Scoring Functions, Parameterized Using N-PLS, for Structure-Based Drug Discovery." Journal of Chemical Information and Modeling **47**(1): 85-91.

Chelvi T.P. and Ralhan R. (1995). "Designing of thermosensitive liposomes from natural lipids for multimodality cancer therapy." International Journal of Hyperthermia **11**(5): 685-695.

Chen J-P. and Cheng T-H. (2006). "Thermo-Responsive Chitosan-graft-poly(N-isopropylacrylamide) Injectable Hydrogel for Cultivation of Chondrocytes and Meniscus Cells." Macromolecular Bioscience **6**(12): 1026-1039.

Chen J-P. and Cheng T-H. (2009). "Preparation and evaluation of thermo-reversible copolymer hydrogels containing chitosan and hyaluronic acid as injectable cell carriers." Polymer **50**(1): 107-116.

Chen J-P., Leu Y-L., et al. (2011). "Thermosensitive hydrogels composed of hyaluronic acid and gelatin as carriers for the intravesical administration of cisplatin." Journal of Pharmaceutical Sciences **100**(2): 655-666.

Cho K.Y., Chung T.W., et al. (2003). "Release of ciprofloxacin from poloxamer-graft-hyaluronic acid hydrogels in vitro." International Journal of Pharmaceutics **260**(1): 83-91.

Csoka A.B., Frost G.I., et al. (2001). "The six hyaluronidase-like genes in the human and mouse genomes " Matrix Biology **20**(8): 499-508.

Csoka A.B., Scherer S.W., et al. (1999). "Expression Analysis of Six Paralogous Human Hyaluronidase Genes Clustered on Chromosomes 3p21 and 7q31." Genomics **60**(3): 356-361.

Daskiewicz J-B. and Barron D. (2003). "Substituent Effects in the Bf3-Mediated Acylation of Phenols with Cinnamic Acids." Natural Product Research **17**(5): 347-350.

De Geest B.G., Urbanski H.P., et al. (2005). "Synthesis of monodisperse biodegradable microgels in mcirofluidic devices." Langmuir **21**: 10275-10279.

Egerton P.L., Pitts E., et al. (1981). "Photocycloaddition in solid poly(vinyl cinnamate). The photoreactive polymer matrix as an ensemble of chromophore sites." Macromolecules **14**(1): 95-100.

EnCor Biotechnology Inc. (2008). "Formulations of commonly used buffers and media." Retrieved November 5, 2009, from http://www.encorbio.com/protocols/media.htm.

Ercole F., Davis T.P., et al. (2010). "Photo-responsive systems and biomaterials: photochromic polymers, light-triggered self-assembly, surface modification, fluorescence modulation and beyond." Polymer Chemistry **1**(1): 37-54.

Esposito Vinizi V., Chin W.W., et al. (2010). Handbook of Partial Least Squares, Springer.

FDA (2009). "Medical Devices." XACT Soft acrylic UV light-absorbing posterior chamber intraocular lens - P080021. Retrieved January 20 2011, from http://www.fda.gov/AboutFDA/ContactFDA/default.htm.

Fernandez G. "Principal Component Analysis." Retrieved May 29, 2011, from http://www.ag.unr.edu/saito/classes/ers701/pca2.pdf.

Fitzpatrick S.D., Mazumder M.A.J., et al. (2010). "PNIPAAm-grafted-collagen as an injectable, in situ gelling, bioactive cell delivery scaffold." Biomacromolecules **11**: 2261-2267.

Fitzpatrick S.D., Mazumder M.A.J., et al. (2011). "Cell-adhesive thermo-gelling PNIPAAm/ hyaluronic acid cell delivery hydrogels for non-invasive retinal therapy." to be determined: 20.

Ganachaud F., Monteiro M.J., et al. (2000). "Molecular Weight Characterization of Poly(N-isopropylacrylamide) Prepared by Living Free-Radical Polymerization." Macromolecules **33**(18): 6738-6745.

García-Muñoz S., Kourti T., et al. (2003). "Troubleshooting of an Industrial Batch Process Using Multivariate Methods." Industrial & Engineering Chemistry Research **42**(15): 3592-3601.

Garcia A., Marquez M., et al. (2006). "Photo-, Thermally, and pH-Responsive Microgels†." Langmuir **23**(1): 224-229.

Gattás-Asfura K.M., Weisman E., et al. (2005). "Nitrocinnamate-Functionalized Gelatin: Synthesis and "Smart" Hydrogel Formation via Photo-Cross-Linking." Biomacromolecules **6**(3): 1503-1509.

Ge X., Trabbic-Carlson K., et al. (2006). "Purification of an elastin-like fusion protein by microfiltration." Biotechnology and Bioengineering **95**(3): 424-432.

Geelen P.A.P. (2008). Light switchable coatings. TU-terrein, Netherlands, Technische Universiteit Eindhoven. **PhD:** 144.

Ghosh P., Hutadilok N., et al. (1994). "Interactions of hyaluronan (hyaluronic acid) with phospholipids as determined by gel permeation chromatography, multi-angle laser-light-scattering photometry and 1H-NMR spectroscopy." International Journal of Biological Macromolecules **16**(5): 237-244.

Guha R., Stanton D.T., et al. (2005). "Interpreting Computational Neural Network Quantitative Structure−Activity Relationship Models: A Detailed Interpretation of the Weights and Biases." Journal of Chemical Information and Modeling **45**(4): 1109-1121.

Ha D.I., Lee S.B., et al. (2006). "Preparation of Thermo-Responsive and Injectable Hydrogels Based on Hyaluronic Acid and Poly(N-isopropylacrylamide) and Their Drug Release Behaviors." Macromolecular Research **14**(1): 87-93.

Hansen C.M. (2004). "50 Years with solubility parameters--past and future." Progress in Organic Coatings **51**(1): 77-84.

Haserodt S., Aytekin M., et al. (2011). "comparison of the sensitivity, specificity, and molecular weight accuracy of three different commercially available Hyaluronan ELISA-like assays." Glycobiology **21**(2): 175-183.

He J., Yan B., et al. (2011). "Both Core- and Shell-Cross-Linked Nanogels: Photoinduced Size Change, Intraparticle LCST, and Interparticle UCST Thermal Behaviors." Langmuir **27**(1): 436-444.

He X., Wu X., et al. (2011). "Synthesis and self-assembly of a hydrophilic, thermo-responsive poly(ethylene oxide) monomethyl ether-block-poly(acrylic acid)-block-poly(N-isopropylacrylamide) copolymer to form micelles for drug delivery." Reactive and Functional Polymers **71**(5): 544-552.

Health Canada. (2006). Seniors and Agining - Vision Care. H. Canada, Government of Canada.

Heath F., Haria P., et al. (2007). "Varying Polymer Architecture to Deliver Drugs." The AAPS Journal **9**(2): E235-E240.

Heskins M. and Guillet J.E. (1968). "Solution Properties of Poly(N-isopropylacrylamide)." Journal of Macromolecular Science: Part A - Chemistry **2**(8): 1441-1455.

Hoare T. (2006). Multi-responsive Microgels: Synthesis, Characterization, and Applications. Chemical Engineering. Hamilton, ON, McMaster University. **PhD ChemEng:** 284.

Hoare T. (2009). Polymers Part III: Polymer Modification, CheE 704 Course Notes. McMaster University**:** 1-26.

Hoare T. and McLean D. (2006). "Kinetic prediction of functional group distributions in thermosensitive microgels." J. Phys. Chem. B **110**(41): 20327-20336.

Hoare T. and Pelton R. (2004). "Functional Group Distributions in Carboxylic Acid Containing Poly(N-isopropylacrylamide) Microgels." Langmuir **20**(6): 2123-2133.

Hoare T. and Pelton R. (2004). "Highly pH and temperature responsive microgels functionalized with vinylacetic acid." Macromolecules **37**(7): 2544-2550.

Hu R., Chen Y-Y., et al. (2010). "Synthesis and characterization of in situ photogelable polysaccharide derivative for drug delivery." International Journal of Pharmaceutics **393**(1-2): 97-104.

Hulubei C. and Rusu E. (2006). "NEW FUNCTIONAL POLY(BISMALEIMIDE-ETHER)S: SYNTHESIS AND CHARACTERIZATION." Polymer-Plastics Technology and Engineering **40**(2): 17.

International Program on Chemical Safety. (1982). Environment Health Criteria 23, Lasers and Optical Radiation, United Nations Environment Programme, the International Labour Organisation, the International Radiation Protection Association**:** 191.

Itano N., Sawai T., et al. (1999). "Three isoforms of mammalian hyaluronan synthases have distinct enzymatic properties." The Journal of Biological Chemistry **274**(35): 25085-25092.

Ito Y. and Fujita H. (1999). "Unusual [2+2] Photocycloaddition between Tryptamine and 3-Nitrocinnamic Acid in the Solid State." Chemistry Letters **29**(3): 288-289.

Izunobi J.U. and Higginbotham C.L. (2011). "Polymer Molecular Weight Analysis by 1H NMR Spectroscopy." Journal of Chemical Education **88**(8): 1098-1104.

Jeong B., Bae Y.H., et al. (1996). "Biodegradable block copolymers as injectable drug-delivery systems." Nature **388**: 860-862.

Jiang J., Qi B., et al. (2007). "Polymer Micelles Stabilization on Demand through Reversible Photo-Cross-Linking." Macromolecules **40**(4): 790-792.

Jung H., Jang M.K., et al. (2009). "Synthesis and Characterization of Thermosensitive Nanoparticles Based on PNIPAAm Core and Chitosan Shell Structure." Macromolecular Research **17**(4): 265-270.

Kadlubowski S. (2009). "Nanogels & Microgels." Retrieved July 12, 2011, from http://www.mitr.p.lodz.pl/biomat/nanogel.html.

Kato M., Ichijo T., et al. (2003). "Novel synthesis of photocrosslinkable polymers." Journal of Polymer Science: Part A: Polymer Chemistry **9**(8): 2109-2128.

Kelly S.M. (1995). "Anisotropic Networks." Journal of Materials Chemistry **5**(12): 2047-2061.

Kesselman L., Shinwary S., et al. (2011). Reactive Microfluidic Production of Degradable Microgels for Drug Delivery. AlChE, Minneapolis Convention Center.

Kettaneh-Wold N. (1992). "Analysis of mixture data with partial least squares." Chemometrics and Intelligent Laboratory Systems **14**(1-3): 57-69.

Khan M., Brunklaus G., et al. (2008). "Transient States in [2 + 2] Photodimerization of Cinnamic Acid: Correlation of Solid-State NMR and X-ray Analysis." Journal of the American Chemical Society **130**(5): 1741-1748.

Kim H-T. and Park J-K. (1998). "Thermal degradation of poly(vinyl cinnamate)." Polymer Bulletin **41**: 325-331.

Kolb H., Fernandez E., et al. (1995). The Organization of the Retina and Visual System. Salt Lake City, UT, USA, University of Utah Health Sciences Center. **1**.

Lambeth R.H., Ramakrishnan S., et al. (2006). "Synthesis and Aggregation Behavior of Thermally Responsive Star Polymers." Langmuir **22**(14): 6352-6360.

Larsson A., Kuckling D., et al. (2001). "1H NMR of thermoreversible polymers in solution and at interfaces: the influence of charged groups on the phase transition." Colloids and Surfaces A: Physicochemical and Engineering Aspects **190**(1-2): 185-192.

Lee J-W., Kim H-T., et al. (2001). "Relationship between pretilt angle and surface energy of the blended films based on poly(vinyl cinnamate) and alkanoyl cinnamic acid." Synthetic Metals **117**: 267-269.

Leitzke A., Reisz E., et al. (2001). "The reactions of ozone with cinnamic acids: formation and decay of 2-hydroperoxy-2-hydroxyacetic acid." The Royal Society of Chemistry **2**: 793-797.

Lewis F.D., Quillen S.L., et al. (1988). "Lewis acid catalysis of photochemical reactions. 7. Photodimerization and cross-cycloaddition of cinnamic esters." Journal of the American Chemical Society **110**(4): 1261-1267.

Li B., Morris A.J., et al. (2004). "Generalized partial least squares regression based on the penalized minimum norm projection." Chemometrics and Intelligent Laboratory Systems **72**(1): 21-26.

Lim D.W., Nettles D.L., et al. (2007). "Rapid Cross-Linking of Elastin-like Polypeptides with (Hydroxymethyl)phosphines in Aqueous Solution." Biomacromolecules **8**: 1463-1470.

Liu L. (2003). PDMS/PNIPAM Interpenetrating Polymer Networks as Ophthalmic Biomaterials. Chemical Engineering. Hamilton, ON, McMaster University. **MASc:** 149.

López-León T., Ortega-Vinuesa J.L., et al. (2006). "Cationic and Anionic Poly(N-isopropylacrylamide) Based Submicron Gel Particles: Electrokinetic Properties and Colloidal Stability." The Journal of Physical Chemistry B **110**(10): 4629-4636.

Lowenstein J.I. (2011). Macular Hole. Digital Journal of Ophthalmology. Massachusetts, USA, Harvard Medical School.

Lutz J-F., Akdemir O., et al. (2006). "Point by Point Comparison of Two Thermosensitive Polymers Exhibiting a Similar LCST: Is the Age of Poly(NIPAM) Over?" Journal of American Chemical Society **128**(40): 13046-13047.

MacGregor J.F. and Kourti T. (1995). "Statistical process control of multivariate processes." Control Eng. Practice **3**(3): 403-414.

Malonne H., Eeckman F., et al. (2005). "Preparation of poly(N-isopropylacrylamide) copolymers and preliminary assessment of their acute and subacute toxicity in mice." European Journal of Pharmaceutics and Biopharmaceutics **61**(3): 188-194.

Maruyama K., Unezaki S., et al. (1993). "Enhanced delivery of doxorubicin to tumor by long-circulating thermosensitive liposomes and local hyperthermia " Biochimica et Biophysica Acta (BBA) - Biomembranes **1149**(2): 209-216.

Masci G., Giacomelli L., et al. (2004). "Atom Transfer Radical Polymerization of N-Isopropylacrylamide." Macromolecular Rapid Communications **25**(4): 559-564.

McHale R., Aldabbagh F., et al. (2007). "Polymerization of N-isopropylacrylamide in the presence of poly(acrylic acid) and poly(methacrylic acid) containing ω-unsaturated end-groups." Journal of Polymer Science Part A: Polymer Chemistry **45**(18): 4394-4400.

Minsk L.M., Smith J.G., et al. (1959). "Photosensitive polymers. I. Cinnamate esters of poly(vinyl alcohol) and cellulose." Journal of Applied Polymer Science **2**(6): 302-307.

Mone M.J., Volker M., et al. (2001). "Local UV induced DNA damage in cell nuclei results in local transcription inhibition." European Molecular Biology Organization **2**(11): 1013-1017.

Moxon E. "The electromagnetic spectrum." Retrieved December 2, 2010, from http://www.lbl.gov/MicroWorlds/Support.html.

Murugan N.A., Hugosson H.W., et al. (2008). "Solvent Dependence on Conformational Transition, Dipole Moment, and Molecular Geometry of 1,2-Dichloroethane: Insight from Car−Parrinello Molecular Dynamics Calculations." The Journal of Physical Chemistry B **112**(47): 14673-14677.

Muteki K. and MacGregor J.F. (2006). "Rapid Development of New Polymer Blends: The Optimal Selection of Materials and Blend Ratios." Ind. Eng. Chem. Res. **45**: 4653-4660.

Naciri J., Shenoy D.K., et al. (2004). "Molecular structure and pretilt control of photodimerized-monolayers (PDML)." Journal of Materials Chemistry **14**(23): 3468-3473.

Nagata M. and Inaki K. (2009). "Synthesis and characterization of photocrosslinkable poly(l-lactide)s with a pendent cinnamate group." European Polymer Journal **45**(4): 1111-1117.

Nakashima T., Shimizu M., et al. (2000). "Particle control of emulsion by membrane emulsification and its applications." Advanced Drug Delivery Reviews **45**: 47-56.

NASA Official: Netting R. (2007). "The electromagnetic spectrum." Retrieved Demeber 3 2010, from http://science.hq.nasa.gov/kids/imagers/ems/waves3.html.

National Eye Institute (2010, August 2010). "Facts About Age-Related Macular Degeneration." from http://www.nei.nih.gov/health/maculardegen/armd_facts.asp.

Nguyen D.V. and Rocke D.M. (2002). "Partial least squares proportional hazard regression for application to DNA microarray survival data." Bioinformatics **18**(12): 1625-1632.

Nichols E. (2011). Rapid Product Development. Chemical Engineering. Hamilton, Ontario, Canada, McMaster University. **M.A.Sc. Chem. Eng.:** 100.

Novack G.D. (2008). "Ophthalmic Drug Delivery: Development and Regulatory Considerations." Clinical Pharmacology & Therapeutics **85**(5): 539-543.

Ogawa K., Nakayama Y., et al. (2003). "Preparation and characterization of thermosensitive polyampholyte nanogels." Langmuir **19**(8): 3178-3184.

Ohya S. and Matsuda T. (2005). "Poly (N-isopropylacrylamide) (PNIPAM)-grafted gelatin as thermoresponsive three-dimensional artificial extracellular matrix: molecular and formulation parameters vs. cell proliferation potential." Journal of Biomaterials Science, Polymer Edition **16**(7): 809-827.

Ohya S., Nakayama Y., et al. (2001). "Material design for an artificial extracellular matrix: Cell entrapment in poly (N-isopropylacrylamide) (PNIPAM)-grafted gelatin hydrogel." Journal of Artificial Organs **4**(4): 308-314.

Ohya S., Nakayama Y., et al. (2001). "Thermoresponsive Artificial Extracellular Matrix for Tissue Engineering: Hyaluronic Acid Bioconjugated with Poly(N-isopropylacrylamide) Grafts." Biomacromolecules **2**(3): 856-863.

Okushima S., Nisisako T., et al. (2004). "Controlled Production of Monodisperse Double Emulsions by Two-Step Droplet Breakup in Microfluidic Devices." Langmuir **20**(23): 9905-9908.

Paczkowski J. (1991). "Cinnamates. 5. Light-Sensitive Polycinnamates with Internal Charge Transfer. The Study of the Local Dielectric Constant and Viscosity." Macromolecules **24**: 2172-2177.

Pecinovsky C.S., Hatakeyama E.S., et al. (2008). "Polymerizable Photochromic Macrocyclic Metallomesogens: Design of Supramolecular Polymers with Responsive Nanopores." Advanced Materials **20**(1): 174-178.

Pelton R.H. and Chibante P. (1986). "Preparation of Aqueous Latices with N-Isopropylacrylamide." Colloids and Surfaces **20**: 247-256.

Perny S., Le Barny P., et al. (2000). "Molecular orientation and liquid crystal alignment properties of new cinnamate-based photocrosslinkable polymers." Liquid Crystals **27**(3): 341-348.

Perny S., Le Barny P., et al. (2000). "Photoinduced orientation in poly(vinylcinnamate) and poly(7-methacryloyloxycoumarin) thin films and the consequences on liquid crystal alignment." Liquid Crystals **27**(3): 329-340.

Philipson L.H. and Schwarts N.B. (1984). "The six hyaluronidase-like genes in the human and mouse genomes*." The Journal of Biological Chemistry **259**(8): 5017-5023.

Plunkett K.N., Zhu X., et al. (2006). "PNIPAM Chain Collapse Depends on the Molecular Weight and Grafting Density." Langmuir **22**(9): 4259-4266.

PolymerSource. "pNIPAM data sheet." Retrieved June 12, 2011, from http://www.polymersource.com/dataSheet/P6669-NIPAM.pdf.

ProSensus Inc. (2011). ProSensus Multivariate Help Documentation v11.02 documentation. . ProSensus MulitVariate Titorial. Hamilton, ON, Canada, ProSensus.

Rai S.K., Duh F-M., et al. (2001). "Candidate tumor suppressor HYAL2 is a glycosylphosphatidylinositol (GPI)-anchored cell-surface receptor for jaagsiekte sheep retrovirus, the envelope protein of which mediates oncogenic transformation." Proc. Natl. Acad. Sci., U.S.A **98**(8): 4443-4448.

Ravve A. (2006). Photocrosslinkable Polymers. Light-Associated Reactions of Synthetic Polymers Springer New York**:** 199-245.

Rimmer S., Soutar I., et al. (2009). "Switching the conformational behaviour of poly(N-isopropyl acrylamide)." Polymer International **58**(3): 273-278.

Rockel A., Hertel J., et al. (1986). "Permeability and secondary membrane formation of a high flux polysulfone hemofilter." Kidney Int **30**(3): 429-432.

Ruzin S. (2005, August 10, 2005). "Buffers." Plant Microtechnique and Microscopy. Retrieved July 8, 2010, from http://microscopy.berkeley.edu/Resources/instruction/buffers.html.

Samimi H.A., Mamaghani A., et al. (2009). "Studies on the Synthesis and Dynamic NMR Properties of 2-(Benzylidene amino)-N-[(R)-2-hydroxy-2-methyl-1-phenylpropyl]acetamide." J. Iran. Chem. Soc., **7**(1): 185-189.

Schmidt G.M.J. (1971). "Photdimerization in the solid state." Pure and Applied Chemistry **27**(4): 647-678.

Segura T., Anderson B.C., et al. (2005). "Crosslinked hyaluronic acid hydrogels: a strategy to functionalize and pattern." Biomaterials **26**(4): 359-371.

Selvam P., Babu K.V., et al. (2005). "Studies on photocrosslinkable copolymers of 4-methacryloyloxyphenyl-3',4'-dimethoxystyryl ketone and methyl methacrylate." European Polymer Journal **41**(4): 831-841.

Sheardown H., Brook M.A., et al. (2009). Photo-responsive delivery system. U. S. P. A. Publication. **19:** 14.

Shen Z., Terao K., et al. (2006). "Synthesis and phase behavior of aqueous poly(N-isopropylacrylamide-co-acrylamide), poly(N-isopropylacrylamide-co-N,N-dimethylacrylamide) and poly(N-isopropylacrylamide-co-2-hydroxyethyl methacrylate)." Colloid & Polymer Science **284**(9): 1001-1007.

Sirpal S., Gattás-Asfura K.M., et al. (2007). "A photodimerization approach to crosslink and functionalize microgels." Colloids and Surfaces B: Biointerfaces **58**(2): 116-120.

Sivakumaran D. (2010). Injectable in situ gellable hydrogel-microgel composites for drug delivery. Chemical Engineering. Hamilton, ON, McMaster University. **M.A.Sc:** 120.

Stile R.A., Burghardt W.R., et al. (1999). "Synthesis and Characterization of Injectable Poly(N-isopropylacrylamide)-Based Hydrogels That Support Tissue Formation in Vitro." Macromolecules **32**(22): 7370-7379.

Tan B.H., Ravi P., et al. (2006). "Synthesis and Characterization of Novel pH-Responsive Polyampholyte Microgels." Macromolecular Rapid Communications **27**(7): 522-528.

Tan H., Ramirez C.M., et al. (2009). "Thermosensitive injectable hyaluronic acid hydrogel for adipose tissue engineering." Biomaterials **30**(36): 6844-6853.

TdB Consultancy (2010). "FITC-Dextran Data File." Retrieved June 2, 2011, from www.tdbcons.se/tdbcons/attachment/datafilefitcdex.pdf.

The MathWorks Inc. (2000). Optimization Toolbox: For Use with MATLAB, User's Guide, Version 2. Natick, MA, The MathWorks.

Tong Z., Zeng F., et al. (1999). "Inverse Molecular Weight Dependence of Cloud Points for Aqueous Poly(N-isopropylacrylamide) Solutions." Macromolecules **32**(13): 4488-4490.

Tornaletti S. and Pfeifer G.P. (1996). "UV damage and repair mechanisms in mammalian cells." BioEssays: Review Article **18**(3): 221-228.

Tumarkin E. and Kumacheva E. (2009). "Microfluidic generation of microgels from synthetic and natural polymers." Chemical Society Reviews **38**: 2161-2168.

VeriMed Healthcare Network (2009, August 6 2008). "Glaucoma." Retrieved February 6, 2011, from http://www.ncbi.nlm.nih.gov/pubmedhealth/PMH0002587/.

Versari A., Parpinello G.P., et al. (2010). Prediction of total antioxidant capacity of red wine by Fourier transform infrared spectroscopy. Food Control, Elsevier Ltd. **21:** 786-789.

Vijayanand P.S., Kato S., et al. (2007). "Novel Photosensitive Polymer: Synthesis, Characterization and Thermal Properties of Polymer having Pendant Photocrosslinkable Group." Journal of Macromolecular Science, Part A: Pure and Applied Chemistry **44**(7): 727-734.

Vinogradov S.V. (2006). Colloidal microgels in drug delivery applications. Sharjah, EMIRATS ARABES UNIS, Bentham.

Weiner A.L. and Gilger B.C. (2010). "Advancements in ocular drug delivery." Veterinary Ophthalmology **13**(6): 395-406.

Wells L.A. (2010). Photoresponsive Drug Delivery from Anthracene - Modified Hydrogels. Chemical Engineering. Hamilton, McMaster University. **PhD:** 226.

Wells L.A., Furukawa S., et al. (2011). "Photoresponsive PEG-Anthracene Grafted Hyaluronan as a Controlled-Delivery Biomaterial." Biomacromolecules **12**(4): 923-932.

West D.C., Hampson I.N., et al. (1985). "Angiogenesis induced by degradation products of hyaluronic acid." Science, New Series **228**(4705): 1324-1326.

Williams J., Rubin M., et al. (1969). Photopolymerization and photocrosslinking of polymers. Photochemistry, Springer Berlin / Heidelberg. **13:** 227-250.

Wold S., Sjöström M., et al. (1986). "Multivariate design." Analytica Chimica Acta **191**: 17-32.

Wybrańska K., Szczubiałka K., et al. (2008). "Photochemical molecular imprinting of cholesterol." Journal of Inclusion Phenomena and Macrocyclic Chemistry **61**(1): 147-151.

Yin X., Hoffman A.S., et al. (2006). "Poly(N-isopropylacrylamide-co-propylacrylic acid) copolymers that respond sharply to temperature and pH." Biomacromolecules **7**(5): 1381-1385.

Yoo J-H., Cho I., et al. (2004). "Sequence-Controlled Ethylene/Vinyl Cinnamate Coploymers: Synthesis and Application to the Photoalignment of Liquid Crystals." Journal of Polymer Science: Part A: Polymer Chemistry **42**: 5401-5406.

Yoshida M. and Lahann J. (2008). "Smart Nanomaterials." ACS Nano **2**(6): 1101-1107.

Yu T.L., Lu W-C., et al. (2004). "Solvents effect on the physical properties of semi-dilute poly(N-isopropyl acryl amide) solutions." Polymer **45**(16): 5579-5589.

Yusa S-i., Yamago S., et al. (2007). "Thermo-Responsive Diblock Copolymers of Poly(N-isopropylacrylamide) and Poly(N-vinyl-2-pyrroridone) Synthesized via Organotellurium-Mediated Controlled Radical Polymerization (TERP)." Macromolecules **40**(16): 5907-5915.

Zeng F., Tong Z., et al. (1999). "Molecular chain properties of poly (N-isopropyl acrylamide)." Science in China Series B: Chemistry **42**(3): 290-297.

Zhao C., Zhuang X., et al. (2009). "Synthesis of biodegradable thermo- and pH-responsive hydrogels for controlled drug release." Polymer **50**: 4308-4316.

Zheng Y., Andreopoulos F.M., et al. (2001). "A Novel Photoscissile Poly(ethylene glycol)-Based Hydrogel." Advanced Functional Materials **11**(1): 37-40.

Appendices

A1: PCA Results on X and Y form final modeling data

A1.1 PCA on X

Performing a PCA on either x or y data can help establish which original x variables are correlated and how influential they are to the latent variables. The principal component loadings (vectors) P1vs.P2 are in Figure A1.1, where we can see the relationships between all 14 x variables. The variables grouped together are highly correlated and move in the same direction. For example, DMF is positively correlated with reaction temperature; correspondingly, DMF reactions were typically performed at higher temperatures due to the higher boiling point of DMF.

This PCA on X gave a model with 7 components with R2 ~0.9063 and Q2 ~ 0.6484. All monomers are spread out far apart in the P1-P2 space; physically, this spread is related to the fact that reducing the fraction of one monomer results in an increase in the fraction of another monomer. Note that NIPAM is close to a cluster of variables: AIBMe, AESH, and reaction temperature. This tells us that in general with increased amount of NIPAM, followed an increased amount of initiator (AIBMe) and more AESH for certain chemistries with those reactants involved. The type of solvent and amount of solvent used are expressed as an inverse concentration (the volume of solvent in liters per total monomer moles). This was chosen so as to ensure the model interpretations were proportional to concentration volume and not inversely proportional to volume (as typical concentration units mol/L represent).

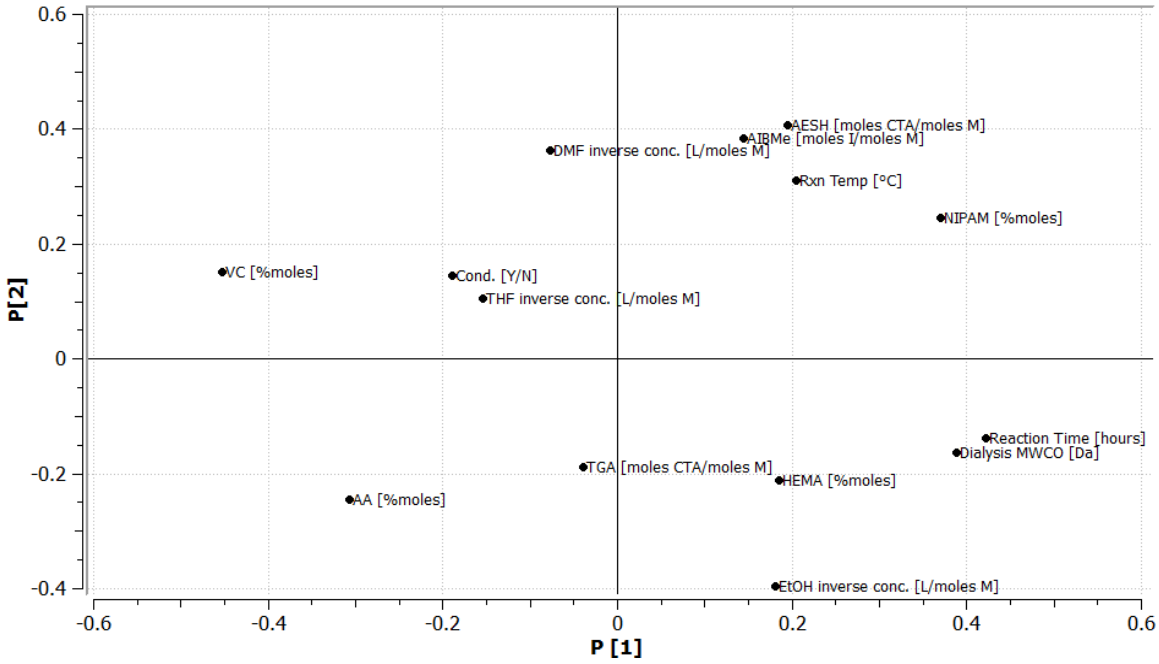

Figure A1.1: P1vs.P2 from PCA on X

In a PCA analysis, there are no coefficients bar plots and instead the variable importance plot (VIP) tells how important a variable is to a model. The P1 bar plot shows the direction of influence of each x variable in the system. Therefore to determine which variables are most influential (as well as their magnitude and direction), it is useful to view both VIP and P1 bar plot simultaneously as in Figure A.1.2. In doing so, the user can decide which variable(s) could be excluded from the model and eliminate insignificant variables; this was done in a trial model but did not improve the model predictability in the model currently considered.

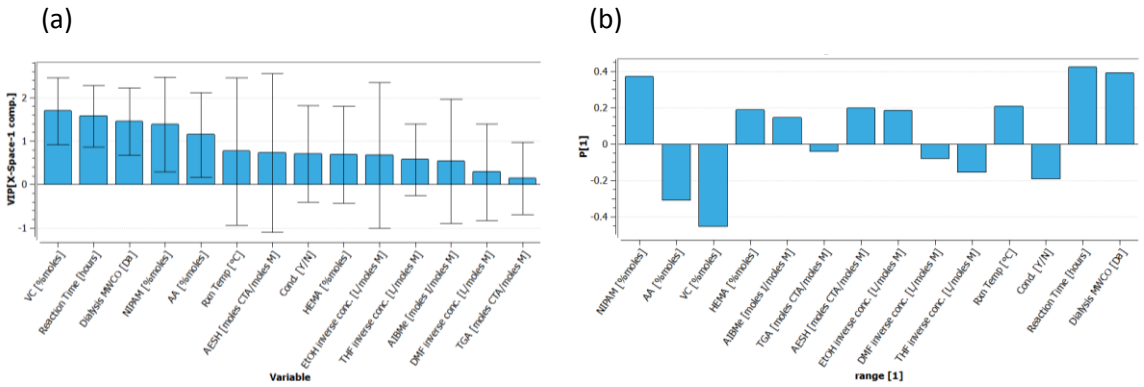

Figure A.1.2: Plots of (a) VIP and (b) P1 bar for component 1

From this information, we can see that the most influential and significant x variables on the first component are VC (negative) followed by reaction time (positive), and dialysis MWCO (positive).

A1.2 Analysis of Y Data

Performing a PCA on y gives an R2 ~0.7834 and Q2 ~0.6214 with two components. In Figure A.1.3, the higher VC/NIPAM (NMR actual ratio) is oppositely correlated to both solubility and cloud point in the first component. So more VC in the product leads to lower solubility and lowers the T_{cp} of the polymer. Also, the amount of AA incorporated is more closely correlated with both solubility and cloud point compared to VC or HEMA. This supports the use of PLS for interpreting complex chemical systems, as it can be used to find more accurate relationships among different chemistries made by changing more than one input variable at a time. In addition, PCA can clearly elucidate all correlations present in the data in a single analysis, detecting potential correlations that may be ignored or obscured by directly comparing two variables.

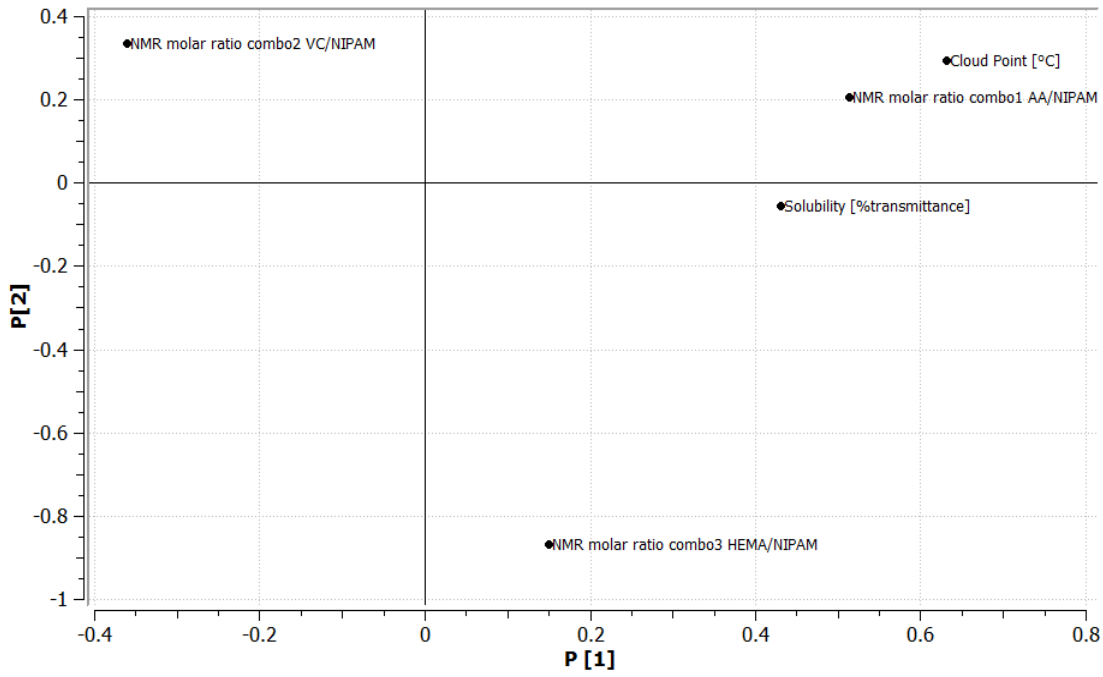

Figure A.1.3: P2vs.P1 loading plot from PCA on y data

A2: Steps to follow for the application of PLS Modeling to polymer designing

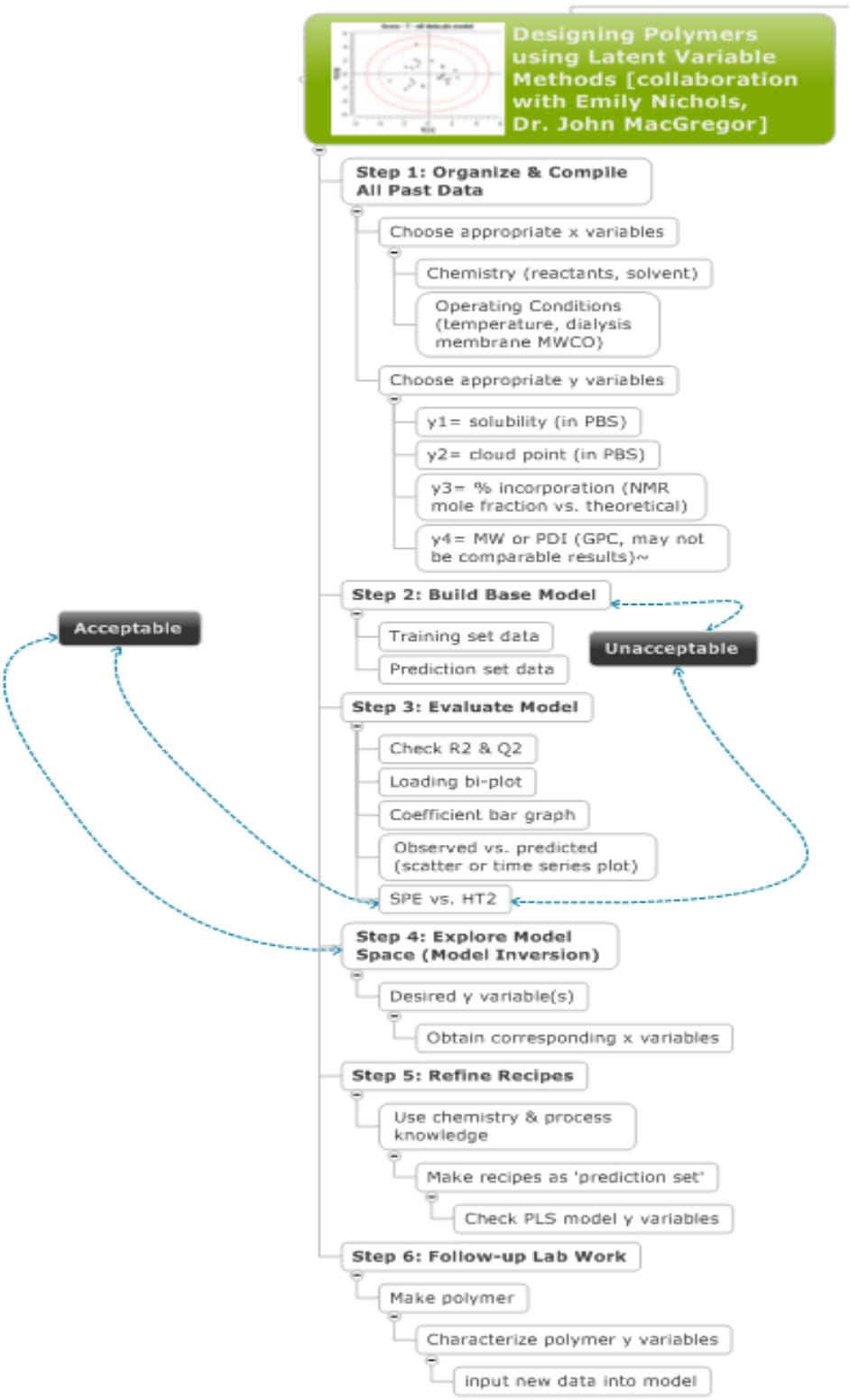

A3: pNIPAM standards GPC relational curve

M_n actual refers to manufacturer data provided with samples (Polymer Source, Sigma-Aldrich) and M_n measured refers to the GPC result calculated using polystyrene calibration standards in THF as the elution solvent.

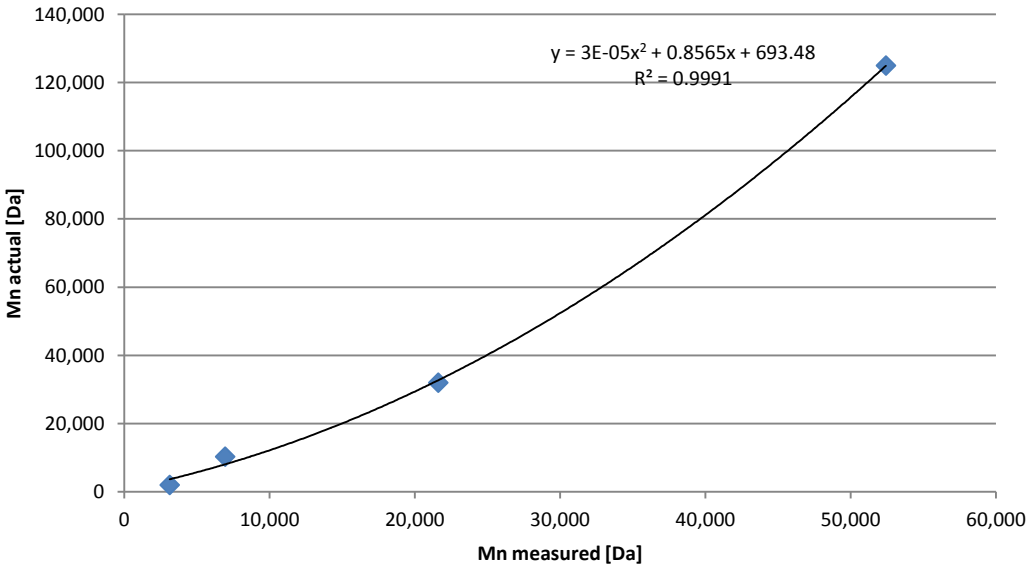

A4 Appendix for titration curve example

The analysis of the conductometric titration curve for sample 3M-1 pNIPAM-AA (BIS) as:

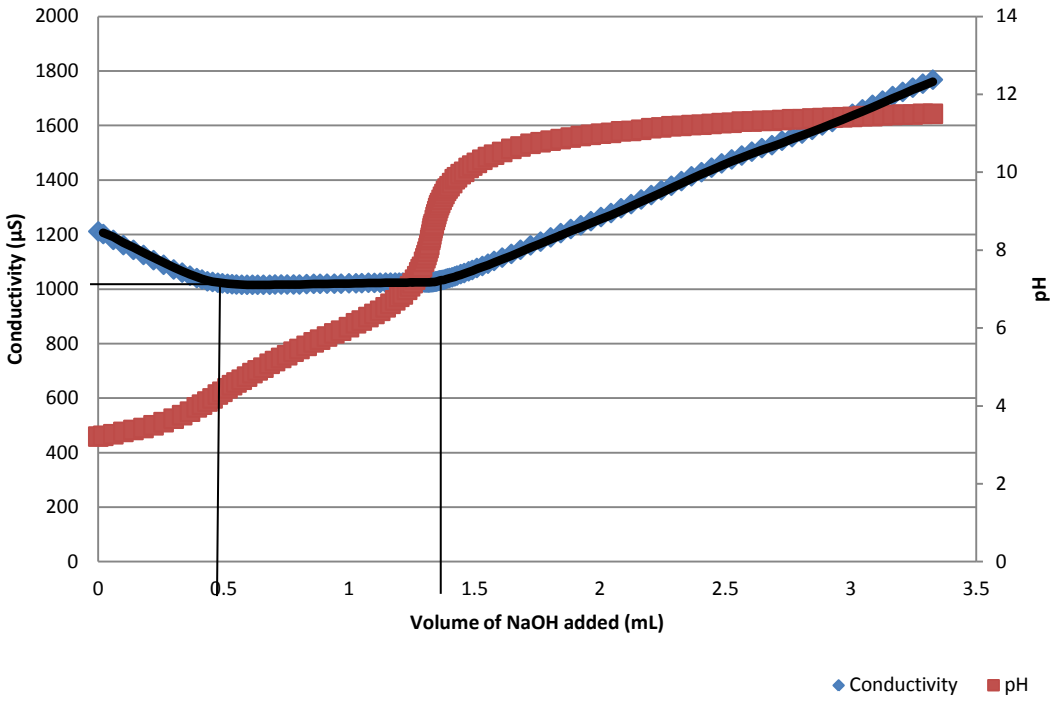

points chosen	volume (mL)	Conductivity (µS)
point 1	0.434	1028.3
point 2	1.285	1024.4

delta vol (L)	0.00085
NaOH (M)	0.1
moles of AA	0.000085
mass AA (g)	0.00612
Mass ratio (%)	**12.25**
MW AA (g/mol)	72.06
mass of sample (g)	0.050